UNIVERSIDADE DA CORUÑA

Generation and characterization of mesenchymal cell lines for osteochondral regeneration research

María Piñeiro Ramil

UDC Doctoral Thesis 2021

Programa de Doutoramento en Ciencias da Saúde

Directoras:
Silvia María Díaz Prado
Clara Sanjurjo Rodríguez

A Dra. Silvia María Díaz Prado, profesora da Área de Anatomía e Embrioloxía Humana do Departamento de Fisioterapia, Medicina e Ciencias Biomédicas da Universidade da Coruña, e a Dra. Clara Sanjurjo Rodríguez, investigadora posdoutoral do grupo de investigación en Terapia Celular e Medicina Rexenerativa da Universidade da Coruña,

CERTIFICAN QUE:

Dna. María Piñeiro Ramil, graduada en Biotecnoloxía pola Universidade de Salamanca e máster en Bioloxía Molecular, Celular e Xenética pola Universidade da Coruña, realizou baixo a nosa dirección o traballo "Xeración e caracterización de liñas celulares mesenquimais para investigación en rexeneración osteocondral", e que dito traballo reúne as condicións necesarias de orixinalidade e rigor científico para ser defendido publicamente e optar á mención de doutora internacional en Ciencias da Saúde.

A Coruña, 17 de xaneiro de 2021

Dra. Silvia María Díaz Prado

Dra. Clara Sanjurjo Rodríguez

Parte da investigación incluída nesta tese de doutoramento foi realizada baixo a supervisión do Dr. Manuel Bañobre López, líder do grupo de investigación *Nanomedicine* do *International Iberian Nanotechnology Laboratory (INL)* de Braga (Portugal), durante unha estadía de investigación predoutoral no ano 2019.

A mis abuelos

Me gustaría agradecer, en primer lugar, su altruismo a los donantes de las muestras. Sin ellos, este trabajo no podría haberse llevado a cabo.

En segundo lugar, quisiera agradecer a mis directoras de tesis, las doctoras Silvia María Díaz Prado y Clara Sanjurjo Rodríguez, el haberme dado la oportunidad de hacer este trabajo en el grupo de investigación en Terapia Celular y Medicina Regenerativa (TCMR) del Instituto de Investigación Biomédica de A Coruña (INIBIC). Gracias por confiar en mí, por dedicarme vuestro tiempo, por enseñarme tanto, y por guiarme durante todo el proceso de realización de esta tesis, desde el primer día en que puse un pie en el laboratorio hasta la escritura desde estas líneas.

También me gustaría agradecer a los doctores Isaac Fuentes Boquete y Javier de Toro Santos su apoyo y su ayuda, y al director científico del INIBIC, el Dr. Francisco Blanco García, el haberme facilitado el acceso a las instalaciones y a las muestras necesarias para realizar esta investigación. Gracias también a todos los técnicos y profesionales de la agrupación estratégica CICA-INIBIC: Purificación Filgueira Fernández, Beatriz Cruz Caamaño, Noa Goyanes Rey, Sara Relaño Fernández, Estefanía Cives, María Moreno... Mi agradecimiento especial a la Dra. Tamara Hermida Gómez, Tamy, y a María José Sánchez Dopico, Mariajo, por haber estado siempre dispuestas a resolver mis dudas, por tontas que fueran, y por hacer del laboratorio de Cultivos Celulares uno de los sitios más divertidos en los que pasar el rato (¡no os hacéis una idea de cuánto se nota que no estáis!).

Gracias a mis compañeros del INIBIC por haber compartido conmigo estos años. A Silvia, por aguantar todas mis crisis, por ayudarme siempre que has podido, por soportar que hable sola en la poyata… después de estos años conmigo, tienes el cielo ganado. A Miriam, por animar las mañanas en el laboratorio, y por no perder nunca el buen humor ni las ganas de hacer ciencia, a pesar de todo. A Pau, porque empezamos y terminamos este camino juntas; gracias, porque sé que siempre puedo contar contigo. A Durán, por animar mis días con sus comentarios y sus caras de sueño. A Alba, por estar a mi lado todos estos años y ser mi compañera de batallas perdidas. A todos los demás, incluso los que ya no están; especialmente a Rocío, por haberme enseñado y acompañado durante mi primera etapa en el laboratorio; y a Cris, por los momentos buenos y malos que hemos compartido, pero sobre todo por nuestros tés y nuestras conversaciones interminables sobre gatos.

I would also like to thank the AmTheNa group from INL: Dr. Manuel Bañobre and Dr. Juan Gallo, for letting me be a part of their amazing research, and for their

guidance and implication in a project that would never have been possible without them; and all the team members: Nuria, Marta, Stefania, Milene, Cátia, Vera, Victor, thank you all so much for helping me during my stay and making me feel part of the AmTheNa family.

Gracias a la Deputación da Coruña, Consellería de Cultura, Educación e Ordenación Universitaria (Xunta de Galicia) y Fondo Social Europeo 2014/2020, por haberme financiado como investigadora durante la realización de esta tesis. Al programa inMOTION INDITEX-UDC por haber financiado mi estancia predoctoral, permitiéndome optar a la mención internacional. Me gustaría agradecer también el apoyo financiero de las siguientes instituciones y organismos, sin el cual esta investigación no habría sido posible: Fundación Española de Reumatología, Instituto de Salud Carlos III, Rede Galega de Terapia Celular y Grupos con Potencial de Crecemento (Xunta de Galicia) y CIBER-BBN. También agradezco a Bruna Parma, de Opocrin S.p.A., el suministro de los biomateriales de colágeno I. Gracias, además, a Xesús Mosquera y Alicia Pallas, por su impecable trabajo en la revisión y corrección de este manuscrito.

Por último, pero no menos importante, me gustaría agradecer a mi familia. Gracias a mis padres porque nunca habría llegado hasta aquí sin su confianza y su apoyo. Gracias a Pan por haber estado a mi lado durante todos estos años, y por aguantar mis desvaríos sobre las células "mezenquimales". Gracias a mis amigos, los que están cerca y los que están lejos, y muy especialmente a Elena y Mortuk, que son los que siempre aguantan todas mis quejas. Gracias, en definitiva, a todos los que me han acompañado durante este tiempo, incluidos los de tres y cuatro patas.

Gracias, de corazón.

INDEX

LIST OF ABBREVIATIONS

ACI: Autologous chondrocyte implantation

ACTB: Beta-actin

ADSCs: Adipose tissue-derived stem cells

AI: Adipogenic induction.

APN: Adiponectin

ATM: Ataxia-telangiectasia mutated protein kinase

ATR: ATM and Rad3-related protein kinase

BM: Basal medium.

CCK-8: Cell Counting Kit-8

CDKs: Cyclin-dependent kinases

CD29: Integrin β1

CD34: Hematopoietic progenitor cell antigen 1 (HPCA1)

CD44: Homing cellular adhesion molecule (HCAM)

CD45: Leukocyte common antigen (LCA)

CD73: Ecto-5'-nucleotidase (NT5E)

CD90: Thymocyte differentiation antigen 1 (Thy-1)

CD105: Endoglin

CHO: Chinese hamster ovary

ColI: Type I collagen

COX2: Cyclooxigenase 2

CPCs: Chondroprogenitor cells

DNA: Deoxyribonucleic acid

ECM: Extracellular matrix

eGFP: Enhanced green fluorescent protein

EO: Endochondral ossification

E2F: E2F transcription factor 1

FABP4: Fatty acid binding protein 4

FCWF-4: *Felis catus* whole foetus cells

Fe_3O_4: Magnetite

Fe_3O_4@PAA: IONs composed of magnetite and polyacrylic acid (PAA)

FIPV: Feline infectious peritonitis virus

GAPDH: Glyceraldehyde 3-phosphate dehydrogenase

GFP: Green fluorescent protein

HBV: Hepatitis B virus

HCV: Hepatitis C virus

HDMB: Hexadimethrine bromide

HIV: Human immunodeficiency virus

HPRT1: Hypoxanthine phosphoribosyltransferase 1

HPV: Human papillomavirus

HSC: Hematopoietic stem cells

HSV-1: Herpes simplex virus type-1

hTERT: Human telomerase reverse transcriptase (TERT)

ICP-OES: Inductively coupled plasma optical emission spectrometry

IL-1β: Interleukin 1β

IL6: Interleukin 6

IL8: Interleukin 8

iMSC: Immortalized MSC

IO: Intramembranous ossification

ION: Iron oxide nanoparticle

K: Kelvin

LB: Luria-Bertani medium

LBA: LB broth with 100 μg/mL ampicillin

LPL: Lipoprotein lipase

LPMCs: Lamina propria mononuclear cells

MDM2: MDM2 proto-oncogene

min: Minute

mL: Millilitre

mM: Millimolar

MSCs: Mesenchymal stromal cells

ng: Nanogram

PAA: Polyacrylic acid

PBMCs: Peripheral blood mononuclear cells

PBS: Phosphate-buffered saline

PCNA: Proliferating cell nuclear antigen

PDs: Population doublings

PEG: Polyethylene glycol

PEMF: Pulsed electromagnetic field

PGA: Polyglycolic acid

PLA: Polylactic acid

PLC: Poly caprolactone

PPIA: Peptidylprolyl isomerase A

p14/ARF: Cyclin-dependent kinase inhibitor, 2A isoform p14ARF

p16: Cyclin-dependent kinase inhibitor 2A, isoform p16INK4a

p21: Rac family small GTPase 1

p53: Tumor protein p53

OA: Osteoarthritis

OCN: Bone gamma-carboxyglutamate protein (Osteocalcin)

OCT4B1: Homo sapiens POU class 5 homeobox 1 (POU5F1), transcript variant 4

OD: Optical density

OI: Osteogenic induction

OP: Osteoporosis

OPCs: Osteoprogenitor cells

qPCR: Quantitative real-time polymerase chain reaction

RAS: HRas proto-oncogene, GTPase

Rb: RB transcriptional co-repressor 1

REL: Relative expression level

RMF: Rotating magnetic field

RNA: Ribonucleic acid

RNA18S: RNA 18S ribosomal N1

ROS: Reactive oxygen species

RT: Room temperature

Runx2: Runt-related transcription factor 2

s: Second

SA-ß-Gal: Senescence-associated ß-galactosidase

SMF: Static magnetic field

Sox9: SRY-box transcription factor 9

Sp7: Sp7 transcription factor (Osterix)

SQUID: Superconducting quantum interference device

SV40LT: Simian virus 40 large T antigen

T: Tesla

TBP: TATA-binding protein

TERC: Telomerase RNA component

TERT: Telomerase reverse transcriptase

TGF-β3: Transforming growth factor β-3

T-MSC: SV40LT-transduced MSC

TUBB: Beta-tubulin

UBC: Ubiquitin C

UV: Ultraviolet

VPA: Valproic acid

YWHAZ: Tyrosine 3-monooxygenase/ tryptophan 5-monooxygenase activation protein zeta

5%FBS/DMEM: DMEM with 5%FBS and 1% P/S

10%FBS/DMEM: DMEM with 10%FBS and 1% P/S

20%FBS/DMEM: DMEM with 20%FBS and 1% P/S

φNX-A: Phoenix amphotropic cells

µg: Microgram

×*g***:** Times gravity

°C: Degree Celsius

LIST OF FIGURES

LIST OF TABLES

RESUMO

A rexeneración do óso e da cartilaxe tras sufrir un traumatismo ou unha enfermidade dexenerativa segue sendo un gran desafío clínico. Debido á súa capacidade de auto-renovación e multi-diferenciación, as células mesenquimais estromais *(MSC)* son unha fonte celular moi prometedora para a rexeneración destes tecidos, pero a investigación neste campo está limitada pola tendencia das *MSC* á senescencia ao seren expandidas en cultivo. A inmortalización das *MSC* permítelles superar a senescencia, o que supón un impulso para os avances na investigación. Neste estudo desenvolveuse un método para inmortalizar *MSC* derivadas de doantes de idade avanzada mediante inoculación centrífuga de dous xenes de inmortalización: o antíxeno T grande do virus de simio 40 *(SV40LT)* e a transcriptase reversa da telomerase humana *(hTERT)*. As *MSC* inmortalizadas son fenotipicamente similares ás *MSC* primarias e son capaces de diferenciarse cara ás tres liñaxes esqueléticas, aínda que se inclinan cara á ruta de diferenciación osteoxénica. Os condrocitos articulares e os sinoviocitos pódense inmortalizar empregando o mesmo método, pero os condrocitos inmortalizados son metabolicamente diferentes dos condrocitos articulares primarios. Estas células poden ser útiles como parte de modelos *in vitro* de rexeneración dos tecidos articulares ou de enfermidade osteocondral.

RESUMEN

La regeneración del hueso y el cartílago tras sufrir un traumatismo o una enfermedad degenerativa continúa siendo un gran desafío clínico. Debido a su capacidad de auto-renovación y multi-diferenciación, las células mesenquimales estromales *(MSC)* son una fuente celular prometedora para la regeneración de estos tejidos, pero la investigación en este campo se ve limitada por la tendencia de las *MSC* a la senescencia en cultivo. La inmortalización de las *MSC* les permite superar la senescencia, impulsando así los avances en la investigación. En este estudio, se ha desarrollado un método para inmortalizar *MSC* derivadas de donantes de edad avanzada mediante inoculación centrífuga de dos genes de inmortalización: el antígeno T grande del virus de simio 40 *(SV40LT)* y la transcriptasa reversa de la telomerasa humana *(hTERT)*. Las *MSC* inmortalizadas son fenotípicamente similares a las *MSC* primarias y son capaces de diferenciarse hacia los tres linajes esqueléticos, aunque tienen tendencia a seguir la ruta de diferenciación osteogénica. Los condrocitos articulares y los sinoviocitos se pueden inmortalizar utilizando el mismo método, pero los condrocitos inmortalizados son metabólicamente diferentes de los condrocitos articulares primarios. Estas células pueden ser útiles como parte de modelos *in vitro* de regeneración de los tejidos articulares o de enfermedad osteocondral.

ABSTRACT

Regeneration of bone and cartilage after trauma or age-related degenerative diseases remains a major clinical challenge. Due to their self-renewal and multi-differentiation potential, mesenchymal stromal cells (MSCs) are a promising cell source for bone and cartilage regeneration, but research on this field is impaired by MSCs' predisposition to senescence when culture-expanded. Immortalization of MSCs allows them to bypass senescence, thus boosting the advances in MSC research. In this study, a method has been developed to immortalize MSCs derived from elderly donors by spinoculation of two immortalization genes: simian virus 40 large T antigen (SV40LT) and human telomerase reverse transcriptase (hTERT). Immortalized MSCs are phenotypically similar to primary MSCs and are able to differentiate to the three skeletal lineages, although their multi-differentiation potential is unbalanced towards the osteogenic pathway. Articular chondrocytes and synoviocytes can also be immortalized by the same method, but immortalized chondrocytes are metabolically different from primary articular chondrocytes. These immortalized cells can be useful as part of *in vitro* models of osteochondral regeneration and disease.

I. Introduction

1. Bone: composition, structure and function

Bone is a highly dynamic and vascularized tissue with the ability to remodel and regenerate itself after traumatic injury (Vas *et al.*, 2017). Just like other connective tissues, bone is made up of cells and their extracellular matrix (ECM). The bone ECM has an inorganic part, composed of calcium phosphate in the form of hydroxyapatite crystals, and an organic part, containing type I collagen, proteoglycans and proteins such as osteocalcin, osteonectin, osteopontin and bone sialoprotein (Iaquinta *et al.*, 2019). The inorganic part of the ECM confers hardness to the bones, while the organic part confers flexibility (Hart *et al.*, 2017).

There are three types of cells present in the bones that contribute to their homeostasis: osteoblasts, osteocytes and osteoclasts. Osteoblasts arise from pre-osteoblasts, also called osteoprogenitor cells (OPCs), which are derived from mesenchymal stromal cells (MSCs) from the bone marrow, and their functions are the deposition of the ECM and the regulation of osteoclasts activity. When they get embedded in their own ECM, osteoblasts differentiate into osteocytes, which participate in mechanotransduction and ECM calcification. Osteoclasts are derived from monocytes and take part in bone remodelling by secreting acids and proteolytic enzymes, which destroy the bone ECM, under the influence of certain cues. Osteocytes can recognize damaged bone areas and recruit osteoclasts to the remodelling site (Goonoo and Bhaw-Luximon, 2018) (**Figure 1**).

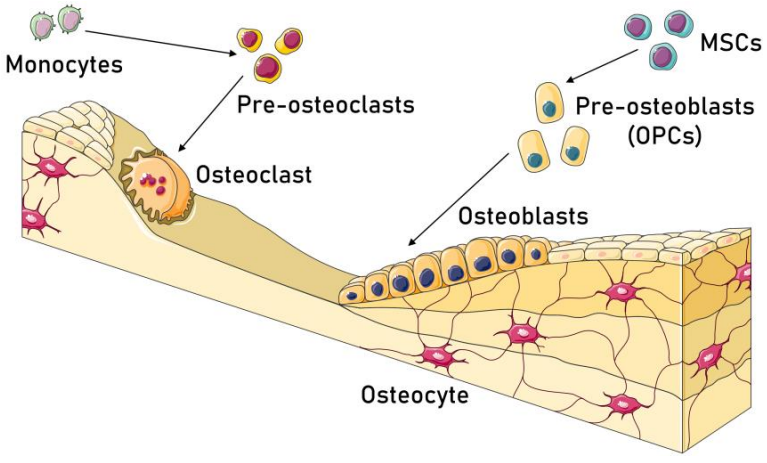

Figure 1. Cell types present in bone tissue. Osteoclasts are derived from monocytes and destroy the bone ECM. Osteoblasts are derived from OPCs, which derive from MSCs, and secrete the bone ECM. Osteocytes are osteoblasts that got embedded in their own ECM and participate in mechanotransduction. MSC: mesenchymal stromal cell; OPC: osteoprogenitor cell (pre-osteoblast). This figure was created using images from SMART Servier Medical Art (**smart.servier.com**).

In the human adult body, bone tissue has two structurally different forms: cortical bone and trabecular bone (Su *et al.*, 2019). Cortical bone has the highest density and is organized in osteons, each consisting of concentric layers of mineralized matrix with enclosed osteocytes, surrounding a central vascular canal. Cortical bone surrounds trabecular bone, whose structure is less homogeneous (**Figure 2**). Trabecular bone comprises a porous network that contains the red bone marrow, where haematopoiesis occurs (Paniagua *et al.*, 2007; Osterhoff *et al.*, 2016; Goonoo and Bhaw-Luximon, 2018; Iaquinta *et al.*, 2019).

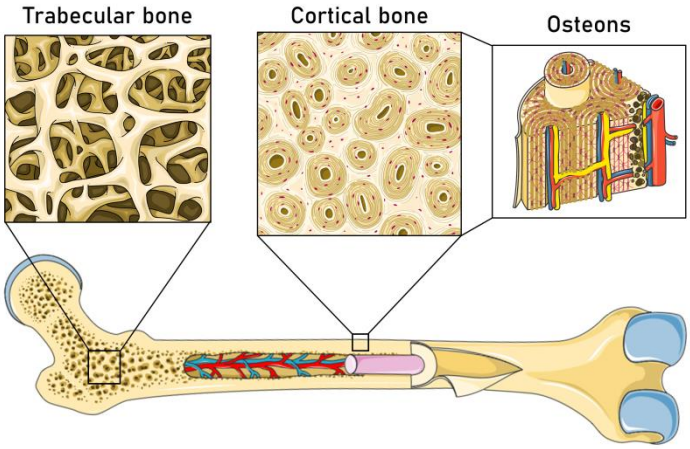

Figure 2. Types of bone tissue in the human adult body. Trabecular bone is more porous and less organized, while cortical bone is more dense and organized in osteons. Osteons consist of concentric layers of bone, with enclosed osteocytes, around a central vascular canal. This figure was created using images from SMART Servier Medical Art (**smart.servier.com**).

The main functions of the bones include providing mechanical support, protecting internal organs, supporting locomotion and being a reservoir of minerals, mainly calcium and phosphate. These functions depend on bone homeostasis, which is maintained by the coupling between osteoclast-mediated bone resorption and osteoblast-mediated bone formation. An imbalance in this mechanism results in different skeletal disorders (Iaquinta *et al.*, 2019; Su *et al.*, 2019).

2. Cartilage: composition, structure and function

Articular cartilage is a highly hydrated, avascular and aneural tissue that covers the articular surface of bones in synovial joints. Articular cartilage contains a hyaline ECM composed of water, type II collagen fibres, glycosaminoglycans and proteoglycans, mainly aggrecan. Chondrocytes are the only cell type present in cartilage and account for only 1–2% of the total cartilage volume. Their functions

are maintaining cartilage homeostasis and producing the ECM, which is responsible for the biomechanical properties of cartilage (Goldring and Goldring, 2016; Armiento *et al.*, 2018). These cells are derived from chondroblasts, which arise from MSC-derived chondroprogenitor cells (CPCs) (Heras and Gahunia, 2020).

Articular cartilage is anatomically organized in four zones: the superficial zone, transitional zone, the deep zone and the calcified layer (**Figure 3**).

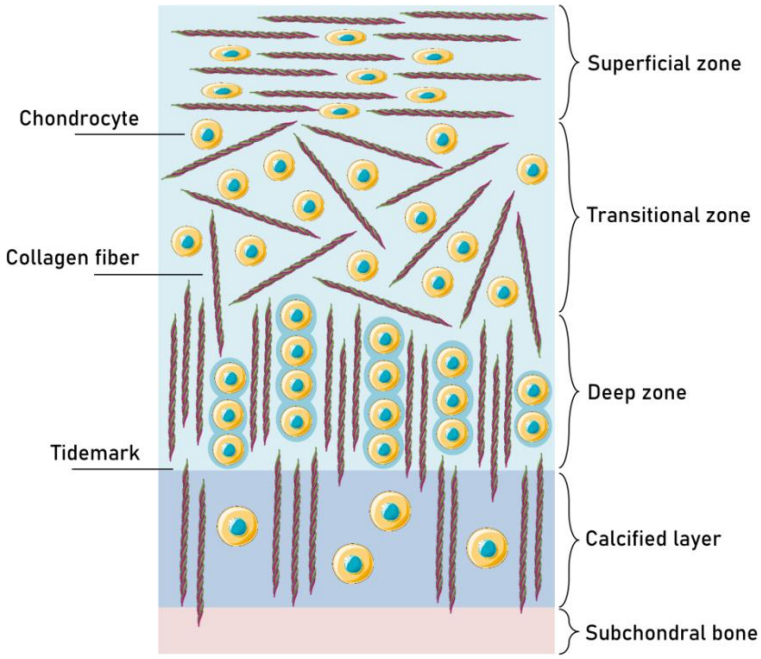

Figure 3. Layers found in articular cartilage, from the articular surface (top) to the subchondral bone (bottom). Chondrocyte morphology and collagen fibre alignment vary among layers. The tidemark separates the cartilage from the calcified layer and prevents vascularization of upper layers. This figure was created using images from SMART Servier Medical Art (**smart.servier.com**).

The superficial zone has the highest collagen and water content. In this zone, chondrocytes show a flat morphology and collagen fibres are aligned parallel to the joint surface. The transitional zone has less collagen and water than the superficial layer and is composed of spheroidal chondrocytes immersed in an ECM with obliquely-organized collagen fibres and high proteoglycan content. The deep zone has the lowest water content and the highest proteoglycan content. In this zone, collagen fibres are aligned perpendicular to the joint surface and chondrocytes are arranged in columnar orientation and surrounded by a collagen VI-rich pericellular matrix, forming the chondrons. Finally, the calcified layer is located above the subchondral bone and below the tidemark, which inhibits vascular penetration of

the upper zones. The calcified cartilage layer has very sparse, hypertrophied chondrocytes. It anchors the collagen fibres of the deep zone to subchondral bone, thus securing the cartilage to the bone (Fox, Bedi and Rodeo, 2009; Liu *et al.*, 2017; Baumann *et al.*, 2019).

In the joints, articular cartilage distributes the load between the adjoining bones and, in combination with synovial fluid, reduces friction (Armiento *et al.*, 2018; Baumann *et al.*, 2019). Due to its load-bearing function, articular cartilage is susceptible to damage during sports activities and wears over time (W. Zhang *et al.*, 2016). Given its lack of vascularization, its low cellularity and the thickness of its ECM, the self-repair capacity of articular cartilage is very limited. Cartilage defects derived from trauma may progress to further deterioration, causing joint pain and disability (Jeon and Elisseeff, 2016; Le *et al.*, 2020).

3. Bone and cartilage diseases

Defects in bone and cartilage caused by trauma or degenerative diseases are common clinical conditions that significantly affect the quality of life of the patients (Lu *et al.*, 2019). Due to the increase in life expectancy of the population, the incidence of bone and cartilage diseases such as osteoporosis (OP) and rheumatic diseases, including osteoarthritis (OA), is rapidly rising (Roseti *et al.*, 2017).

OP is the most common bone disease. This pathology is characterized by bone mass and density loss and, consequently, increased bone fragility and fracture risk (Phetfong *et al.*, 2016; Chang *et al.*, 2018). Despite the bone's ability to repair itself, 5–10% of fractures show either delayed healing or complete failure to adequately heal, and the development of new treatments to improve bone healing is therefore necessary (Stewart *et al.*, 2015). In addition, prolonged pharmacological OP treatment causes serious side effects; thus, cell therapy is emerging as an alternative treatment. Due to their ability to regenerate bone, MSCs are a promising cell source for OP and fracture non-union treatments. However, much more research is needed to properly evaluate and standardize MSC-based techniques before their clinical application in bone regeneration (Phetfong *et al.*, 2016; Vas *et al.*, 2017; Marolt Presen *et al.*, 2019).

OA is the most common age-related joint disorder and affects both cartilage and bone. OA is characterized by chondrocyte stress and ECM degradation, processes

which are initiated by injuries that activate maladaptive repair responses, including pro-inflammatory pathways of innate immunity (Kraus *et al.*, 2015). These pro-inflammatory stimuli induce a homeostasis imbalance in the cartilage, with predominant catabolic activity. Pro-inflammatory cytokines such as interleukin 1β (IL-1β) are overexpressed in early osteoarthritic cartilage and stimulate the catabolic activities of synovial cells and chondrocytes. IL-1ß changes the expression of genes such as interleukin 6 (IL6), interleukin 8 (IL8) and prostaglandin E2, an enzymatic product of cyclooxigenase 2 (COX2), which represses ECM production and promotes cartilage degradation (Vaamonde-García *et al.*, 2012; Lv *et al.*, 2019). OA chondrocytes produce matrix-degrading enzymes, exacerbating the breakdown of the tissue, and these biomechanical and biochemical changes lead to joint space narrowing and loss of function of the joint. Conversely, the imbalance of bone homeostasis leads to predominant anabolic activity in which the bone becomes sclerotic. As OA progresses, bone spurs called osteophytes form at the margins of the joints, and inflammation of the synovial membrane leads to further degeneration of the tissues (W. Zhang *et al.*, 2016; Baumann *et al.*, 2019) (**Figure 4**).

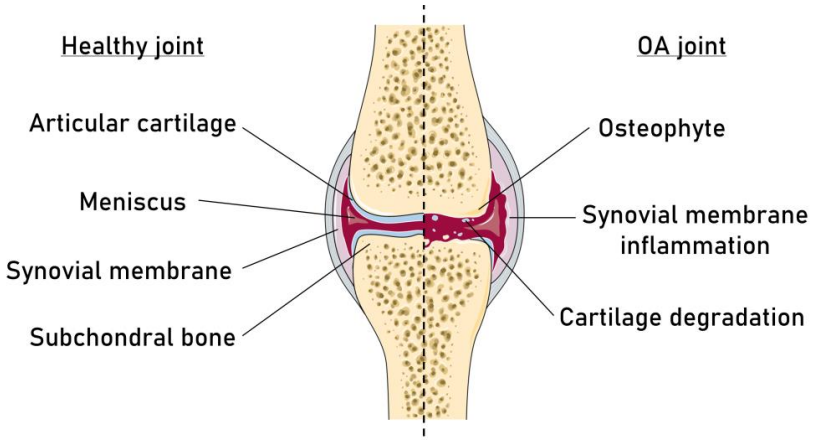

Figure 4. Schematic representation of a healthy joint and an OA joint. In OA, homeostasis imbalance leads to cartilage degradation. During disease progression, osteophytes are formed and inflammation of the synovial membrane contributes to the degradation of joint tissues. This figure was created using images from SMART Servier Medical Art (**smart.servier.com**).

Currently, there is no effective treatment for OA able to restore the physiological properties of the affected joints, and prosthetic replacement is necessary at the final clinical stage. Different cell treatments, based on autologous MSCs and chondrocytes, have been developed with the aim of forming a repair tissue with structural, biochemical and functional characteristics equivalent to those of native articular cartilage. In spite of these efforts, no technique has been able to

consistently regenerate hyaline articular cartilage in clinical trials yet (Piñeiro-Ramil *et al.*, 2018; Le *et al.*, 2020).

4. Mesenchymal stromal cells

Bone marrow-derived MSCs are self-renewing, multipotent progenitors of skeletal lineages. They give rise to osteoblasts during development and bone remodelling, generate adipocytes during growth and bone marrow remodelling, and also form cartilage under certain circumstances. *In vivo*, MSCs are located in bone marrow cavities, around the bone marrow sinusoids and the trabecular bone surface (Kouroupis *et al.*, 2018), where they establish and maintain the hematopoietic microenvironment necessary for the growth and maturation of hematopoietic stem cells (HSCs) (Bianco and Robey, 2015). *In vitro*, they have been defined as plastic-adherent, colony-forming cells that can differentiate into osteogenic, adipogenic and chondrogenic lineages after exposure to specific factors and express certain surface antigens while lacking expression of hematopoietic markers (Dominici *et al.*, 2006; Zhou *et al.*, 2014; Uder *et al.*, 2018) (**Figure 5**).

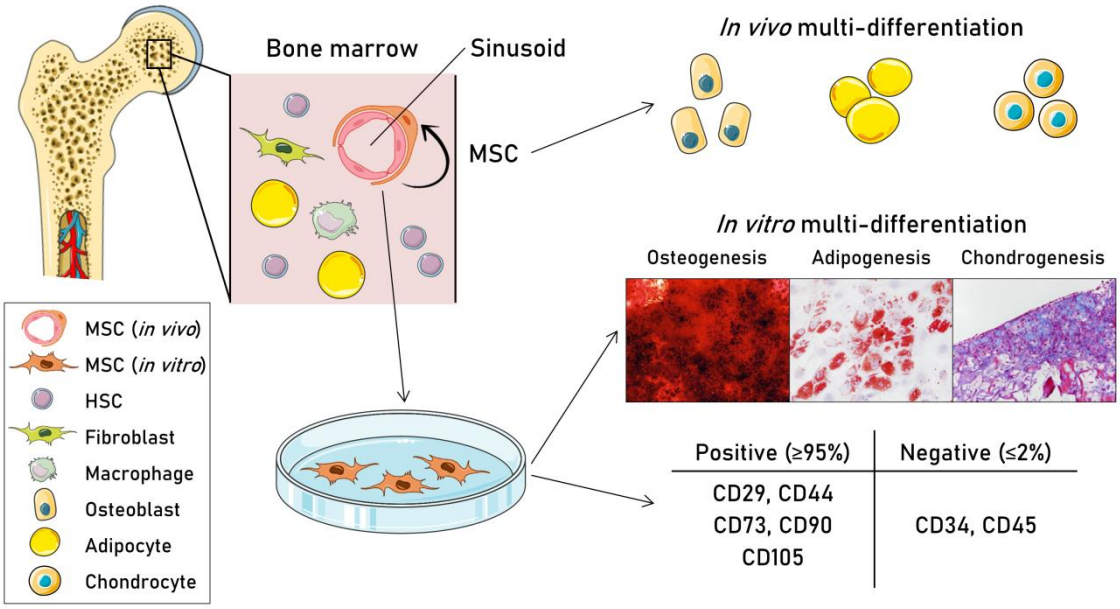

Figure 5. Schematic representation of the characteristics of MSCs. *In vivo*, MSCs are found in the bone marrow stroma around sinusoids and bone trabeculae and can give rise to osteoblasts, adipocytes and chondroblasts. *In vitro*, MSCs are identified by their adherence to plastic, their multi-differentiation ability and the expression of a set of cell surface markers. MSC: mesenchymal stromal cell; HSC: hematopoietic stem cell. This figure was created using images from SMART Servier Medical Art (smart.servier.com) and BioRender (biorender.com).

Nowadays, therapeutic options capable of restoring the physiological properties of bone and cartilage after trauma or degenerative diseases are still lacking (Grayson *et al.*, 2015; Tamaddon *et al.*, 2018), and regeneration of these tissues remains a major clinical challenge (Lu *et al.*, 2019). Due to their multipotency and self-renewal capacity, MSCs are a promising cell source for bone and cartilage regeneration (Samsonraj *et al.*, 2017; Szychlinska *et al.*, 2017; Zhou, Tsai and Li, 2017; Kouroupis *et al.*, 2018). However, this research field has a major limitation, which is that MSCs progressively lose their proliferation and multi-differentiation capacities when culture-expanded (Samsonraj *et al.*, 2017; Szychlinska *et al.*, 2017; Zhou, Tsai and Li, 2017; Yang *et al.*, 2018).

Human MSCs can achieve a maximum of 30–40 population doublings (PDs) *in vitro* before they lose their proliferation potential (Böcker *et al.*, 2008; Koch *et al.*, 2013; Bourgine *et al.*, 2014), and their proliferative and differentiation potential decrease with donor age (Baker, Boyette and Tuan, 2015; Szychlinska *et al.*, 2017; Knuth *et al.*, 2018). This means that research using MSCs derived from aged donors is hindered by both limited *in vitro* expansion and donor-related reduction of proliferation. For this reason, their potential for tissue regeneration in age-related bone and cartilage diseases has yet to be fully elucidated (Lunyak, Amaro-Ortiz and Gaur, 2017; Iaquinta *et al.*, 2019).

5. Cell senescence

The process by which cultured cells irreversibly lose their proliferation potential is known as cell senescence. Cell senescence is caused by telomere shortening or other types of cellular stress and results in the acquisition of a senescent phenotype, characterized by enlarged cytoplasm, increased lysosomal content and senescence-associated ß-galactosidase (SA-ß-Gal) activity. Telomere shortening and the resulting chromosomal instability cause the so-called replicative senescence, while other types of cellular stress, including DNA damage or oncogenic signals, cause stress-induced premature senescence. Senescent cells retain their metabolic activity and can remain viable *in vitro* for long periods of time (Carnero *et al.*, 2015; Lunyak, Amaro-Ortiz and Gaur, 2017; Schmeer *et al.*, 2019).

5.1 Stress-induced senescence

The initial *in vitro* growth arrest of human primary MSCs is presumed to be due to stress-induced senescence, which is regulated by p53 and Rb-related pathways. Both p53 and Rb proteins are regulated by post-translational modifications. In unstressed growing cells, p53 is ubiquitinated by the E3-ubiquitin ligase MDM2 and then degraded by the proteasome, while Rb is phosphorylated by cyclin-dependent kinases (CDKs). The phosphorylation of Rb promotes its disassociation from E2F and allows for the expression of E2F-dependent genes, which are necessary for cell division (Moll and Petrenko, 2003; Alberts *et al.*, 2008) (**Figure 6**).

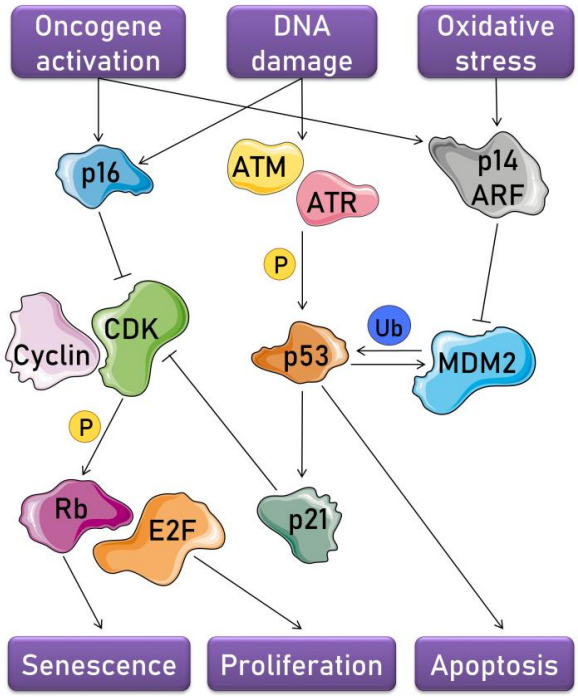

Figure 6. Senescence regulation by p53-p21 and p16-Rb pathways. Upon DNA damage, p53 is released from its binding to MDM2, promoting the transcription of p21 and the binding of Rb to E2F transcription factors, which prevents cell proliferation and promotes senescence. During oncogenic or oxidative stress, p14 prevents the ubiquitination of p53 by MDM2. This figure was created using images from SMART Servier Medical Art (**smart.servier.com**).

Cellular stressors such as DNA damage, oncogenic signals such as Ras proto-oncogene activation, and reactive oxygen species (ROS) promote senescence through the activation of several CDK inhibitors. DNA damage sensors ATM/ATR activate transcription factor p53 by phosphorylation, allowing for its release from MDM2. Phosphorylated p53 promotes the transcription of CDK inhibitor p21, which results in transient cell growth arrest. Oncogenic or oxidative stress stimulates

the production of p14/ARF, which also inhibits the ubiquitination of p53 by MDM2. If these stress/DNA damage situations are not resolved by the cell, p16 is activated, thus supressing Rb phosphorylation by inhibition of CDKs. Unphosphorylated Rb controls cell proliferation by binding and inhibiting E2F transcription factors, turning transient growth arrest into irreversible senescence (Alberts *et al.*, 2008; An, Sáenz Robles and Pipas, 2012; Ozono, Yamaoka and Ohtani, 2013; Lunyak, Amaro-Ortiz and Gaur, 2017; Bourgeois and Madl, 2018). A cell can resume proliferation after the activation of the p53-p21 pathway if p53 is inhibited; however, cells that senesce via the p16-Rb pathway are unable to re-enter the cell cycle, even after the inhibition of p53, Rb or p16 (Sultana *et al.*, 2018).

5.2 Replicative senescence

Telomeres are tandem repeats of a hexameric sequence, TTAGGG, which cap the end of chromosomes and protect them from fusion and degradation. In human adult cells, telomeres are shortened at each cell division because of the "DNA end-replication problem" (Schmidt and Cech, 2015; J. Zhang *et al.*, 2016). DNA polymerases can synthesize DNA only in a 5' to 3' direction and require an RNA primer, synthesized by the DNA primase, with an available 3' end. Since eukaryotic telomeres carry a 3' overhang, both the leading- and lagging-strand ends potentially face end-replication problems (Wellinger, 2014) (**Figure 7**).

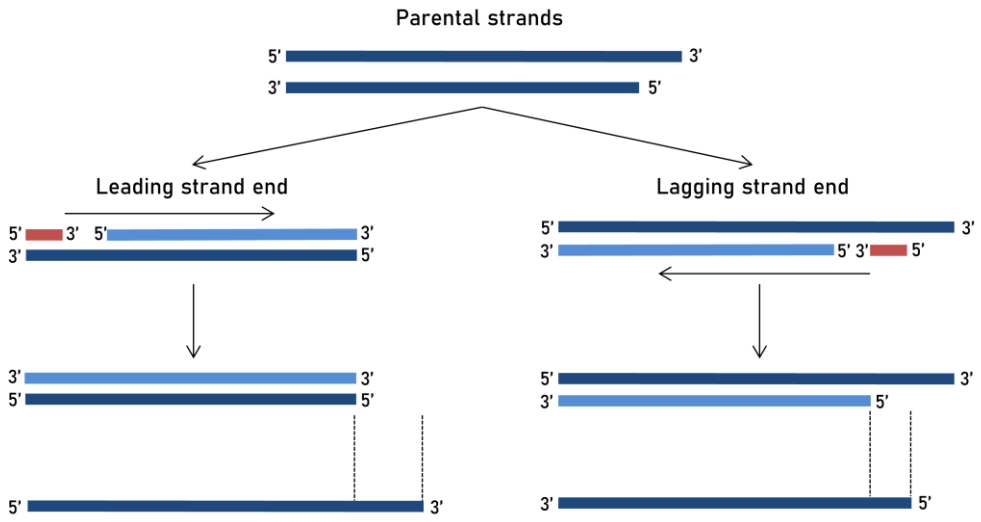

Figure 7. The "DNA end replication problem". Dark blue shows parental strands, light blue shows daughter strands and red shows RNA primers. Arrows show DNA synthesis direction (from 5' to 3'). Dashed vertical lines show how long the daughter strands would need to be to avoid sequence losses at the end of telomeres.

Progressive telomere erosion due to the proliferation of cells eventually triggers the DNA damage response through ATM/ATR, when telomeres are critically short. This induces the activation and stabilization of p53, p53-p21-mediated cell-cycle exit (**Figure 6**) and, finally, the senescence of the cell, since eroded telomeres cannot be repaired in the absence of telomerase, which is not expressed in somatic tissues (J. Zhang *et al.*, 2016; Lunyak, Amaro-Ortiz and Gaur, 2017; Leão *et al.*, 2018). Telomere shortening may also induce p21 expression in a p53-independent manner (Chen *et al.*, 2017) and Rb-independent repression of E2F transcription factors, mediated by p21 and other CDK inhibitors (Moiseeva *et al.*, 2015).

During *in vitro* culture, the same processes that promote senescence *in vivo* take place: due to the propagation of the cells, telomeres are shortened, DNA damage is accumulated and other types of cell stress are produced (Wagner *et al.*, 2009; Medeiros Tavares Marques *et al.*, 2017). As a result of *in vitro* aging, MSCs display telomere shortening, decline of their growth rate and colony forming capacity, and changes in their differentiation potential from osteogenic to adipogenic (Honoki and Tsujiuchi, 2013), termed "adipogenic switch" (Ok, Song and Hwang, 2018). The predisposition of aged MSCs to senesce *in vitro* may be overcome by immortalization, which can be achieved by transduction of certain genes.

6. Cell immortalization

Immortalization is the process by which cells acquire an unlimited proliferation potential through the bypass of senescence (Carnero *et al.*, 2015). Since the main regulators of senescence are proteins p53 and Rb (**Figure 6**), it is necessary to interfere with their pathways in order to avoid senescence. A number of viral genes, such as simian virus 40 large T antigen (SV40LT) and human papillomavirus (HPV) E6/E7, have been used for this purpose.

6.1 Immortalization genes

Simian virus 40 large T antigen

The simian virus 40 is a polyomavirus, a family of non-enveloped virus with circular double-stranded DNA. Polyomaviruses produce two common early proteins, large T antigen and small t antigen. These viruses interfere with the regulation of the cell cycle and induce transformation *in vivo* and *in vitro* mainly by the action of large T

antigen. Simian virus 40 has been used as a model for polyomavirus infection, since it is easier to replicate in cell culture than human polyomaviruses and its T antigen (SV40LT) is very well characterized (An, Sáenz Robles and Pipas, 2012; An, Brodsky and Pipas, 2015).

SV40LT induces a DNA damage response, leading to the up-regulation of the enzymes involved in DNA replication and repair, but it also binds p53, preventing the expression of p53-dependent genes and thus cell cycle arrest and apoptosis. Rb proteins are also bound and inactivated by SV40LT, which allows for the expression of E2F-dependent genes and induces the resumption of cell proliferation (An, Sáenz Robles and Pipas, 2012; Rotondo *et al.*, 2019).

Because of these characteristics, SV40LT has been widely used for immortalizing various cell types, including bone marrow-derived MSCs (Harigaya and Handa, 1985; Thalmeier *et al.*, 1994; Lee *et al.*, 2015), OPCs from dental follicle (Wu *et al.*, 2015), periosteum (Alexander *et al.*, 2015) and coronal sutures (Song *et al.*, 2017), and CPCs from osteoarthritic cartilage (Jayasuriya *et al.*, 2018). SV40LT expression increases the lifespan of MSCs and raises their proliferation rate, but even SV40LT-transduced cells may eventually senesce. Lee *et al.* (2015) reported that SV40LT-transduced MSCs decreased its growth rate and senesced after more than 80 passages, indicating that this antigen is not enough for complete immortalization of MSCs.

HPV E6/E7 proteins work similarly to SV40LT, inhibiting p53 and Rb functions to avoid growth arrest (Pal and Kundu, 2020). HPV E6/E7 genes have also been used to immortalize bone marrow-derived MSCs (Hung *et al.*, 2004; Mori *et al.*, 2005), and E6/E7-transduced MSCs have also been reported to senesce after 70 PDs, suggesting a limited effect of E6/E7 in prolonging lifespan (Mori *et al.*, 2005).

This eventual growth arrest could be caused by telomere shortening, since neither SV40LT nor E6/E7 proteins can promote telomere replication. However, the chromosomal instability resulting from telomere shortening, together with p53 inhibition, increases the mutability of the genome. In this situation, a mutation that triggers telomerase re-expression may arise (Carnero *et al.*, 2015) and confer an unlimited proliferation potential to the cells.

Telomerase reverse transcriptase

Telomerase is a ribonucleoprotein complex consisting of a catalytic subunit with reverse transcriptase activity (TERT) and a RNA component (TERC), which serves as a template for the synthesis of telomeric repeats (J. Zhang *et al.*, 2016). The single-stranded 3' overhang of the telomeres is the region where the RNA component (TERC) anneals, and nucleotides are added to the 3' end of DNA until the 5' end of the template is reached. Telomerase is then repositioned at the new 3' end of the chromosome and continues synthesizing additional repeats (Schmidt and Cech, 2015; Heidenreich and Kumar, 2017). Finally, DNA polymerase, with the help of DNA primase, synthesizes the complementary strand (**Figure 8**).

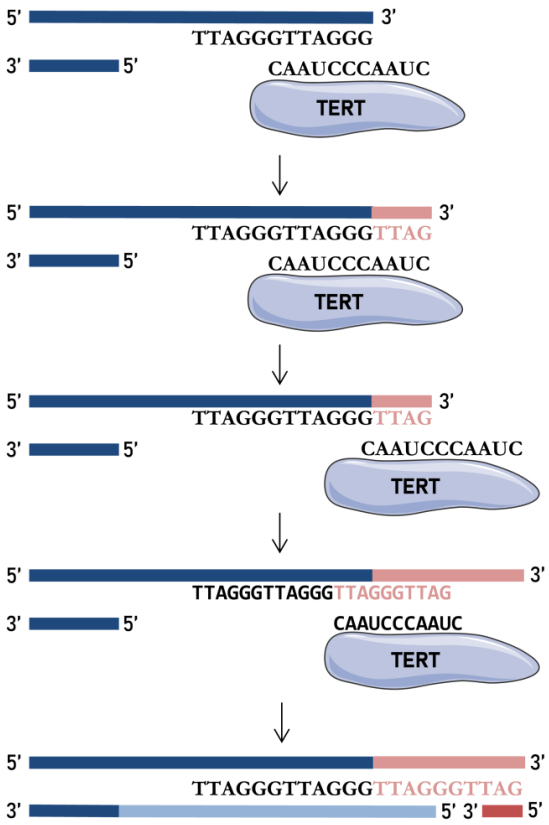

Figure 8. Replication of telomeres by telomerase. Dark blue shows parental and daughter strands, light red shows newly synthetized DNA by telomerase, light blue shows newly synthetized DNA by DNA polymerase and red shows RNA primer.

The level of expression of human TERT (hTER T) in adult stem cells is very low and insufficient to counteract telomere attrition over time (J. Zhang *et al.*, 2016; Heidenreich and Kumar, 2017). Human primary MSCs undergo progressive

telomere shortening during *in vitro* expansion and, if hTERT expression is not up-regulated, telomeres shorten until a critical threshold at which cells enter senescence. Transduction of hTERT has been employed to generate MSC lines but, since hTERT cannot prevent stress-induced senescence, it has also failed to immortalize bone marrow-derived MSCs (Okamoto *et al.*, 2002; Takeda *et al.*, 2004; Mori *et al.*, 2005; Koch *et al.*, 2013; Dale *et al.*, 2015) and adipose tissue-derived stem cells (ADSCs) (Balducci *et al.*, 2014).

For this reason, several authors have reported that hTERT-transduced MSCs display growth rates and lifespans similar to those of primary MSCs (Okamoto *et al.*, 2002; Skårn *et al.*, 2014; Duan and Chen, 2015). Okamoto *et al.* (2002) observed that p16 expression was up-regulated in hTERT-transduced MSCs throughout *in vitro* expansion, finally leading to senescence despite the maintenance of telomere length. However, hTERT transduction may be enough to immortalize bone marrow-derived MSCs from young and/or healthy donors (Simonsen *et al.*, 2002; Bourgine *et al.*, 2014; Skårn *et al.*, 2014), which are less prone to suffering stress-induced senescence.

Transduction of hTERT has also been employed in combination with E6/E7 (Okamoto *et al.*, 2002; Takeda *et al.*, 2004; Mori *et al.*, 2005; Funes *et al.*, 2007; Tsai *et al.*, 2010) or SV40LT (Koch *et al.*, 2013; Balducci *et al.*, 2014). This combination of genes led to an unlimited proliferation potential, which could not be obtained by the transduction of only one gene (Mori *et al.*, 2005; Balducci *et al.*, 2014). In the study by Balducci *et al.* (2014), the combination of hTERT with SV40LT was more efficient at improving the growth rate of ADSCs than the combination of hTERT and E6/E7, but both combinations of genes allowed cells to overcome senescence.

6.2 Immortalization methods

Immortalization of human primary cells is usually achieved by transduction with retroviral or lentiviral vectors. The main limitation of retroviral vectors is their inefficiency in infecting slowly dividing cells (Simmons and Alberola-Ila, 2016). This may be one of the reasons why many immortalized MSC lines have been generated from healthy and/or young donors (Bourgine *et al.*, 2014; Liu *et al.*, 2014; Skårn *et al.*, 2014), since the *in vitro* proliferation of aged and/or diseased donor-derived MSCs is usually impaired. Immortalized MSC lines could be useful as part of *in vitro* models for osteochondral regeneration and disease, and bone and cartilage diseases such as

OA and OP are far more common in the elderly population. In order to immortalize slowly dividing-MSCs derived from elder donors, strategies to enhance infection efficiency should be employed.

Spinoculation has been used for decades to improve viral infection of several types of cells *in vitro* (**Table 1**), although the process responsible for spinoculation-induced enhancement of infection has not been discovered yet (Yan *et al.*, 2015). However, spinoculation-induced enhancement of infection is known to depend on cell type (Introna *et al.*, 1998; Simmons and Alberola-Ila, 2016) and is also related to centrifugation speed (Yan *et al.*, 2015) in a cell type-dependent manner (Guo *et al.*, 2011). Therefore, spinoculation parameters must be optimized for each transduction system (virus and target cell type). Since spinoculation-induced enhancement of infection is also related to virus concentration, it is possible to increase it by prolonging post-transfection incubation of packaging cells before retrovirus harvesting (Steele *et al.*, 2014; Yan *et al.*, 2015; Anastasov *et al.*, 2016; Munisvaradass *et al.*, 2017). As virus half-life at 37°C is shorter than at 32°C, the efficiency of the process increases when packaging cells incubation and centrifugal infection are performed at 32°C (Kotani *et al.*, 1994; Aasen *et al.*, 2008; Raya *et al.*, 2010; Munisvaradass *et al.*, 2017).

Table 1. List of spinoculation experiments found in the literature, detailing target cell type, type of virus used, chemical adjuvants employed and spinoculation conditions. PBMCs: peripheral blood mononuclear cells; HSCs: hematopoietic stem cells; LPMCs: lamina propria mononuclear cells; CHO: Chinese hamster ovary; FCWF-4: *Felis catus* whole foetus cells; HIV: human immunodeficiency virus; HBV: hepatitis B virus; HCV: hepatitis C virus; HSV-1: herpes simplex virus type-1; FIPV: feline infectious peritonitis virus; HDMB: hexadimethrine bromide; PEG: polyethylene glycol; RT: room temperature. Modified from Piñeiro-Ramil *et al.* (2020).

Target cell type	Virus	Adjuvants	Spinoculation conditions	Reference
PBMCs	Lentivirus	10 μg/mL HDMB and 1000 μg/mL P338	800 ×*g* 90 min RT	Anastasov *et al.*, 2016
$CD3^+$ T cells	Lentivirus	8 μg/mL HDMB	800 ×*g* 90 min 32°C	Munisvaradass *et al.*, 2017
$CD4^+$ T cells	HIV	None	1200 ×*g* 120 min RT	Kohler *et al.*, 2016
HSCs and immune cells	Retrovirus or lentivirus	5 μg/mL HDMB	460 ×*g* 60-90 min RT	Simmons and Alberola-Ila, 2016

Target cell type	Virus	Adjuvants	Spinoculation conditions	Reference
PBMCs	HIV	None	1200 ×*g* 120 min 30°C	Sampah *et al.*, 2015
HepG2 cell line (hepatocellular carcinoma)	HBV	4% PEG-8000	1000 ×*g* 60 min RT	Yan *et al.*, 2015
LPMCs	HIV	None	1200 ×*g* 120 min RT	Steele *et al.*, 2014
$CD4^+$ T cells	HIV	None	300-1200 ×*g* 2 hours RT	Guo *et al.*, 2011
Keratinocytes and fibroblasts	Retrovirus	1-5 μg/mL HDMB	750 ×*g* 45 min 32°C	Aasen *et al.*, 2008; Raya *et al.*, 2010
Huh7.5.1 cell line (hepatocellular carcinoma)	HCV	None	500-1000 ×*g* 30-120 min RT	Ye *et al.*, 2008
CHO cell lines (epithelial)	HSV-1	None	1200 ×*g* 120 min 37°C	Scanlan *et al.*, 2005
HSCs	Retrovirus	0.8 μg/mL HDMB	300 ×*g* 45 min RT	Introna *et al.*, 1998
FCWF-4 (macrophages)	FIPV	None	400 ×*g* 0-180 min RT	Hohdatsu, Tatekawa and Koyama, 1995
HUT-78 cell line (T cells)	Retrovirus	8 μg/mL HDMB	1600 ×*g* 90 min 32°C	Kotani *et al.*, 1994

For greater enhancement of infection, chemical adjuvants for transduction and inductors of transgene expression can be used. Hexadimethrine bromide (HDMB, also known as Polybrene) is the most common adjuvant for retroviral infection, but it should be used over short application times and at low concentrations due to its high cellular toxicity (Lin *et al.*, 2012; Anastasov *et al.*, 2016). The combination of HDMB and spinoculation may have a synergistic effect in enhancing infection (Stranford *et al.*, 2017), but centrifugation-induced stress produced during spinoculation could increase cell susceptibility to HDMB toxicity (Lin *et al.*, 2012).

The histone deacetylase inhibitor valproic acid (VPA, 2-propyl-valeric acid) could be used to induce transgene expression (Cervera *et al.*, 2015; Fang *et al.*, 2017). VPA not only prevents the transcriptional silencing of genes (Wulhfard *et al.*, 2010), but also reduces cell proliferation (Wulhfard *et al.*, 2010; Jäger *et al.*, 2013), and could exert a negative (Wulhfard *et al.*, 2010) or positive effect on cell viability, depending on concentration and cell type (Jäger *et al.*, 2013; Cervera *et al.*, 2015). Thus, its

concentration needs to be adjusted for each transduction system in order to enhance transgene expression without affecting cell viability and proliferation.

7. Features of immortalized mesenchymal cell lines

After transduction with immortalization genes, it is necessary to check whether the expression of immortalization genes allows transduced cells to bypass senescence. Once an immortalized MSC line has been generated, it is essential to characterize it and verify that immortalized cells retain the characteristics of primary parental cells: multi-differentiation potential (into osteoblasts, chondrocytes and adipocytes) and expression of mesenchymal surface markers. It is also important to investigate if immortalization has led to the acquisition of oncogenic potential.

7.1 Multi-differentiation potential

Osteogenic potential

Osteogenic potential is the ability of MSCs and OPCs to generate bone tissue. *In vivo*, MSCs participate in bone formation during growth and fracture healing through intramembranous ossification (IO) or endochondral ossification (EO). In IO, MSCs differentiate into osteoblasts, which deposit the bone ECM. In contrast, during EO, MSCs first differentiate into chondrocytes and form a cartilage template that is gradually replaced by new bone synthesized by osteoblasts (Su *et al.*, 2018). *In vitro*, MSCs are able to differentiate into osteoblasts and deposit a mineralized extracellular matrix after exposure to osteogenic stimuli (Mohamed-Ahmed *et al.*, 2018). Runt-related transcription factor 2 (Runx2) and osterix (Sp7) are the key transcription factors that promote osteogenic differentiation of MSCs (Hu *et al.*, 2018). Osteogenesis is the default differentiation pathway for MSCs (Bourgine *et al.*, 2014; Somoza *et al.*, 2014) and the most commonly retained differentiation lineage at later passages.

After immortalization, MSCs are still able to form bone *in vitro*, as shown by standard histochemical stainings (Alizarin Red, Von Kossa and Alkaline Phosphatase) and osteogenesis-related gene expression analysis (Skårn *et al.*, 2014; James *et al.*, 2015; Liu *et al.*, 2015; Harkness *et al.*, 2016; Liang *et al.*, 2016; Sugimoto *et al.*, 2017; Leber *et al.*, 2017; Abarrategi *et al.*, 2018; Blaschke *et al.*, 2018; Kusuyama *et al.*, 2018; Sreekumar *et al.*, 2018). Importantly, immortalized MSCs retain the ability

to form bone *in vivo* (Simonsen *et al.*, 2002; Larsen *et al.*, 2009; Bourgine *et al.*, 2014), one of the fundamental characteristics of an MSC (Bianco and Robey, 2015).

When compared with the primary MSCs from which they were derived, several immortalized MSC lines showed greater *in vitro* osteogenic potential (Böcker *et al.*, 2008; Lee *et al.*, 2015). The osteogenic potential of immortalized OPCs from the periosteum was also increased in comparison with primary cells (Alexander *et al.*, 2015), as was the osteogenic potential of immortalized ADSCs (Balducci *et al.*, 2014). Conversely, non-immortalized hTERT-transduced MSCs and ADSCs showed a reduction in their osteogenic potential (Balducci *et al.*, 2014; Dale *et al.*, 2015) similar to the loss of differentiation potential observed in culture-expanded primary MSCs.

Chondrogenic potential

Chondrogenic potential is the capacity of MSCs and CPCs to form cartilage. *In vivo*, bone marrow MSCs form cartilage during endochondral processes, such as bone formation and fracture healing. However, MSC-derived cartilage differs from articular cartilage in terms of structure, chemical composition and function. *In vitro*, MSCs can form cartilage-like tissue in aggregate culture after exposure to chondrogenic stimuli, but chondrogenically-induced MSCs tend to acquire a hypertrophic phenotype (Somoza *et al.*, 2014). If suitable scaffolds, growth factors and culture conditions are employed, chondrogenically-induced MSCs overexpress chondrogenesis-related genes such as SRY-box transcription factor 9 (Sox9), type II collagen and aggrecan, but also express high amounts of type X collagen (Sanjurjo-Rodríguez *et al.*, 2014; Stölzel *et al.*, 2015; Neybecker *et al.*, 2020).

Overall, the chondrogenic potential of immortalized MSCs is similar to or lower than that of their primary parental MSCs (Okamoto *et al.*, 2002; Bourgine *et al.*, 2014; Dale *et al.*, 2015; Armbruster *et al.*, 2017). Although Sox9 and type II collagen up-regulation have been detected in chondrogenically-induced immortalized MSCs, these cells showed the same predisposition to hypertrophy as primary MSCs, with type X collagen expression (Bourgine *et al.*, 2014; Armbruster *et al.*, 2017) and low quality-cartilage production (Nürnberger *et al.*, 2019; Piñeiro-Ramil *et al.*, 2019). However, immortalized MSCs with low chondrogenic potential are able to stimulate the differentiation of co-cultured chondrocytes (Skårn *et al.*, 2014) in the same way as primary MSCs (de Windt *et al.*, 2014).

Unlike bone marrow-derived MSCs, CPCs from articular cartilage produce a predominantly hyaline extracellular matrix (Williams *et al.*, 2010; Fellows *et al.*, 2017). CPCs from the articular cartilage of the knee were found to retain their chondrogenic potential after immortalization with either SV40LT (Jayasuriya *et al.*, 2018) or hTERT (Koelling *et al.*, 2009). Immortalized CPCs are able to undergo spontaneous chondrogenesis in 3D culture (Koelling *et al.*, 2009) and up-regulate the expression of Sox9, type II collagen and aggrecan when cultured in chondrogenic medium. However, immortalized CPCs derived from OA cartilage also up-regulate the expression of type X collagen and increase the release of matrix-degrading enzymes upon chondrogenic induction (Jayasuriya *et al.*, 2018).

Adipogenic potential

Adipogenic potential is the ability of MSCs to differentiate into adipocytes. *In vivo*, MSCs are the progenitors of bone marrow adipocytes (Bianco, 2014). *In vitro*, when MSCs are cultured under adipogenic stimuli, lipid vesicles are formed in their cytoplasm (Mohamed-Ahmed *et al.*, 2018). There is an inverse relationship between osteogenesis and adipogenesis (Bianco, 2014). During OP, the capacity of MSCs to differentiate into osteoblasts is reduced and their ability to differentiate into adipocytes is increased, a phenomenon known as "adipogenic switch" (Hu *et al.*, 2018) that is also observed during *in vitro* aging of MSCs (Ok, Song and Hwang, 2018).

Immortalized bone marrow-derived MSCs usually maintain their adipogenic potential, as shown by Oil Red O staining and up-regulation of adipogenesis-related genes such as adiponectin (APN), fatty acid-binding protein 4 (FABP4) and lipoprotein lipase (LPL) (Ali *et al.*, 2016; Harkness *et al.*, 2016; Galarza Torre *et al.*, 2018; Fayyad *et al.*, 2019). Immortalized dental follicle-derived OPCs (Wu *et al.*, 2015) and articular cartilage-derived CPCs (Koelling *et al.*, 2009; Jayasuriya *et al.*, 2018) are able to differentiate into adipocytes *in vitro* as well. However, the adipogenic potential of MSCs may be reduced after immortalization (Funes *et al.*, 2007; Dale *et al.*, 2015; James *et al.*, 2015). In immortalized MSC line 3A6, adipogenic potential was reduced and osteogenic potential was increased in comparison with its parental E6/E7-transduced cell line (Tsai *et al.*, 2010).

It has been described that multipotent cells from adult tissues have tissue-specific differentiation potential: while MSCs have higher osteogenic potential, ADSCs

possess higher adipogenic capacity (Mohamed-Ahmed *et al.*, 2018). In the same way, whereas immortalized MSCs and OPCs may show greater osteogenic potential (Böcker *et al.*, 2008; Alexander *et al.*, 2015; Lee *et al.*, 2015) and lower adipogenic potential (Funes *et al.*, 2007; Dale *et al.*, 2015; James *et al.*, 2015) than their primary parental cells, immortalized ADSCs may increase their adipogenic potential after immortalization (Wolbank *et al.*, 2009). Yet again, non-immortalized hTERT-transduced ADSCs have lower adipogenic potential than their primary parental cells (Balducci *et al.*, 2014).

7.2 Surface marker expression

In 2006, the International Society for Cell Therapy proposed a set of cell surface markers to identify human MSCs, including the expression of CD73, CD90 and CD105, and the lack of expression of hematopoietic markers (CD34 and CD45) (Dominici *et al.*, 2006). Since then, the list of surface antigens detected on MSCs has grown enormously. In addition to the surface markers from the classic set, proteins CD29 and CD44 are also expressed by MSCs from all species (Uder *et al.*, 2018). CD29 (human integrin β1) is involved in MSC migration *in vivo* (Ode *et al.*, 2011); CD44 (homing cellular adhesion molecule or HCAM) is a receptor for hyaluronic acid and acts as a co-receptor for other molecules (Mellor *et al.*, 2013); CD73 (ecto-5'-nucleotidase or NT5E) and CD90 (thymocyte differentiation antigen 1 or Thy-1) participate in transduction pathways of the immune system, as well as in cell-cell and cell-matrix interactions; and CD105 (endoglin) is a co-receptor of TGF-β and participates in the modulation of the response to this molecule (Ode *et al.*, 2011).

Nevertheless, none of the surface markers proposed by the International Society for Cell Therapy is specific for MSCs, and their expression is not clearly related to their multi-differentiation potential either (Cleary *et al.*, 2016; Uder *et al.*, 2018). Since MSCs are heterogeneous populations, the level of expression of these proteins may change due to passaging and may also vary among different culture conditions (Duan and Chen, 2015; Uder *et al.*, 2018), and thus their expression in primary cells does not guarantee that they will be expressed by immortalized cells. For instance, CD105 expression has been found to be reduced in bone marrow-derived MSCs (Abarrategi *et al.*, 2018), periosteum-derived OPCs (Alexander *et al.*, 2015) and ADSCs (Balducci *et al.*, 2014) after immortalization.

7.3 Oncogenic potential

As a result of immortalization gene transduction, cells may acquire an infinite life span at the expense of increasing genetic instability. This genetic instability may eventually lead to aberrant growth control (loss of contact inhibition and anchorage dependence) and malignancy (Freshney, 2005). MSCs have been described to be resistant to malignant transformation (Abarrategi *et al.*, 2018; Caplan *et al.*, 2019) and are able to obtain an unlimited proliferation potential without aberrant growth control or oncogenic features (Okamoto *et al.*, 2002; Simonsen *et al.*, 2002; Böcker *et al.*, 2008; Abarrategi *et al.*, 2018).

Immortalized MSCs transduced with E6/E7 and hTERT genes have shown to be non-tumorigenic unless transduced with an additional proto-oncogene (Abarrategi *et al.*, 2018). However, oncogenic mutations could arise during passaging (Burns *et al.*, 2017). In this regard, culture conditions are important, since immortalized MSCs seeded at low densities during long periods of time could become tumorigenic (Abdallah *et al.*, 2005; Takeuchi *et al.*, 2015). Low-density seeding provides an advantage for clones with oncogenic mutations, which display higher growth rates: the lower the density seeding, the faster the accumulation of these oncogenic clones in the population. Importantly, after undergoing oncogenic transformation, immortalized MSCs experience changes in their phenotype and their multi-differentiation potential (Abarrategi *et al.*, 2018).

8. Tissue engineering for osteochondral regeneration

Bone and cartilage conditions can be chronic, such as OA and OP; acute, such as trauma; or result from other conditions, such as cancer or infection. These conditions, as well as their surgical treatments, often lead to clinically relevant loss of tissue (Smith and Grande, 2015). Bone and cartilage defects and diseases are the leading causes of disability among elderly patients, and their incidence is expected to rise along with the median age of the population (Bomer *et al.*, 2015; Akter and Ibanez, 2016; W. Zhang *et al.*, 2016; Piñeiro-Ramil *et al.*, 2018).

Tissue engineering is an interdisciplinary science which applies the principles of engineering and life sciences towards the development of biological substitutes able to regenerate tissues and restore their function (Caddeo, Boffito and Sartori, 2017). Tissue engineering techniques require three elements: first, a scaffold to provide

structure for tissue growth; second, cells to produce the desired tissue; and finally, physical or chemical cues that drive cell proliferation and differentiation. Scaffolds for the regeneration of bone and articular cartilage have been extensively investigated, but there is still no consensus on the best material, cell source or technique for osteochondral regeneration (Smith and Grande, 2015). Although many efforts have been made, very few tissue engineering techniques have been translated into clinical practice, and the ideal scaffold for engineering bone and cartilage substitutes has not yet been developed (Grayson *et al.*, 2015; Deng *et al.*, 2018; Ghassemi *et al.*, 2018; Piñeiro-Ramil *et al.*, 2018; Lu *et al.*, 2019).

8.1 Bone tissue engineering

The development of bone substitutes is necessary to counteract its loss in various circumstances, such as bone diseases, fracture non-unions, congenital bone malformations and tumour resections (Akter and Ibanez, 2016). Autologous bone grafting is the clinical gold standard for bone restoration because of its osteoinductive and osteoconductive properties and its histocompatibility. However, this technique implies invasive bone collection from healthy sites, which limits the amount of donor tissue (Jeon and Elisseeff, 2016; Ng *et al.*, 2017; Iaquinta *et al.*, 2019). Allografts and xenografts have drawbacks as well, including donor scarcity, disease transmission risk and adverse immune reactions. For these reasons, bone tissue engineering has emerged as an alternative therapeutic strategy to promote bone regeneration (Ng *et al.*, 2017; Iaquinta *et al.*, 2019).

Despite the potential of tissue engineering for bone regeneration, efficacy of the current available methods is still far from optimal and needs to be improved (Goonoo and Bhaw-Luximon, 2018). Bone tissue engineering requires porous scaffolds that provide mechanical support, are able to integrate with the surrounding bone and promote vascularization. Both biological polymers, such as collagen and hyaluronic acid, and synthetic polymers, such as polylactic acid (PLA), polyglycolic acid (PGA) and poly caprolactone (PLC), have been used as scaffolds for bone tissue engineering (Akter and Ibanez, 2016; Ng *et al.*, 2017; Vas *et al.*, 2017). Type I collagen is the main component of the organic part of bone ECM and has become the preferred scaffold for bone regeneration applications. Its advantages include high biocompatibility, low immunogenicity and presence of several cell-binding sequences involved in integrin-mediated cell attachment (Nijsure and Kishore, 2018).

Different cell types have been used to populate scaffolds for bone tissue engineering, including embryonic stem cells, MSCs, ADSCs and differentiated OPCs (Colnot, 2011; Vas *et al.*, 2017). Bone marrow-derived MSCs can form bone-like tissue when cultured in porous scaffolds under osteoinductive conditions, and they are the most studied cell source for bone regeneration (Ng *et al.*, 2017). Due to their unlimited proliferation potential and osteogenic capacity, immortalized MSCs are a suitable tool for screening different regeneration approaches and scaffolds for bone tissue engineering.

Magnetic field-based approaches for bone regeneration

MSCs are mechanosensitive and capable of undergoing mechanically-induced osteogenic differentiation (Ng *et al.*, 2017). The process by which MSCs sense and respond to mechanical stimuli is termed mechanotransduction and is mediated by structural proteins, such as integrins and actin fibres. Mechanotransduction signalling pathways can be activated through the application of magnetic force, a technique known as magnetic actuation. The application of magnetic force is thought to deform the cell membrane, change its permeability and activate its mechanosensors, including integrins. These changes have been found to accelerate osteoblast differentiation, bone regeneration and mineralisation (Ross *et al.*, 2015; Santos, Reis and Gomes, 2015; Yun *et al.*, 2016; Xia *et al.*, 2018).

Generally, magnetic actuation has two main components: the supplied magnetic field and the responsive magnetic effectors, namely magnetic nanoparticles. Magnetic fields include static magnetic fields (SMFs), pulsed electromagnetic fields (PEMFs), and rotating magnetic fields (RMFs). Even for the same type of magnetic field, different intensities and frequencies induce different effects on the cells. Both SMFs (Kim *et al.*, 2015) and PEMFs (Petecchia *et al.*, 2015) were found to induce the osteogenic differentiation of MSCs, but the exact mechanism by which the magnetic force exerts a positive effect on MSCs and bone-healing still remains unclear (Xia *et al.*, 2018).

Magnetic-assisted tissue engineering involves cell or scaffold labelling with magnetic nanoparticles. If cells or scaffolds are magnetically labelled, the application of a magnetic field generates a magnetic force that induces their structural deformation and the activation of mechanotransduction signalling pathways (Santos, Reis and Gomes, 2015). Because of their biocompatibility and superparamagnetic properties,

iron oxide nanoparticles (IONs) <20 nm in diameter have numerous biomedical uses (Ansari *et al.*, 2019). IONs can be internalized by MSCs (Guldris *et al.*, 2017) and promote their osteogenic differentiation (Wang *et al.*, 2016). Scaffolds can be also magnetized with IONs (Meng *et al.*, 2010; Samal *et al.*, 2015), and further enhancement of osteogenic differentiation can be achieved by combining magnetic scaffolds with magnetic fields (Arjmand *et al.*, 2018; Xia *et al.*, 2018).

8.2 Cartilage tissue engineering

Different cell-based surgical treatments for cartilage defects have been used in clinical practice for decades. These treatments include microfracture surgery, which consists in penetrating the subchondral bone to allow migration of MSCs from the bone marrow to the cartilage defect; autologous chondrocyte implantation (ACI), in which the cartilage defect is filled with *in vitro*-grown chondrocytes and covered by a periosteal flap; and matrix-induced ACI, in which *in vitro*-grown chondrocytes are seeded on collagen or hyaluronic acid matrix prior to implantation. These surgical interventions have drawbacks, including donor site morbidity, mechanical instability and unwanted fibrocartilage formation (Makris *et al.*, 2015; Jeon and Elisseeff, 2016).

The limitations associated with the aforementioned techniques have led to the development of new therapeutic strategies based on tissue engineering (Vinatier and Guicheux, 2016). A wide range of natural and synthetic materials, such as alginate, collagen, PLA and PGA, have been investigated as scaffolds for cartilage repair (Akter and Ibanez, 2016). Hydrogels are promising scaffolds for cartilage tissue engineering, owing to their high water content, their similarity to the native ECM and their ability to match irregular defects (Liu *et al.*, 2017).

Suitable cell sources for cartilage tissue engineering include MSCs, CPCs and chondrocytes (Makris *et al.*, 2015). The use of MSCs circumvents the limitations of chondrocyte-based treatments in terms of their accessibility and minimization of donor morbidity (Le *et al.*, 2020), but strategies to allow their differentiation into articular chondrocytes and reduce hypertrophy still need to be further investigated.

II. Objectives

In spite of their multipotency and self-renewal ability, the usefulness of MSCs for bone and cartilage regeneration has not been fully elucidated. Research involving MSCs is impaired by the predisposition of these cells to senesce *in vitro*, especially when they are derived from aged donors. Age-related bone and cartilage diseases, such as OA and OP, significantly affect the quality of life of the patients, but suitable therapeutic options for bone and cartilage regeneration have not yet been developed. The generation of MSC lines derived from these patients, capable of overcoming senescence while keeping the essential mesenchymal features, can boost osteochondral regeneration research. In addition, these MSC lines can be a useful tool for the development of *in vitro* models of these diseases.

Therefore, the general goal of this doctoral thesis was the generation and characterization of MSC lines by immortalization of bone marrow-derived MSCs from OA patients and aged donors, useful for the study of joint tissue repair.

The specific objectives proposed to achieve this goal were:

1. Generate human MSC lines derived from bone marrow from OA patients and non-OA aged donors.
    1.1. Establish a suitable protocol for the immortalization of senescence-prone, slowly dividing MSCs.
    1.2. Obtain OA and non-OA MSC lines by transduction of both immortalization genes: SV40LT and hTERT.
    1.3. Verify the expression of transgenes and the bypass of senescence in the MSC lines generated.
2. Analyse the phenotype and functionality of the human MSC lines generated.
    2.1. Characterize phenotypically the generated cell lines by studying the expression of MSC surface markers in primary and immortalized MSCs.
    2.2. Characterize functionally the generated MSC lines by studying the multi-differentiation potential of primary and immortalized MSCs.
    2.3. Study the oncogenic potential of the generated MSC lines.
3. Isolate clones from the generated MSC lines and study their osteogenic potential.

4. Test magnetic-based approaches for bone tissue engineering using highly osteogenic clones.
5. Validate the immortalization protocol in other cell types present in the synovial joint: chondrocytes and synoviocytes.

III. Materials and methods

1. Isolation and culture of primary human cells

The present study was reviewed and approved by the research ethics committee of A Coruña-Ferrol, Spain (2016/588) (**Annex I**). All samples were collected from patients who underwent orthopaedic surgery and who gave written informed consent (**Annex II**).

1.1 Mesenchymal stromal cells

Bone marrow-derived MSCs were isolated from thirteen donors: eight patients with hip OA (aged 45 to 94 years, five males and three females) and five patients with hip fracture without OA (aged 65 to 95 years, four males and one female). Bone marrow of femoral heads was washed with Dulbecco's modified Eagle's medium (DMEM; Lonza, Madrid, Spain) with 5% foetal bovine serum (FBS, Gibco, Thermo Fisher Scientific, Madrid, Spain) and 1% penicillin/streptomycin (P/S, Gibco) (5%FBS/DMEM) to obtain bone marrow cells. After filtration through a 100 μm-pore filter and centrifugation at 430 ×*g* for 10 min, cells were plated in adherent culture dishes (Costar Corning Incorporated, New York, USA) and grown in DMEM with 20% FBS and 1% P/S (20%FBS/DMEM) at 37°C and 5% CO_2 (Sanjurjo-Rodríguez *et al.*, 2014; Piñeiro-Ramil *et al.*, 2020). Cell subculture was performed with 0.1% trypsin-EDTA (Gibco) when cell confluence reached 80-90%. In order to remove fibroblasts and macrophages from cell cultures, a 15-min pre-plating technique (Durgam *et al.*, 2016) was employed in the first and second passages.

1.2 Articular chondrocytes

Samples of articular cartilage were collected from two patients with hip OA who underwent orthopaedic surgery (aged 81 and 88 years, one male and one female). Articular cartilage was sliced into small pieces and subjected to enzymatic digestion with 0.25% trypsin (Gibco) in DMEM with 1% P/S for 10 minutes and with 2 mg/mL type IV collagenase (Sigma-Aldrich Química S.A., Madrid, Spain) in 5%FBS/DMEM overnight at 37°C in agitation (Díaz-Prado *et al.*, 2012). The isolated chondrocytes were filtrated through a 100 μm-pore filter, centrifuged at 430 ×*g* for 10 min, resuspended in DMEM with 10% FBS and 1% P/S (10%FBS/DMEM), counted using a Neubauer counting chamber (Thermo Fisher Scientific) and plated in adherent culture dishes. When cell confluence reached 70%,

one of the cell cultures was used for one spinoculation experiment. The other cell culture was employed in chondrogenesis and inflammation experiments as a control of primary cells.

1.3 Fibroblast-like synoviocytes

One sample of synovial tissue was collected from a patient without OA who underwent leg amputation (aged 88 years, male), after obtaining written informed consent. Synovial tissue was cut into small fragments and placed in a 100-mm adherent culture dish. After a few minutes, culture medium (10%FBS/DMEM) was added and synovial explants were incubated at 37°C. Once synoviocytes had outgrown, tissue fragments were discarded and cells were expanded in 10%FBS/DMEM (Rosengren, Boyle and Firestein, 2007). Subculture was performed when cell confluence reached 90%.

2. Plasmid purification and sequencing

Plasmids pBABE-puro-SV40LT (Addgene plasmid #13970), deposited by Thomas Roberts (Zhao *et al.*, 2003), and pBABE-hygro-eGFP-hTERT (Addgene plasmid #28169), deposited by Kathleen Collins (Wong, Kusdra and Collins, 2002), were obtained from Addgene as stab cultures of transformed *Escherichia coli* DH5-α. Stab cultures were used for streaking on Luria-Bertani (LB) agar (VWR International, Radnor, Pennsylvania, USA) with 100 μg/mL ampicillin (Sigma-Aldrich Química S.A., Madrid, Spain). After a 16-hour incubation at 37°C, single colonies were picked and grown at 37°C with agitation in 5 mL LB broth (Thermo Fisher Scientific) supplemented with 100 μg/mL ampicillin (LBA). After overnight incubation, plasmid DNA was isolated from bacterial cultures employing the GeneJET Plasmid Miniprep Kit (Thermo Fisher Scientific).

Plasmid DNA quantity and purity were determined using a ND-1000 UV-Vis Spectrophotometer (NanoDrop Technologies LLC, Thermo Fisher Scientific). DNA sequencing was performed in a 3130xl Genetic Analyzer (Applied Biosystems, Invitrogen, Thermo Fisher Scientific) using the BigDye Terminator v3.1 Cycle Sequencing Kit (Thermo Fisher Scientific) with specific primers (**Table 2**) to verify the presence of the genes of interest in the purified plasmids.

Table 2. Primers employed for plasmid sequencing.

Primer	Reference sequence	Primer sequence 5'→3'
pBABE_F1	Addgene NGS Result	GTCTCTCCCCCTTGAACCTC
hTERT_R	NM_198253.3	GGAGTAGCAGAGGGAGGCCG

Bacterial glycerol stocks corresponding to the verified colonies were established by adding 500 µL of overnight-grown liquid culture to 500 µL of 50% glycerol solution (Sigma-Aldrich Química S.A.). These stocks were stored at -80°C and subsequently employed as inoculums. For retrovirus production, plasmid DNA was amplified by growing bacteria in 100 mL of LBA overnight and purified using the Genopure Plasmid Midi Kit (Roche, Sigma-Aldrich Química S.A.).

3. Production of retroviruses and infection of primary cells

Phoenix Amphotropic (ATCC CRL-3213) cells (φNX-A) (Swift *et al.*, 2001) were plated on 100 mm adherent culture dishes (Costar Corning Incorporated), grown in 10%FBS/DMEM and transfected employing a single plasmid (either pBABE-puro-SV40LT or pBABE-hygro-eGFP-hTERT). For transfection of each culture dish, 10 µg of plasmid were mixed with Opti-MEM (Gibco) up to a volume of 970 µL, as described elsewhere (Piñeiro-Ramil *et al.*, 2020). Then, 30 µL of X-tremeGENE HP DNA Transfection Reagent (Roche, Sigma-Aldrich Química S.A.) were added, and this mixture was incubated for 25 minutes at room temperature and added dropwise to culture dishes.

Transfected φNX-A cells were incubated at 37°C during 24 hours, whereupon culture medium was changed and cells were incubated at 32°C for retrovirus production (Aasen *et al.*, 2008; Raya *et al.*, 2010). After 24 or 48 hours incubation at 32°C (**Table 3**), supernatants were collected and filtered through a 0.45 µm pore size membrane filter (Millipore, Burlington, Massachusetts, USA) to remove φNX-A, and 8 µg of HDMB (Sigma-Aldrich Química S.A.) were added per mL of retroviral supernatant (Balducci and Alessandri, 2016; Munisvaradass *et al.*, 2017). This retroviral supernatant was employed for infection of MSCs (3rd–5th passage), freshly digested chondrocytes and synoviocytes (2nd passage) at 70% of confluence, cultured in 6-well adherent culture dishes. A volume of 1.5 mL of retroviral supernatant was added to each well (**Figure 9**), and no viruses were added to one well of each dish, which was used as a negative control for antibiotic selection.

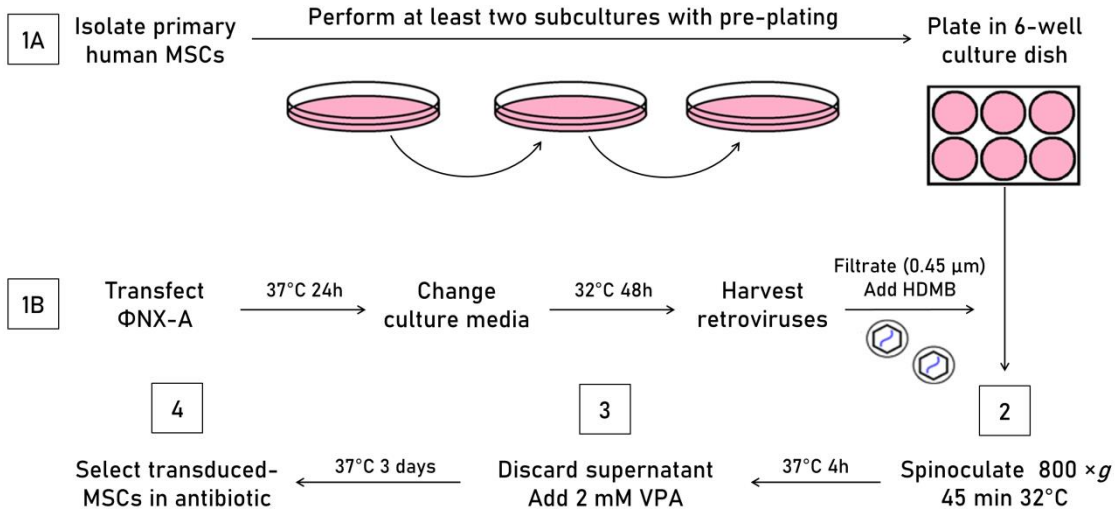

Figure 9. Human MSCs immortalization protocol. MSCs are isolated from bone marrow, subcultured with pre-plating and plated in 6-well culture dishes (1A). φNX-A cells are transfected with a plasmid containing SV40LT or hTERT sequence and incubated 48 h at 32°C for retrovirus production. Retroviruses are harvested and mixed with HDMB (1B), and this mixture is employed for MSCs infection by spinoculation (2). Four hours after spinoculation, retroviral supernatant is discarded and VPA is added (3). After a three–day incubation with VPA, transduced MSCs are selected in antibiotic (4). MSCs: mesenchymal stromal cells; φNX-A: Phoenix amphotropic cells; HDMB: hexadimethrine bromide; VPA: valproic acid.

Different spinoculation experiments were performed, including co-infections of MSCs with both SV40LT and hTERT retroviruses and infections with single SV40LT or hTERT viruses. Two centrifugation speeds (1000 and 800 ×*g*) and three time-points (60, 45 and 30 min) were assayed for spinoculation (**Table 3**), which was performed at 32°C. After spinoculation, MSCs were incubated during 4 hours at 37°C, whereupon retroviral supernatants were replaced by fresh culture medium with different concentrations of VPA (Cayman Chemical Company, Ann Arbor, Michigan, USA) (Cervera *et al.*, 2015) (**Table 3**), used to induce transgene expression. Selection of the optimal VPA concentration was analysed using a viability test (**Section 8**). After three days, culture medium was replaced by selection culture medium containing 2.5 µg/mL puromycin (Thermo Fisher Scientific) and/or 75 µg/mL hygromycin (AMRESCO, VWR International) (**Figure 9**).

Table 3. Different variations of the transduction protocol assayed: retrovirus employed, φNX-A culture conditions, spinoculation parameters and VPA concentration. MSCs: mesenchymal stromal cells; #: Cell line number; SV40LT: simian virus 40 large T antigen; hTERT: human telomerase reverse transcriptase; φNX-A: Phoenix amphotropic cells; VPA: valproic acid.

Cells	Donor		Retrovirus	φNX-A culture	Spinoculation	VPA (mM)
	Age (years)	Pathology				
MSCs#1	65	Fracture	SV40LT + hTERT	32ºC 24 hours	1000 ×*g* 60 min	0
MSCs#2	94	OA				
MSCs#1	65	Fracture	SV40LT + hTERT /SV40LT/hTERT	32ºC 24 hours	1000 ×*g* 60 min	0-0.5
MSCs#3	71	OA				
MSCs#4	88	Fracture	SV40LT	32ºC 24 hours	1000 ×*g* 45 min	0.5-2
MSCs#5	69	OA				
MSC#6	67	OA	SV40LT	32ºC 48 hours	800 ×*g* 45 min	0.5-2
MSCs#7	45	OA	SV40LT	32ºC 48 hours	800 ×*g* 30 min	2
MSCs#8	70	OA				
MSCs#9	74	Fracture	SV40LT	32ºC 48 hours	800 ×*g* 45 min	2
MSCs#1	65	Fracture				
MSCs#4	88	Fracture				
MSCs#10	58	OA				
MSCs#11	52	OA	SV40LT	32ºC 48 hours	800 ×*g* 45 min	0.5-5
MSC#12	95	Fracture	SV40LT	32ºC 48 hours	800 ×*g* 45 min	2
MSC#13	88	Fracture				
Chondrocytes	88	OA				
Synoviocytes	88	Amputation				
SV40LT-transduced MSCs, chondrocytes and synoviocytes	-	-	hTERT	32ºC 48 hours	800 ×*g* 45 min	2

4. Characterization of transduced cells

Transduced MSCs characteristics, including morphology, proliferation potential, colony formation ability, surface antigen expression, multi-differentiation potential and oncogenic potential, were analysed and compared, when possible, with those of their primary parental MSCs.

4.1 Analysis of morphology and proliferative capacity

The morphology of primary and transduced MSCs seeded on adherent culture plates was analysed by observation with a Nikon Eclipse TS100 inverted microscope (Nikon Instruments Europe B.V., Amsterdam, Netherlands) coupled to a XM Full HD digital camera (Hangzhou Xiongmai Technologies (XM), Hangzhou, China). Proliferation of transduced cells was calculated as cumulative PDs following the formula in **Equation 1** (Balducci and Alessandri, 2016). Cells were trypsinized and counted using a Neubauer counting chamber to calculate the final and initial cell numbers at each passage. Generation time was calculated for each cell line at each passage as the number of PDs per day. The proliferation rates of all cell lines were analysed by regression, and mean generation times of all cell lines were compared. Expression of PCNA, which is present only in actively proliferating cells, was analysed in primary and transduced MSCs.

$$PD = \frac{\log Nf - \log Ni}{\log 2}$$

Equation 1. Formula employed to calculate population doubling (PD) at each passage, where *Nf* is the final cell number, *Ni* is the initial cell number, and *log* is the natural logarithm.

4.2 Colony formation

One of the characteristics of MSCs is the ability to form colonies. Transduced MSCs seeded in 6-well culture dishes at a density of 500 cells per well were cultured for one week, in order to assess their colony formation ability. Cytological staining was performed to visualize the colonies, as described below (**Section 9.3**).

4.3 Flow cytometric analysis

Expression of surface markers of MSCs (CD29, CD44, CD73, CD90 and CD105) and HSCs (CD34 and CD45) was analysed by flow cytometry in primary and

transduced MSCs. For comparison with another MSC line, the expression of the aforementioned surface markers was also analysed in immortalized MSC line 3a6 (Tsai *et al.*, 2010), kindly provided by Dr. Hung's group. Additionally, expression of surface markers CD44 and CD90 was analysed by flow cytometry in immortalized synoviocytes. Cells were split with 0.1% trypsin-EDTA, washed twice in Fluorescence Activated Cell Sorting (FACS) buffer (BD Biosciences, Madrid, Spain) and incubated at 4°C for 45 minutes with fluorescent-labelled antibodies and isotype controls listed in **Table 4**. After incubation, cells were washed, resuspended in FACS buffer and transferred to polypropylene tubes (NUNC, VWR International). Data acquisition was made using a BD FACSCalibur flow cytometer (BD Biosciences), and the data obtained was analysed using BD Cell-Quest Pro software (BD Biosciences). For each assay, a minimum of 10^5 cell events were acquired. Results are shown as percentage of positive cells.

Table 4. Antibodies conjugated with fluorescein isothiocyanate (FITC), phycoerythrin (PE) or PE/Cy5 used for flow cytometry.

Antibody	Dilution	Specificity	Clone	Source
FITC Mouse IgG1 Isotype Control	1:50	-	ICIG1	Immunostep
PE Mouse IgG1 Isotype Control	1:50	-	B11/6	Immunostep
PECy5 Mouse IgG1 Isotype Control	2:25	-	1F8	Abcam
PE Mouse Anti-Human CD29	3:50	Human integrin β1 (ITGB1)	VJ1/14	Immunostep
PE Mouse Anti-Human CD34	2:25	Hematopoietic progenitor cell antigen 1 (HPCA1)	581	BD Pharmingen
FITC Mouse Anti-Human CD44	1:50	Homing cellular adhesion molecule (HCAM)	IM7	BD Pharmingen
FITC Mouse Anti-Human CD45	3:50	Leukocyte common antigen (LCA)	D3/9	Immunostep
PE Mouse Anti-Human CD73	3:50	Ecto-5'-nucleotidase (NT5E)	AD2	Immunostep
PECy5 Mouse Anti-Human CD90	1:50	Thymocyte differentiation antigen 1 (Thy-1)	5E10	Immunostep
FITC Mouse Anti-Human CD105	1:50	Human Endoglin (ENG)	SN6	AbD Serotec

4.4 Induction of cell differentiation

Primary and transduced MSCs were differentiated into osteoblasts, adipocytes and chondrocytes in order to assess their multi-differentiation potential. Primary and transduced chondrocytes were cultured under chondrogenic stimuli to induce their re-differentiation after *in vitro* expansion.

Two types of experiments were carried out for osteogenic cell differentiation: monolayer differentiation and three-dimensional osteogenesis through endochondral ossification. In monolayer differentiation, 2×10^4 cells were plated on 8-well chamber slides (Millipore) and 10^5 cells were plated on 6-well plates (Costar Corning Incorporated) to perform histological and molecular analysis (**Sections 10-11**). Cells were grown for 21 days in *hMSC Ostegenic Differentiation Medium* (Lonza) and 20%FBS/DMEM (as a control).

In three-dimensional osteogenesis, cell aggregates were formed by the hanging drop method (Hildebrandt, Büth and Thielecke, 2011). Briefly, drops containing 5×10^5 cells were seeded on the lid of a Petri dish filled with PBS. After two days, the aggregates were transferred to a suspension culture system in propylene tubes (J.C. Catalán S.L., Barcelona, Spain) and cultured in *hMSC Chondrogenic Differentiation Medium* (Lonza) with 10 ng/mL of human transforming growth factor β-3 (TGF-β3) (ProSpec-Tany TechnoGene, Rejovot, Israel) for 14 days and in *hMSC Osteogenic Differentiation Medium* for 21 more days (Dang *et al.*, 2016). Control aggregates were cultured in 20%FBS/DMEM for 35 days. Osteogenically induced and control aggregates were analysed histologically (**Section 10**).

For adipogenic cell differentiation experiments, 2×10^4 cells were plated on 8-well chamber slides and 10^5 cells were plated on 6-well plates to perform histological and molecular analysis (**Sections 10-11**). Cells were grown for 21 days in *hMSC Adipogenic Differentiation BulletKit Medium* (Lonza) or *StemPro Adipogenesis Differentiation Kit* (Gibco) and 20%FBS/DMEM (as a control).

For chondrogenic cell differentiation experiments, three-dimensional cell culture was used (Hildebrandt, Büth and Thielecke, 2011). Cell aggregates were formed by the hanging drop method and incubated in *hMSC Chondrogenic Differentiation Medium* with 10 ng/mL of TGF-β3 or in 20%FBS/DMEM (as a control). MSC aggregates were cultured for 21 days and chondrocyte aggregates were cultured for 15 days.

Primary and immortalized chondrocytes were also seeded in 6 mm-diameter sponges of type I collagen (ColI) (Opocrin S.P.A, Modena, Italy) (Sanjurjo-Rodríguez *et al.*, 2014) and maintained in *hMSC Chondrogenic Differentiation Medium* with 10 ng/mL of TGF-β3 for 30 days. After that, cell aggregates and ColI sponges were analysed histologically (**Section 10**).

4.5 Oncogenic potential

The soft agar colony formation assay (Roca-Lema *et al.*, 2019) was performed to investigate the oncogenic potential of the transduced MSCs. For each cell line, 1.5×10^4 cells were inoculated in 0.375% agar (Sigma-Aldrich Química S.A.) and layered on top of a 0.5% agar layer in 12-well culture dishes (Costar Corning Incorporated) (3.75×10^3 cells/well). Cells were incubated for 14 days at 37°C with 5% CO_2 and colony formation was observed and photographed using a Nikon Eclipse TS100 inverted microscope (Nikon Instruments Europe B.V.) coupled to a XM Full HD digital camera (Hangzhou Xiongmai Technologies). Additionally, molecular analysis was performed to quantify expression of tumour-related genes in primary MSCs, transduced MSCs and, as a control for oncogenic potential, osteosarcoma cell line 143B (ATCC CRL-8303) (**Section 11**).

5. Clone isolation

After reaching more than 100 PDs, four SV40LT and hTERT-transduced immortalized MSC (iMSC) lines were seeded at low density (100 cells/dish) on 100 mm adherent culture dishes in 20%FBS/DMEM. After verifying the clonal origin of each colony by microscopic observation with a Nikon Eclipse TS100 inverted microscope, colonies were left to grow until reaching a suitable size for isolation (approximately 50 cells). For clone isolation, cloning cylinders (Sigma-Aldrich Química S.A.) were placed over each selected colony and cells were trypsinized and subcultured in adherent culture dishes. Three clones were isolated from each iMSC line.

6. *In vitro* inflammation model

The response of immortalized chondrocytes to the inflammatory cytokine IL-1β was investigated. Primary chondrocytes, immortalized chondrocytes and immortalized chondrocyte cell line T/C28a2 (Goldring *et al.*, 1994; Finger *et al.*,

2003) were seeded in 6-well adherent culture dishes in 10%FBS/DMEM. Cells were either incubated DMEM containing 0.5% FBS for 48 h before treatment and thereafter stimulated with IL-1β (5 ng/mL) (PeproTech, Rocky Hill, NJ) for 24 hours in serum-free DMEM (Vaamonde-García *et al.*, 2012) or incubated in serum-free DMEM as a control. Molecular analysis was performed thereafter to quantify the expression of inflammation genes (**Section 11**).

7. Study of magnetic field-based approaches for tissue engineering

A highly osteogenic iMSC-derived clone, iMSC#8.A, was employed for testing magnetic-based approaches for bone tissue engineering. The effect of RMF was analysed in both magnetically labelled iMSC#8.A cultured on 6 mm-diameter ColI sponges and non-labelled iMSC#8.A seeded onto magnetically labelled ColI sponges. For magnetic labelling of cells and scaffolds, IONs composed of an inorganic core of magnetite (Fe_3O_4) and a polymeric coating with polyacrylic acid (PAA) (Fe_3O_4@PAA) were prepared following an hydrothermal protocol (Kolen'ko *et al.*, 2014). These experiments were carried out in the International Iberian Nanotechnology Laboratory (Braga, Portugal) under the supervision of Dr. Manuel Bañobre-López.

7.1 Magnetic labelling of ColI sponges

ColI sponges with 6 mm diameter were magnetically labelled by incubation at different concentrations of Fe_3O_4@PAA nanoparticles (1, 5, 10 and 20 g/L Fe_3O_4) overnight. Negative controls were incubated in Milli-Q water. Magnetically labelled ColI sponges were thereafter washed in PBS to remove non-absorbed magnetic nanoparticles and left to dry in a vacuum chamber, whereupon their magnetic properties were analysed using a superconducting quantum interference device (SQUID-VSM, Quantum Design, California, USA) under a maximum applied field of ±2 T at both 300 K and 5 K. Data were normalized to the total sample mass.

ColI sponges were sterilized in UV light, and 2×10^5 iMSC#8.A were seeded in each magnetically labelled or control sponge, including three replicates for each concentration of nanoparticles used (0, 1, 5, 10 and 20 g/L Fe_3O_4) and a control of ColI without previous incubation, washing and drying ("native ColI"). iMSC#8.A contained in a drop of 20 μL were deposited on top of the sponges in 12-well plates (TPP, Merck KGaA, Darmstadt, Germany). The cells-containing drops were left to

be absorbed by the sponges overnight, and then 500 µL of 20%FBS/DMEM (Merck KGaA, Darmstadt, Germany) were added to each well.

7.2 Magnetic labelling of iMSCs

iMSC#8.A were seeded in 6-well plates (TPP, Merck KGaA, Darmstadt, Germany) and incubated with Fe_3O_4@PAA nanoparticles (0, 25, 50 and 100 µg/mL iron) in 20%FBS/DMEM with 1.5 mg/mL poly-L-lysine (Merck KGaA, Darmstadt, Germany) for 24 hours (Guldris *et al.*, 2017) for magnetic labelling. The iron concentration per cell was determined by inductively coupled plasma optical emission spectrometry (ICP-OES) (ICPE-9000, Shimadzu, Kyoto, Japan). Cells were washed twice in PBS and split with 0.1% trypsin-EDTA, and cell pellets were digested in 1 mL of 37% hydrochloric acid (Merck KGaA, Darmstadt, Germany) overnight. Once digested, samples were diluted 1:10 in Milli-Q water. Three replicates of each sample were measured by ICP-OES. Results were expressed as mean ± standard deviation. Additionally, Prussian blue staining was performed to confirm the uptake of IONs by iMSC#8.A (**Section 9.4**).

7.3 Rotating magnetic field stimulation

Both types of constructs (magnetically labelled ColI sponges containing iMSC#8.A and ColI sponges containing magnetically labelled iMSC#8.A) were employed for cell differentiation experiments induced by RMF. For these experiments, ColI sponges incubated with the highest IONs concentration (20 g/L Fe_3O_4) and magnetically labelled iMSC#8.A incubated with the highest iron concentration (100 µg/mL Fe) were used. For the magnetic stimulation of the constructs, a home-made setup consisting in two magnets of 1.3 T, a rotor, a motor and a battery was employed, and the same system without magnets was used as a control (**Supplementary material** PineiroRamil_Maria_TD_2021_Video.mp4). Three experimental conditions (RMF, rotation only and static culture) were studied, and three replicates were included for each condition and time. Samples were analysed histologically (**Section 10**) after 21 days of culture in order to assess cell distribution throughout the scaffold and the production and level of mineralization of the extracellular matrix.

8. Cell viability assays

Cell viability measurements were carried out in three MSC transduction experiments with SV40LT retrovirus in order to determine the optimal concentration of VPA. Cell viability was determined employing the Cell Counting Kit-8 (CCK-8) (Sigma-Aldrich Química S.A.), following the manufacturer's instructions. Absorbance was measured: (1) before spinoculation; (2) after spinoculation, just before addition of VPA; (3) after a three-day incubation in culture medium containing 0.5, 1, 2, 3 or 5 mM VPA; and (4) after selection of transduced cells in 20%FBS/DMEM containing 2.5 μg/mL puromycin. Absorbance measurements were performed in triplicate using a NanoQuant Infinite M200 microplate reader (Tecan Ibérica Instrumentación S.L., Barcelona, Spain), with a measurement wavelength of 450 nm and a reference wavelength of 650 nm (**Figure 10**).

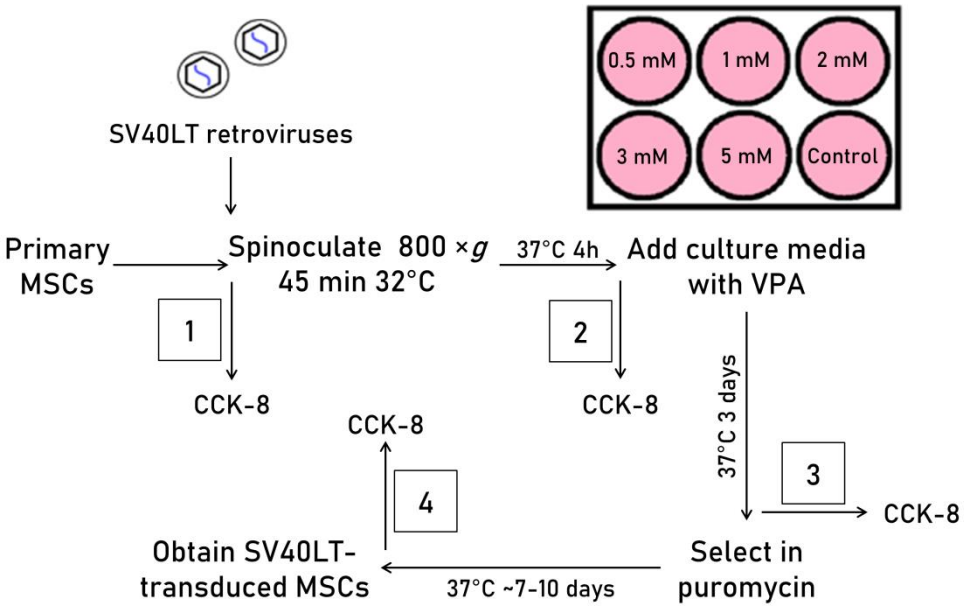

Figure 10. Diagram of experiments performed for optimization of VPA concentration. Cell viability measurements were performed before spinoculation (1); after spinoculation, just before addition of VPA (2); after a three-day incubation with VPA (3); and after selection in puromycin (4), employing CCK-8. MSCs: mesenchymal stromal cells; SV40LT: simian virus 40 large T antigen; VPA: valproic acid; CCK-8: Cell Counting Kit-8.

Viability of iMSC#8.A seeded on magnetically labelled ColI sponges was measured with Aqua-Bluer indicator (MultiTarget Pharmaceuticals, LLC, Denver, USA) 2, 7 and 15 days after seeding. Fluorescence measurements were carried out in a BioTek microplate reader (Agilent Technologies, California, USA) with 540 nm wavelength

for excitation and 590 nm wavelength for emission, and data were collected with Gen5 software (Agilent Technologies).

9. Cytological analysis

9.1. Immunofluorescence assay

Transduced cells were cultured in 8-well chamber slides (Millipore) to test the expression of SV40LT and hTERT. Cells were washed with phosphate-buffered saline (PBS; Dako, Agilent Technologies Spain S.L., Barcelona, Spain), fixed with 4% paraformaldehyde, quenched with 1% glycine, permeabilized with 0.5% Triton X-100 and blocked with 4% bovine serum albumin (all from Sigma-Aldrich Química S.A.). Subsequent incubation with two primary antibodies, mouse anti-SV40LT (SV40LT clone Pab 108; 1:100; Santa Cruz Biotechnology, Dallas, Texas, USA) and rabbit anti-GFP labelled with Alexa Fluor 488 dye (A-21311; 1:500; Invitrogen), was performed at 4ºC overnight.

After incubation with primary antibodies, cells were washed three times with PBS and incubated with a goat anti-mouse secondary antibody labelled with Alexa Fluor 594 dye (A-11032; 1:1000; Invitrogen) at room temperature for one hour. After three additional washes in PBS, a two-minute incubation with Hoechst (bisBenzimide H 33342 trihydrochloride, Sigma-Aldrich Química S.A.) was performed. Slides were mounted with Glycergel aqueous mounting medium (Dako) and observed using an Olympus BX61 fluorescence microscope (Olympus Iberia S.A., Barcelona, Spain) coupled to an Olympus DP70 digital camera (Olympus Iberia S.A.). Fluorescence micrographs were obtained employing the cellSens Dimension software (Olympus Iberia S.A.).

9.2 Senescence-associated β-galactosidase activity

Cytochemical staining for SA-ß-Gal activity was performed for each cell line after reaching more than 100 PDs at three different passages, using the Senescence Cells Histochemical Staining kit (Sigma-Aldrich Química S.A.). After 16 hours of incubation, cells were observed and photographed with a Nikon Eclipse TS100 inverted microscope coupled to a XM Full HD digital camera. SA-ß-Gal-positive and negative cells were counted on ten random microscope fields, and percentage of senescent cells was calculated. Results were provided as mean percentage of

senescent cells ± standard error. Primary MSCs at the 4th passage were employed as a control and compared with transduced MSCs.

9.3 Crystal violet

After one week of culture, transduced MSCs were washed with PBS, fixed with 4% paraformaldehyde and stained with crystal violet 0.1% (Sigma-Aldrich Química S.A.) in order to assess their colony formation ability. Crystal violet-stained colonies were observed and photographed using a Nikon SMZ 745T stereomicroscope coupled to a Nikon DS-Fi2 digital camera.

9.4 Prussian blue staining

Prussian blue staining was performed employing the Iron Stain kit (Merck KGaA, Darmstadt, Germany) in order to observe the distribution of IONs inside magnetically labelled iMSC#8.A. After incubation with Fe_3O_4@PAA (100 μg/mL iron), cells were fixed with 4% paraformaldehyde, washed with Milli-Q water, stained with postassium ferrocyanide in hydrochloric acid (1:1), washed again with Milli-Q water and observed in a Nikon Eclipse TS100 inverted microscope coupled to a digital camera (Nikon Instruments Europe B.V.). Micrographs were taken using the NIS-Elements AR software (Nikon Instruments Europe B.V.).

10. Histological analysis

After osteogenic differentiation, cells were fixed with 4% paraformaldehyde and stained with Alizarin Red, and slides were mounted with DPX mounting medium (Surgipath, Leica Microsistemas S.L., Barcelona, Spain). Adipogenically differentiated cells were fixed with 4% paraformaldehyde and stained with Oil Red O, and slides were mounted with Glycergel aqueous mounting medium.

Cell aggregates and ColI sponges were fixed with 3.7% formaldehyde (Panreac Química S.L.U., Barcelona, Spain), embedded in paraffin (Merck Millipore, Merck KGaA, Darmstadt, Germany) and cut in a microtome. Chondrogenically-induced iMSC and ColI sponges containing chondrocytes were stained with Massons' Trichrome and Safranin O in order to study the presence of collagen fibres and proteoglycans in the ECM. Osteogenically-induced iMSC aggregates were stained with Alizarin Red and Von Kossa to evaluate mineralization level and with Massons' Trichrome and Safranin O to investigate the presence of remaining chondrogenic

features. Magnetically labelled ColI sponges containing iMSC#8.A and ColI sponges containing magnetically labelled iMSC#8.A were stained with Alizarin Red and Masson's Thricrome. Slides were mounted with DPX mounting medium.

Additionally, chondrogenically-induced iMSCs aggregates were immunostained to assess the presence of aggrecan and type II collagen in their ECM. Before immunostaining, cell aggregates were pre-treated with chondroitinase ABC (Sigma-Aldrich Química S.A.). Anti-collagen II (clone 5B2.5 (1:25), Thermo Fisher Scientific) and anti-aggrecan (clone BC-3 (1:50), Abcam) primary antibodies were incubated overnight. The Dako REAL EnVision Detection System (Dako) was used for immunostaining visualization, and slides were mounted with DPX mounting medium.

Stained and immunostained slides were observed employing an Olympus BX61 microscope coupled to an Olympus DP70 digital camera. Micrographs were obtained using the cellSens Dimension software. Quantitative analysis of stained areas and intensity of staining was carried out employing the ImageJ software (National Institutes of Health, Bethesda, USA). Optical density (OD) was calculated as a measure of staining intensity, following the formula $OD = \log(max\ intensity / mean\ intensity)$, where log is the natural logarithm. Both optical density and percentage of staining were measured in four different areas of each sample to obtain an average value (Sanjurjo-Rodríguez *et al.*, 2014; Piñeiro-Ramil *et al.*, 2020).

11. Molecular analysis

RNA from cells and cell aggregates cultured in basal medium or under differentiation/inflammation stimuli was isolated employing TRIzol Reagent (Thermo Fisher Scientific) and chloroform (Sigma-Aldrich Química S.A.), precipitated with isopropanol (Sigma-Aldrich Química S.A.) and washed with ethanol (Sigma-Aldrich Química S.A.). Reverse transcription was carried out using the SuperScript VILO cDNA Synthesis kit, following the manufacturer's instructions (Thermo Fisher Scientific), in an Applied Biosystems Veriti 96-Well Thermal Cycler (Thermo Fisher Scientific), using the following program: 10 min at 25°C, 120 min at 42°C and 5 min at 85°C. When available, 2 μg of RNA were retrotranscribed, and the obtained cDNA was diluted 1:100; otherwise, all the RNA was retrotranscribed, and cDNA was diluted accordingly. Quantitative real-time polymerase chain reaction (qPCR) was performed in a LightCycler1 480 Instrument

(Roche), employing LightCycler 480 SYBR Green I Master (Roche) in addition to gene specific primers shown in **Table 5** and using the following program: 10 min of incubation at 95°C, 35-45 cycles of amplification (10 s at 95°C, 5 s at 60°C and 10 s at 70°C), one cycle of melting (5 s at 95°C, 1 min at 65°C and up to 97°C at 0.03°C/s) and 20 s of cooling at 40°C.

Data analysis was done using the LightCycler 480 Relative Quantification software (Roche), and relative gene expression levels (RELs) were calculated employing the qbase+ software (Biogazelle, Zwijnaarde, Belgium). A set of nine candidate reference genes (**Table 5**) was tested on primary and transduced MSCs cultured in basal and differentiation mediums, and the most stable housekeeping was determined by geNorm (Vandesompele *et al.*, 2002). Relative expression levels (RELs) of genes related with osteogenesis, adipogenesis, immortalization, proliferation and multipotency, as well as cartilage-related genes in chondrocyte aggregates, were normalized to the sample with the highest expression of each gene. RELs of tumour-related genes were normalized to osteosarcoma cell line 143B, and RELs of inflammation genes were normalized to the control sample for each cell line. All RELs are shown as mean ± standard error.

Table 5. Primers employed for quantitative real time PCR (qPCR) analysis.

	Gene	Reference sequence	Forward primer 5'→3'	Reverse primer 5'→3'
Reference	Tyrosine 3-monooxygenase/ tryptophan 5-monooxygenase activation protein zeta (YWHAZ)	NM_003406.3	GATCCCCAATGCTTCACAAG	TGCTTGTTGTGACTGATCGAC
	Glyceraldehyde 3-phosphate dehydrogenase (GAPDH)	NM_002046.7	GGAGTCAACGGATTTGGTCGTA	GGCAACAATATCCACTTTACCAGAGT
	TATA-binding protein (TBP)	NM_003194.5	GCCCATAGTGATCTTTGCAGT	CGCTGGAACTCGTCTCACTA
	Peptidylprolyl isomerase A (PPIA)	NM_021130.5	ATGCTGGACCCAACACAAAT	TCTTTCACTTTGCCAAACACC
	Hypoxanthine phosphoribosyltransferase 1 (HPRT1)	NM_000194.3	TGATAGATCCATTCCTATGACTGTAGA	CAAGACATTCTTTCCAGTTAAAGTTG
	Homo sapiens actin beta (ACTB)	NM_001101.5	AGAGCTACGAGCTGCCTGAC	GGATGCCACAGGACTCCA
	Homo sapiens tubulin beta class I (TUBB)	NM_178014.4	ATACCTTGAGGCGAGCAAAA	CTGATCACCTCCCAGAACTTG
	Homo sapiens ubiquitin C (UBC)	NM_021009.7	GGCAAAGATCCAAGATAAGGAA	GGACCAAGTGCAGAGTGGAC
	RNA 18S ribosomal N1 (RNA18S)	NR_145820.1	GGAGAGGGAGCCTGAGAAAC	TCGGGAGTGGGTAATTTGC
Osteogenesis	Homo sapiens runt related transcription factor 2 (RUNX2)	NM_001024630.4	TTACTTACACCCCGCCAGTC	TATGGAGTGCTGCTGGTCTG
	Homo sapiens Sp7 transcription factor (SP7)	NM_001173467.2	TCCCCTGTTGCCATGGTTAT	CCACCCATTCTTCAGGAGGT
	Homo sapiens bone gamma-carboxyglutamate protein (OCN)	NM_199173.5	GGCGCTACCTGTATCAATGG	TCAGCCAACTCGTCACAGTC
Adipogenesis	Homo sapiens adiponectin, C1Q and collagen domain containing (APN)	NM_001177800.1	GGTGAGAAAGGAGATCCAGGT	TGCTGAGCGGTATACATAGGC
	Homo sapiens fatty acid binding protein 4 (FABP4)	NM_001442.2	GGATGATAAACTGGTGGTGGA	CACAGAATGTTGTAGAGTTCAATGC

Tumour-related	Homo sapiens HRas proto-oncogene, GTPase (HRAS)	NM_005343.4	TGCCATCAACAACACCAAGT	ACGTCATCCGAGTCCTTCAC
	Homo sapiens tumor protein p53 (P53)	NM_000546.5	GGCCCACTTCACCGTACTAA	GTGGTTTCAAGGCCAGATGT
	Homo sapiens RB transcriptional corepressor 1 (RB1)	NM_000321.2	TGCATGGCTCTCAGATTCAC	AGTTGGTCCTTCTCGGTCCT
	Homo sapiens E2F transcription factor 1 (E2F1)	NM_005225.3	TGTGCATGAGTCCATGTGTG	GGCCGAAAGTGCAGTTAGAG
Immortalization	Simian virus 40 complete genome (SV40)	NC_001669.1	TGGGGAGAAGAACATGGAAG	AAATGAGCCTTGGGACTGTG
	Homo sapiens telomerase reverse transcriptase (hTERT)	NM_198253.3	GCTAGTGGACCCCGAAGG	CCTCCCTGACGCTATGGTT
Proliferation and Multipotency	Homo sapiens proliferating cell nuclear antigen (PCNA)	NM_002592.2	TAGACTTTCCTCCTTCCCGC	TGCCTCCAACACCTTCTTGA
	Homo sapiens POU class 5 homeobox 1 (POU5F1), transcript variant 4 (OCT4B1)	NM_001285986.2	AGGGAGAGGGAGAAGATGCT	GAAGCAAAGTGAGGGAGCAC
Inflammation	Homo sapiens interleukin 6 (IL6)	NM_000600.4	AGTCCTGATCCAGTTCCTGC	CATTTGTGGTTGGGTCAGGG
	Homo sapiens interleukin 8 (IL8)	NM_001354840.3	CTCCAAACCTTTCCACCCCA	TTCTCCACAACCCTCTGCAC
	Homo sapiens cyclooxygenase-2 (COX2)	NM_000963.4	AGGAGGTCTTTGGTCTGGTG	ACTGCTCATCACCCCATTCA
Cartilage	Homo sapiens SRY-box transcription factor 9 (SOX9)	NM_000346.4	GTACCCGCACTTGCACAAC	TCGCTCTCGTTCAGAAGTCTC
	Homo sapiens collagen type II alpha 1 chain (COL2A1)	NM_033150.3	TGGTGCTAATGGCGAGAAG	CCCAGTCTCTCCACGTTCAC
	Homo sapiens aggrecan (ACAN)	NM_001135.4	CGGTCTACCTCTACCCTAACCA	GAGAAGGAACCGCTGAAATG

IV. Results

1. Establishment of a suitable protocol for MSC immortalization

Sequencing results showed that the genes of interest, SV40LT and hTERT, were present in plasmids pBABE-puro-SV40LT and pBABE-hygro-eGFP-hTERT, respectively (**Annex III**). ΦNX-A were transfected with these plasmids for retrovirus production, and these retroviruses were employed for transduction of MSCs by spinoculation.

1.1 Spinoculation of MSCs with retrovirus produced by ΦNX-A

Variations of several parameters of the transduction method were assayed for immortalization of primary MSCs (**Table 3**). First, spinoculation at 1000 ×*g* for 60 minutes with SV40LT and hTERT retrovirus (co-infection) caused cell death of almost the entire cell population. The same result was obtained with the hTERT retrovirus alone. A decrease in cell death was observed when employing the SV40LT retrovirus alone, but even then, spinoculation resulted in SV40LT-transduced MSCs (T-MSCs) with very low efficiency and only with VPA induction of transgene expression (**Figure 11**).

Even when lowering centrifugation time down to 45 minutes, spinoculation at 1000 ×*g* still produced cell death of most MSCs. Conversely, lowering centrifugation speed to 800 ×*g* resulted in much higher cell survival after spinoculation. When prolonging incubation time for retrovirus production to 48 hours, transduction efficiency was highly improved and a larger population of T-MSCs was obtained. A shorter centrifugation time (30 minutes) reduced transduction efficiency and did not improve cell survival (**Figure 11**). The established parameters (48-hour incubation of transfected ΦNX-A for retrovirus production, spinoculation at 800 ×*g* for 45 minutes and transgene expression induction by addition of 2 mM VPA) were successfully employed for SV40LT transduction of MSCs derived from ten donors (**Table 3**). Puromycin-selected T-MSCs had grown enough to be trypsinized within one week after selection.

The use of these established parameters for a second transduction of T-MSCs with hTERT enabled us to obtain a small population of hTERT-transduced T-MSCs, which were termed immortalized MSCs (iMSCs). In our system, hTERT transduction was less efficient than SV40LT transduction, which is probably due to the fact that the hTERT plasmid sequence is longer, and ΦNX-A transfection

efficiency is therefore lower. It took 2-4 weeks for hygromycin-selected iMSCs to grow enough to be trypsinized and expanded; however, after this period, all six generated iMSC lines (three OA and three non-OA lines) showed high proliferation rates.

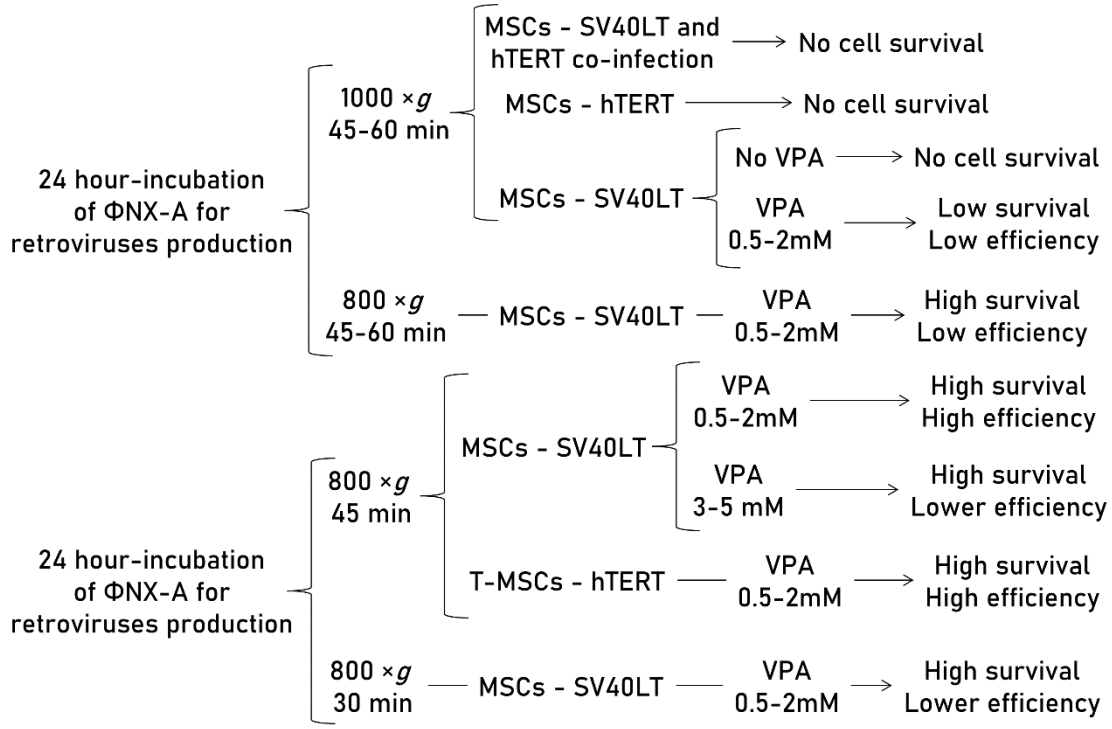

Figure 11. Variations of the assayed transduction protocol: transduction system (retrovirus and cells), φNX-A culture conditions, spinoculation parameters, VPA concentration and obtained result. φNX-A: Phoenix amphotropic cells; MSC: mesenchymal stromal cell; T-MSC: SV40LT-transduced MSC; SV40LT: Simian virus 40 large T antigen; hTERT: human telomerase reverse transcriptase; VPA: valproic acid.

1.2 Optimization of VPA concentration

The Cell Counting Kit-8 (CCK-8) was employed to determine the optimal VPA concentration for transgene expression induction in MSCs. Taking into account that absorbance is proportional to cell population size, it was observed that the cell population was reduced after spinoculation in a very variable way (between 16% and 60%). This reduction was also observed in the cells that have been centrifuged without virus addition. After a three-day incubation with different VPA concentrations, only small changes in cell population were observed (p-value=0.5615). After puromycin selection, a critical decrease in cell population size was detected in all cases except for previous treatments with 0.5 mM and 2 mM

VPA, in which this decrease was less severe. However, no significant differences were found between groups after treatment with different concentrations of VPA (p-value=0.7886) or after selection (p-value=0.0700). Differences between absorbance measurements before and after spinoculation (1), VPA treatment (2) and puromycin selection (3) are represented as percentage reduction of the cell population in **Figure 12**.

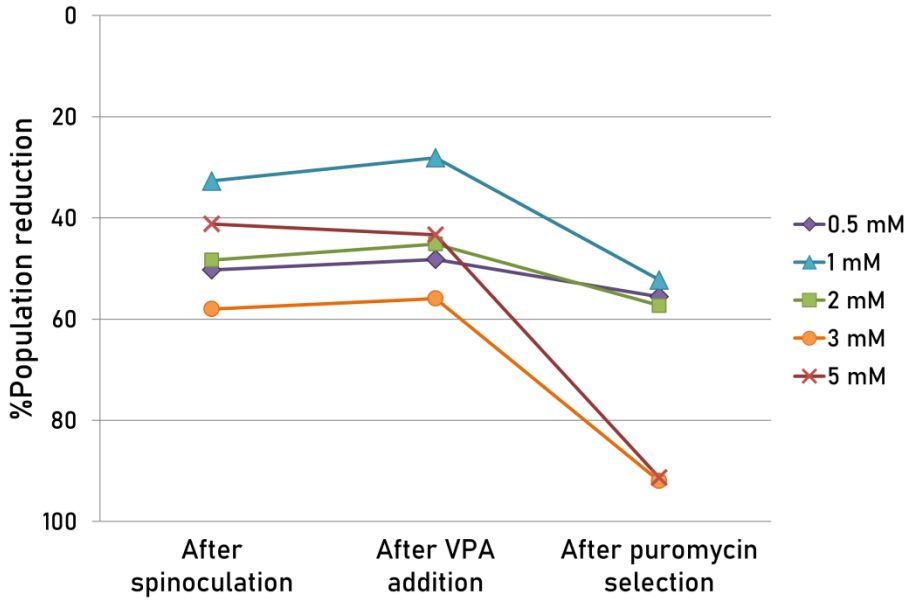

Figure 12. Percentage of cell population reduction after spinoculation (p-value=0.1395) (1), after a three-day incubation with 0.5, 1, 2, 3 or 5 mM VPA (p-value=0.5615) (2), and after puromycin selection of T-MSCs (p-value=0.0700) (3), inferred from percentage differences between absorbance measurements employing CCK-8 (measurement wavelength: 450 nm; reference wavelength: 650 nm). Absorbance measurements were performed for three independent SV40LT transduction experiments (n=3). VPA: valproic acid.

2. Verification of SV40LT and eGFP-hTERT expression in transduced MSCs

In order to prove that iMSCs were properly transduced and expressed both transgenes, SV40LT and GFP (fused to hTERT) immunofluorescence was performed. Expression of both transgenes was detected in the nuclei of iMSC#6, #8, #9, #10, #12 and #13. Immunostained SV40LT was identified by red fluorescence, and eGFP-hTERT was identified by green fluorescence. SV40LT exhibited a "nucleolar exclusion" expression pattern, while eGFP-hTERT showed a more variable pattern, with differences in intensity and location, including strong nucleolar signals and diffuse nucleoplasmic signals (**Figure 13**).

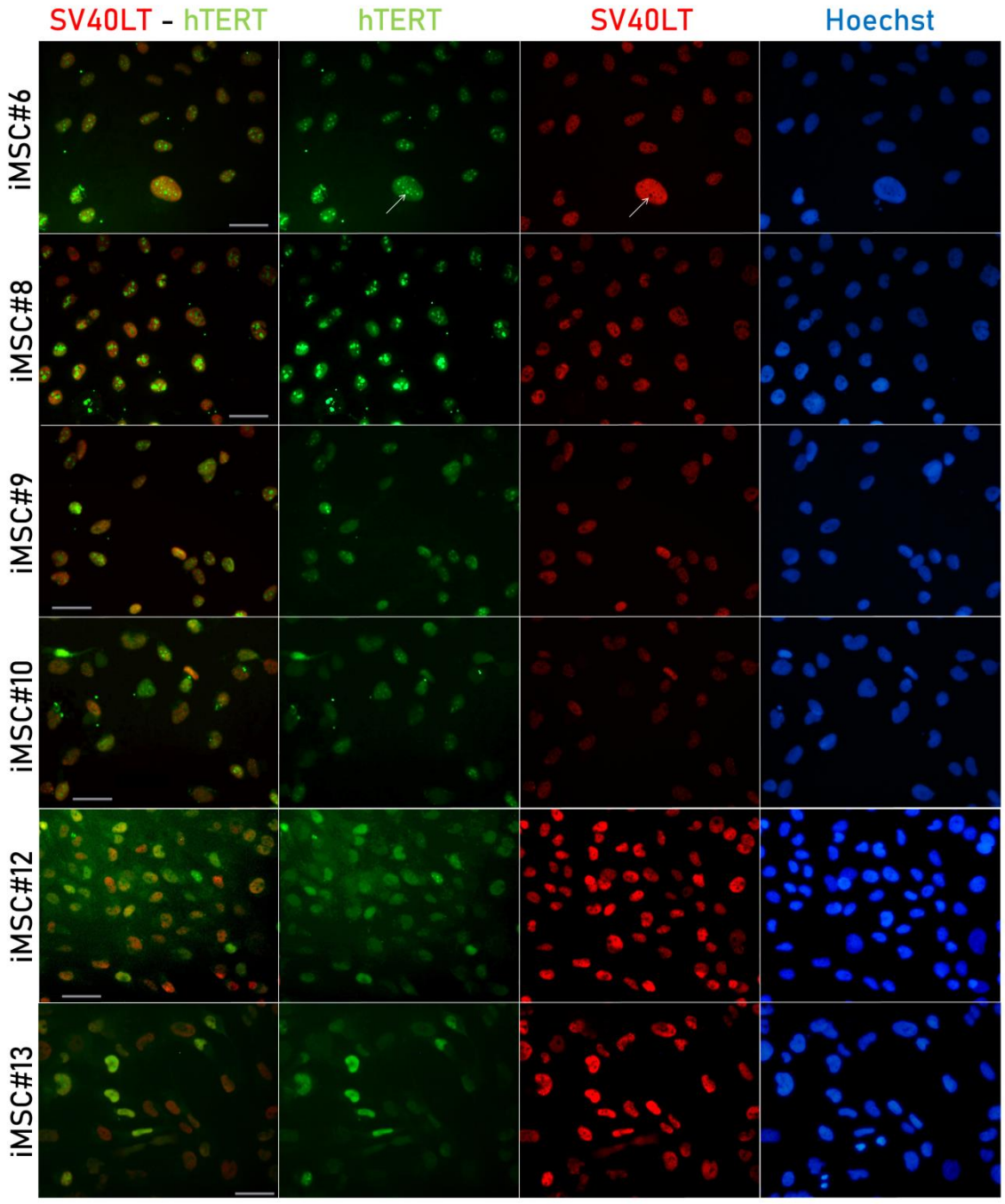

Figure 13. SV40LT and eGFP-hTERT immunostaining of iMSC#6, #8, #9, #10, #12 and #13. SV40LT is shown in red, eGFP-hTERT is shown in green and Hoechst staining is shown in blue. Both nucleoli exclusion of SV40LT and nucleoli association of hTERT in iMSC#6 are marked with white arrows. Scale bar: 50 μm.

In addition, the expression of SV40LT and hTERT was detected in all iMSC lines and not detected in any of the primary parental MSCs by qPCR. RELs of SV40LT and hTERT in iMSC lines are shown in **Table 6**.

Table 6. Relative expression levels (RELs) of SV40LT and hTERT in all iMSC lines. iMSC: immortalized mesenchymal stromal cell; SV40LT: Simian virus 40 large T antigen; hTERT: human telomerase reverse transcriptase.

	iMSC#6	iMSC#8	iMSC#9	iMSC#10	iMSC#12	iMSC#13
SV40LT	0.549±0.022	0.422±0.010	0.285±0.040	0.186±0.021	1.000±0.266	0.775±0.352
hTERT	0.609±0.034	1.000±0.149	0.228±0.017	0.007±0.000	0.168±0.033	0.008±0.002

3. Analysis of the morphology and SA-ß-Gal activity of transduced MSCs

iMSCs displayed a fibroblast-like cell morphology (**Figure 14a**) characteristic of MSCs, with more prominent nucleoli and less cytoplasm than T-MSCs (**Figure 14b**) and primary MSCs at the 4th passage (**Figure 14c**). All iMSC lines showed almost no SA-ß-Gal activity after more than 40 passages (**Figure 15a-f**), the percentage of SA-ß-Gal-positive cells being 2.5±1.1% for iMSC#6, 0.5±0.1% for iMSC#8, 0.8±0.2% for iMSC#9, 2.4±0.8% for iMSC#10, 2.5±0.6% for iMSC#12 and 1.8±0.3 for iMSC#13. Conversely, in two MSC cultures at the 4th passage (derived from two OA patients and one aged non-OA donor), 60% of cells acquired a large and flat morphology and were positive for SA-ß-Gal (**Figure 15g-h**). Regarding SA-ß-Gal activity, significant differences were found between iMSC lines and primary MSCs (p-value < 0.0001) (**Figure 16**).

4. Analysis of the proliferative capacity of transduced MSCs

Mean generation time of iMSCs was 2.0±0.6 days for iMSC#6 between passages 20 and 70; 1.7±0.8 days for iMSC#8 between passages 15 and 50; 1.7±0.6 days for iMSC#9 between passages 15 and 50; 2.0±1.0 days for iMSC#10 between passages 10 and 42; 2.2±0.7 days for iMSC#12 between passages 15 and 52; and 2.0±0.7 days for iMSC#13 between passages 13 and 55. Average generation time for all iMSC lines was 2.0±0.7 days (1.9±0.8 days for OA iMSCs and 2.0±0.7 days for non-OA iMSCs). In comparison, the generation time of T-MSC#6 between passages 7 and 13 was 5.0 days, and the generation time of primary MSC#6 at the 3rd and 4th passages was almost 20.0 days. No significant differences were found between OA and non-OA iMSCs regarding generation time (p-value=0.1345).

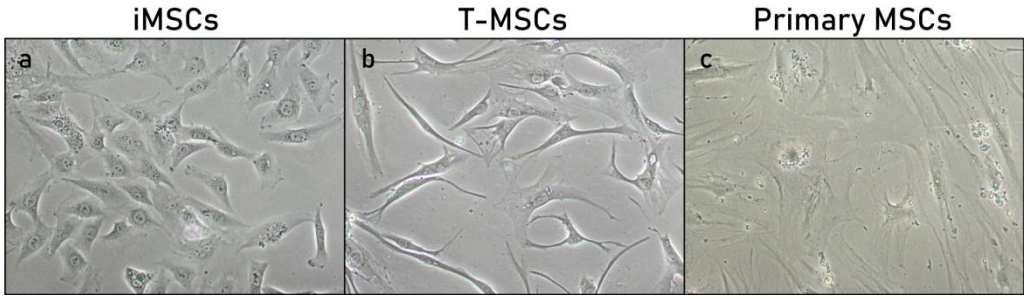

Figure 14. Phase contrast microscopic images of iMSCs (a), T-MSCs (b) and primary MSCs (c). Magnification: 10X. iMSC: immortalized MSC; T-MSC: SV40LT-transduced MSC; MSCs: mesenchymal stromal cells.

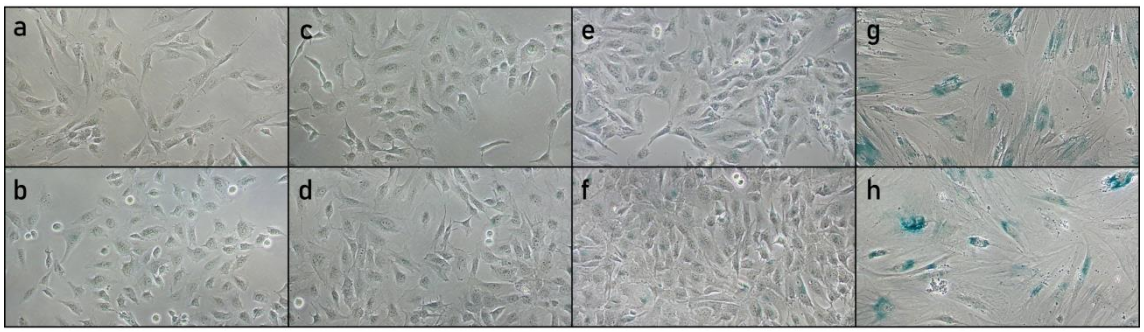

Figure 15. Phase contrast microscopic images of the SA-ß-Gal stained iMSC#6 (a), #8 (b), #9 (c), #10 (d), #11 (e), #12 (f) and primary OA (g) and non-OA (h) MSCs. SA-ß-Gal activity is shown in blue. Magnification: 10X. SA-ß-Gal: senescence-associated ß-galactosidase; iMSC: immortalized MSC; OA: osteoarthritis; MSCs: mesenchymal stromal cells.

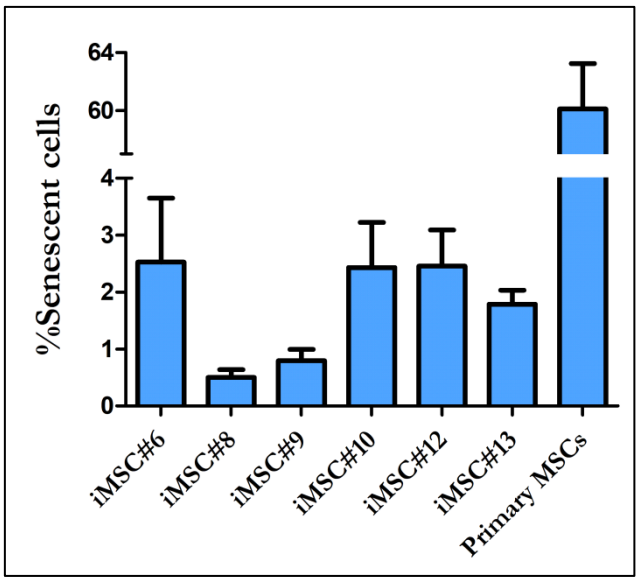

Figure 16. Percentage of SA-ß-Gal-positive senescent cells for each iMSC line and primary MSCs. The error bars represent the standard deviation of measurements at three passages of each iMSC line (n=3) and three different cultures of primary MSCs at the 4th passage (n=3). Significant differences were found between iMSC lines and primary MSCs (p-value <0.0001).

All iMSC lines (#6, #8, #9, #10, #12 and #13) were grown over 100 PDs for more than six months. Regression analysis showed a constant proliferation rate, with a multiple correlation coefficient R>0.95 (**Figure 17**) for all six iMSC lines and a p-value <0.0001.

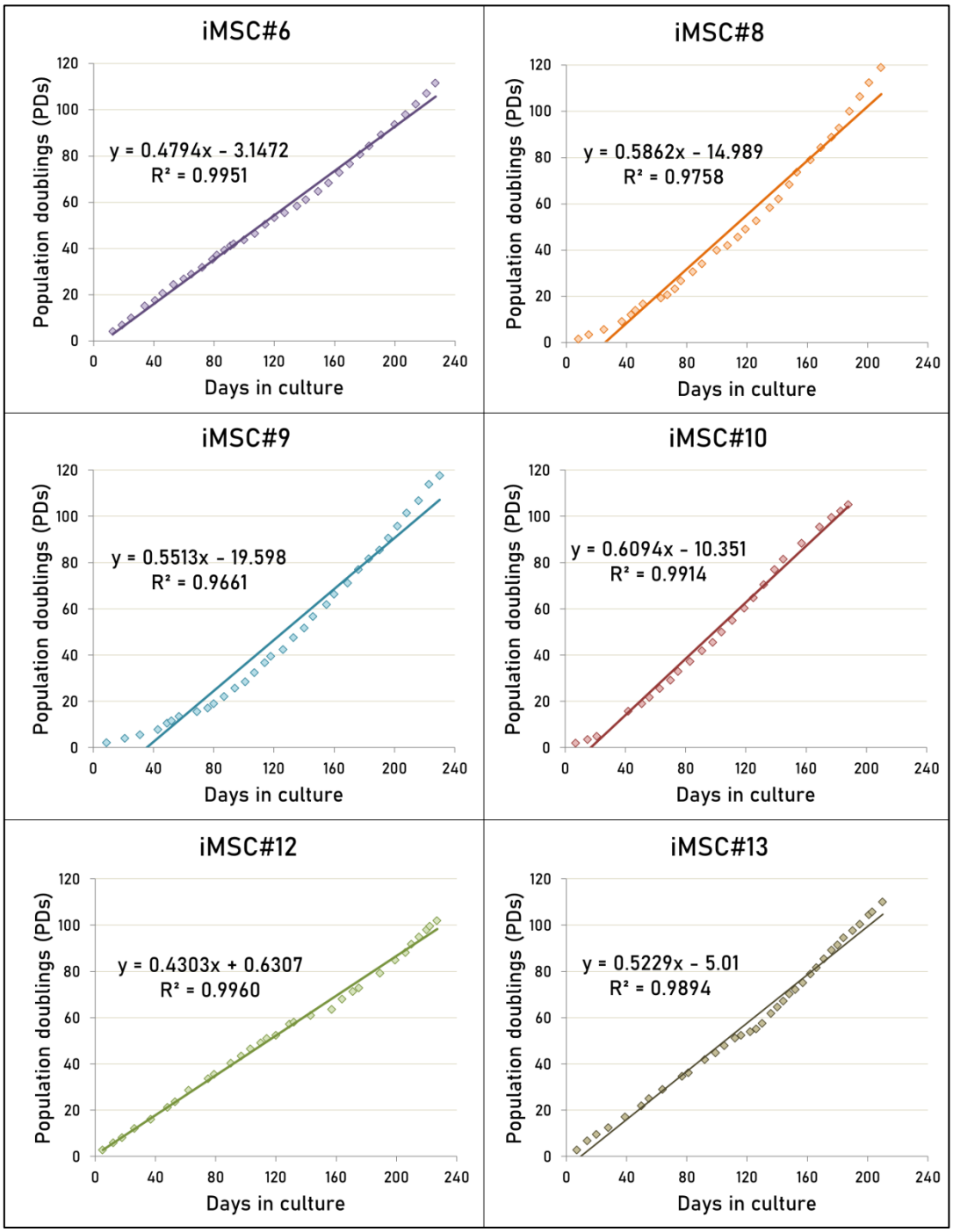

Figure 17. Number of PDs accumulated by iMSC#6, #8, #9, #10, #11 and #12 against days in culture. PDs were calculated as (log *Nf* – log *Ni*)/log 2 (where *Nf* is the final cell population, *Ni* is the number of cells in the inoculum and log is the natural logarithm). PDs: population doublings; iMSC: immortalized mesenchymal stromal cell.

PCNA gene expression was increased in iMSCs compared with primary MSCs (p-value=0.0022) (**Figure 18**), but no significant differences were found between OA and non-OA iMSCs (p-value=1.0000).

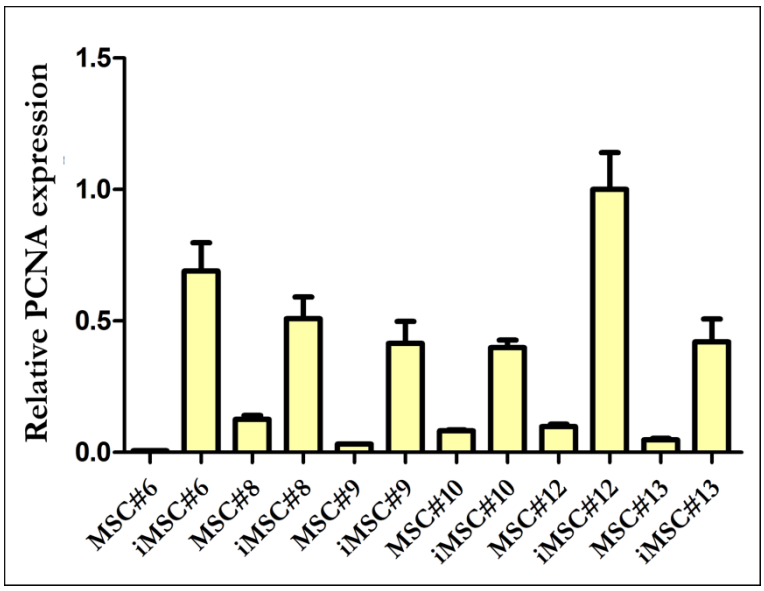

Figure 18. PCNA RELs in primary and immortalized undifferentiated MSCs. PCNA: proliferating cell nuclear antigen; MSC: mesenchymal stromal cell; iMSC: immortalized MSC.

5. Mesenchymal surface marker expression analysis in transduced MSCs

The expression of five mesenchymal (CD29, CD44, CD73, CD90 and CD105) and two hematopoietic (CD34 and CD45) surface markers was analysed in primary MSCs, T-MSCs, iMSCs and immortalized MSC line 3a6. In all cases, >90% of the cells were positive for CD29, CD44 and CD90. T-MSCs showed lower CD73 expression than their primary parental cells and their immortalized hTERT-transduced counterparts. In primary MSCs and iMSCs, >90% of the cells were positive for CD73, except for MSC#12 and all its transduction states and late-passage iMSC#13. CD105 expression was reduced from primary MSCs to iMSCs in cell lines #6 and #8, but increased in cell lines #10 and #12. Moreover, it was reduced in late- versus early-passage iMSCs in cell lines #6, #8, #12 and #13, but increased in cell lines #9 and #10. Two iMSC lines, #8 and #9, showed lower CD105 positivity than immortalized MSC line 3a6, whereas the remaining four iMSC lines (#6, #10, #12 and #13) showed higher positivity. In all cases, <3% of the cells were positive for hematopoietic markers CD34 and CD45, except for primary MSCs #6 and #8, in which almost 10% were positive for CD34 (**Table 7**).

Table 7. Mesenchymal and hematopoietic surface marker expression in primary MSCs, T-MSCs, iMSCs at early and late passages and immortalized MSC line 3a6. Passage is shown as the sum of the number of passages as (1) primary MSCs, (2) T-MSCs and (3) iMSCs. Data from MSC#13 and T-MSC#13 could not be obtained due to cell number limitations. MSC: mesenchymal stromal cell; T-MSC: SV40LT-transduced MSC; iMSC: immortalized MSC.

Cells	Passage	CD29	CD44	CD73	CD90	CD105	CD34	CD45
MSC#6	4	99.2%	99.6%	98.4%	96.2%	85.2%	9.9%	0.1%
T-MSC#6	(4+3)	99.0%	98.9%	96.2%	99.1%	82.3%	1.5%	0.4%
iMSC#6	(4+9+6)	99.2%	98.9%	98.0%	98.3%	81.0%	0.1%	0.0%
iMSC#6 (PD>100)	(4+9+44)	98.2%	98.9%	97.1%	99.5%	73.8%	0.0%	0.0%
MSC#8	4	98.6%	99.4%	98.3%	98.9%	91.6%	9.8%	0.0%
T-MSC#8	(4+4)	93.9%	92.7%	86.3%	95.0%	46.0%	0.4%	0.1%
iMSC#8	(4+2+15)	99.9%	99.6%	99.6%	99.0%	42.1%	0.0%	0.1%
iMSC#8 (PD>100)	(4+2+32)	98.8%	98.8%	98.7%	99.1%	38.4%	0.4%	0.2%
MSC#9	4	96.3%	97.0%	95.5%	96.2%	42.2%	0.6%	0.3%
T-MSC#9	(4+4)	98.4%	97.9%	69.6%	95.5%	71.7%	0.1%	0.2%
iMSC#9	(4+2+15)	98.4%	95.7%	97.3%	92.5%	37.3%	0.2%	0.4%
iMSC#9 (PD>100)	(4+2+35)	98.8%	98.4%	98.7%	99.3%	44.6%	0.9%	0.9%
MSC#10	4	97.9%	97.5%	93.0%	98.7%	76.0%	0.6%	0.3%
T-MSC#10	(4+2)	98.5%	98.1%	85.4%	97.4%	73.7%	0.0%	1.0%
iMSC#10	(4+3+14)	98.9%	98.9%	92.8%	99.1%	74.0%	0.4%	0.2%
iMSC#10 (PD>100)	(4+3+31)	98.4%	98.8%	93.9%	98.4%	82.4%	0.3%	2.7%
MSC#12	3	93.3%	95.2%	71.1%	98.5%	69.8%	0.2%	1.9%
T-MSC#12	(3+4)	98.1%	98.9%	58.7%	98.4%	77.0%	2.1%	0.8%
iMSC#12	(3+4+12)	97.4%	96.8%	85.6%	99.5%	80.1%	0.0%	0.0%
iMSC#12 (PD>100)	(3+4+43)	97.8%	99.3%	82.1%	96.5%	78.1%	0.7%	0.2%
iMSC#13	(3+3+13)	99.3%	99.4%	98.8%	99.9%	97.7%	0.3%	0.9%
iMSC#13 (PD>100)	(3+3+44)	97.9%	98.2%	86.1%	98.3%	90.2%	0.5%	0.6%
3a6	Unknown	99.2%	99.8%	98.0%	98.3%	61.7%	0.1%	0.0%

6. Study of the preservation of MSC multipotency in transduced MSCs

In order to investigate whether transduced MSCs retained multipotency, primary MSCs, T-MSCs and iMSCs were cultured under osteogenic, adipogenic and chondrogenic differentiation conditions, and cell differentiations were evaluated by histological and molecular analysis. Furthermore, the expression of OCT4B1, a splice variant of transcription factor OCT4 related with multipotency, was analysed in undifferentiated iMSCs and their primary parental MSCs. For molecular analysis, YWHAZ was employed as the reference gene, since it was the most stable of the candidate genes tested, as determined by geNorm (**Annex IV**).

6.1 Multipotency

Expression of OCT4B1 was detected in both primary and immortalized MSCs by qPCR. OCT4B1 expression was increased in iMSCs compared with primary MSCs (p-value= 0.0286), but no significant differences were found between OA and non-OA iMSCs (p-value= 0.2000). RELs of OCT4B1 in primary MSCs and iMSCs are shown in **Figure 19**. Its expression could not be analysed in MSC#8 and MSC#9 due to cell number limitations.

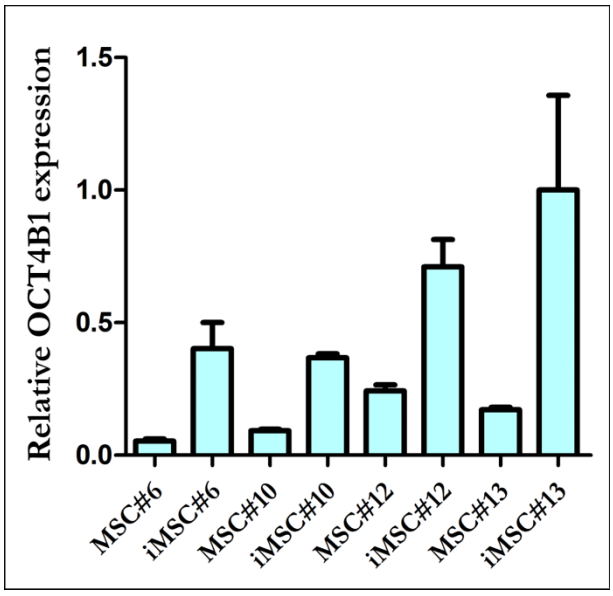

Figure 19. OCT4B1 RELs in primary and immortalized undifferentiated MSCs. OCT4B1: POU class 5 homeobox 1 (POU5F1) transcript variant 4; MSC: mesenchymal stromal cell; iMSC: immortalized MSC.

6.2 Osteogenesis

All primary MSCs, T-MSCs and iMSCs tested were able to differentiate into the osteogenic lineage after 21 days of induction. Primary, T-MSC and iMSC osteogenic potentials were compared in cell lines #6 (OA) and #12 (non-OA) by Alizarin Red staining, which stains calcium phosphate deposits red. In cell line #6, a lower mineralization area after osteogenic induction was detected in primary MSC#6 (6th passage) (**Figure 20a**). The mineralized area was twice as large in T-MSC#6 (12th passage) (**Figure 20b**) and four times as large in iMSC#6 (65th passage) (**Figure 20c**) as in MSC#6, and no mineralization was detected in control cells cultured in 20%FBS/DMEM (**Figure 20 d-f**).

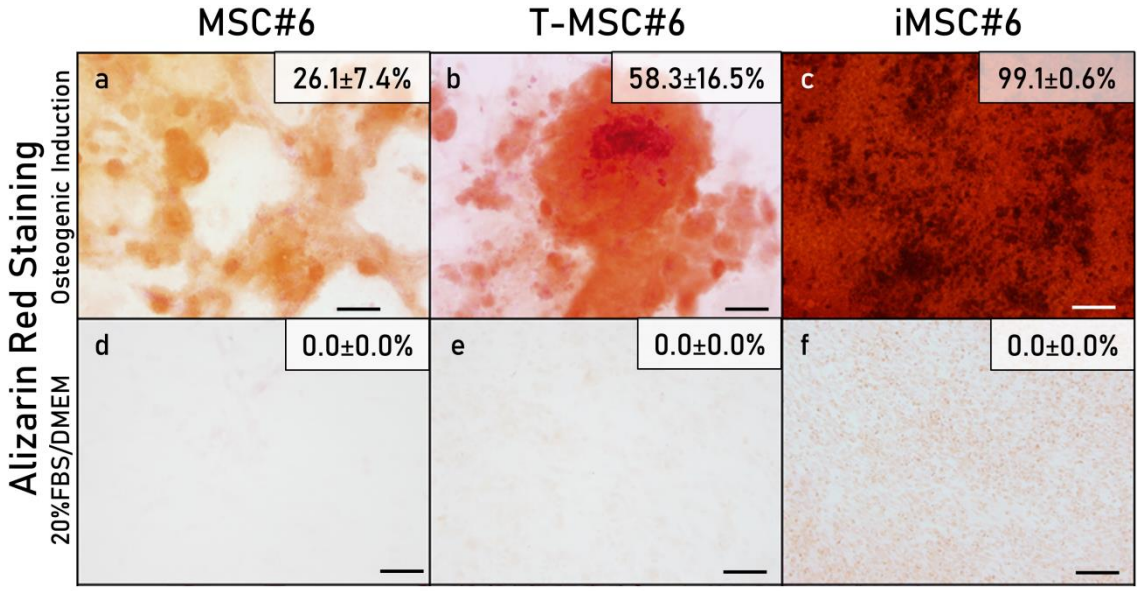

Figure 20. Alizarin Red staining of primary OA MSC#6, T-MSC#6 and iMSC#6 after 21 days of osteogenic induction (a-c) or culture in 20%FBS/DMEM (d-f). Percentage of Alizarin Red stained area for each sample is shown. Scale bar: 100 μm.

In cell line #12, the mineralized area was similar between MSC#12 (4th passage) (**Figure 21a**) and T-MSC#12 (8th passage) (**Figure 21b**) and moderately larger in iMSC#12 (50th passage) (**Figure 21c**). No mineralization was detected in MSC#12 cultured in 20%FBS/DMEM (**Figure 21d**), but a certain degree of mineralization was found in the T-MSC#12 control (**Figure 21e**), while iMSC#12 cultured in control medium were only slightly positive for Alizarin Red (**Figure 21f**).

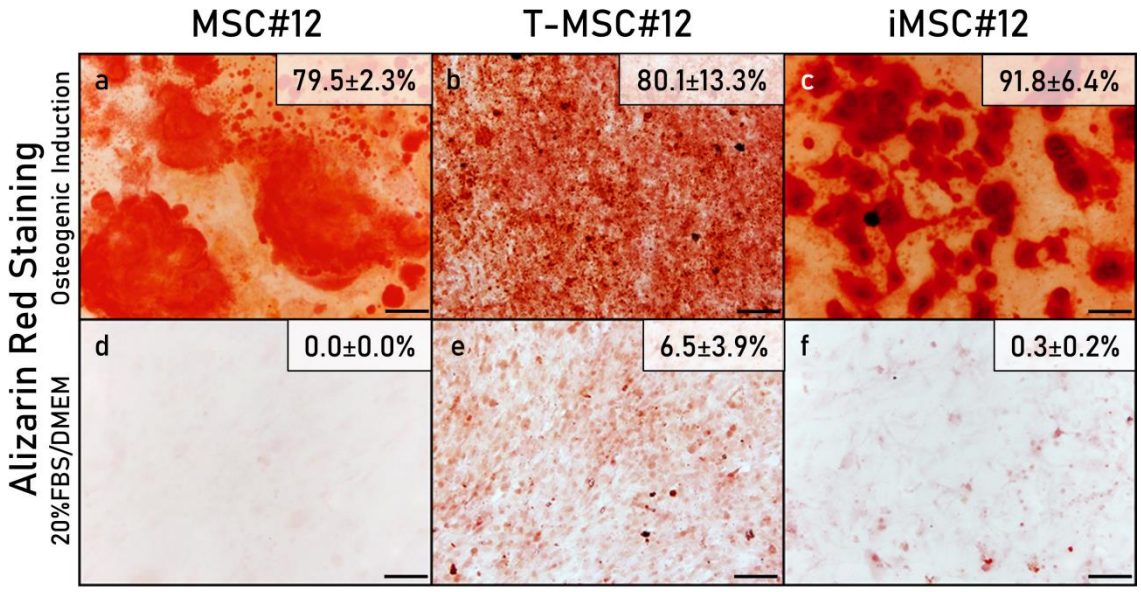

Figure 21. Alizarin Red staining of primary non-OA MSC#12, T-MSC#12 and iMSC#12 after 21 days of osteogenic induction (a-c) or culture in 20%FBS/DMEM (d-f). Percentage of Alizarin Red stained area for each sample is shown. Scale bar: 100 μm.

Furthermore, osteogenic-related gene expression was compared in primary, T-MSCs and iMSCs in cell lines #10 (OA) and #12 (non-OA). In both cell lines, the highest expression of osteocalcin (OCN) was detected in iMSCs. In cell line #10, when cells were cultured under osteogenic stimuli, Runx2 expression was higher in iMSCs than in T-MSCs and higher in T-MSCs than in MSCs, but the highest Sp7 expression was detected in T-MSCs. Conversely, in cell line #12, Runx2 expression was higher in MSCs than in T-MSCs and iMSCs, but the highest Sp7 expression was detected in iMSCs (**Figure 22**).

Osteogenic potential of all iMSC lines was studied by Alizarin Red staining and molecular analysis following culture under osteogenic conditions after reaching more than 100 PDs. iMSC lines #6 (**Figure 23a**), #8 (**Figure 23b**) and #9 (**Figure 23c**) showed the largest areas stained by Alizarin Red, while iMSC lines #10 (**Figure 23d**), #12 (**Figure 23e**) and #13 (**Figure 23f**) showed small zones of weaker mineralization. When comparing osteogenesis-related expression among the six iMSC lines, iMSC#8 showed the highest expression of OCN and iMSC#12 showed the highest expression of transcription factors Runx2 and Sp7 (**Figure 24**).

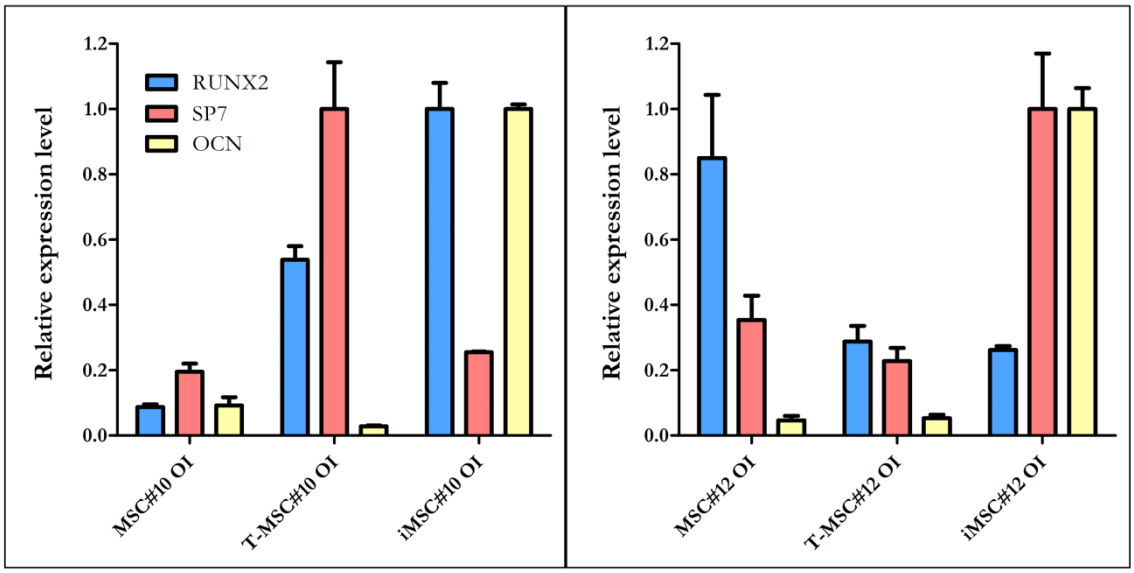

Figure 22. Runx2, Sp7 and OCN RELs in primary MSCs, T-MSCs and iMSCs #10 (OA) and #12 (non-OA). Runx2: Runt-related transcription factor 2; Sp7: Sp7 transcription factor (osterix); OCN: bone gamma-carboxyglutamate protein (osteocalcin); OI: osteogenic induction.

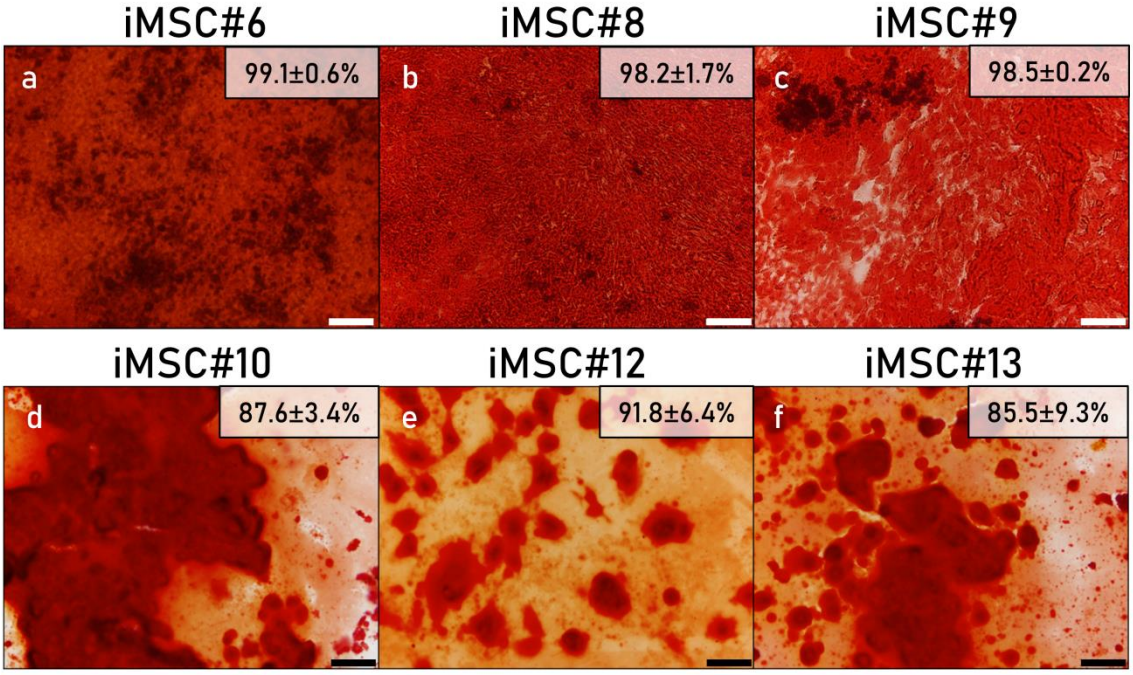

Figure 23. Alizarin Red staining of iMSC lines #6 (a), #8 (b), #9 (c), #10 (d), #12 (e) and #13 (f) after 21 days of osteogenic induction. Percentage of Alizarin Red stained area for each sample is shown. Scale bar: 100 μm.

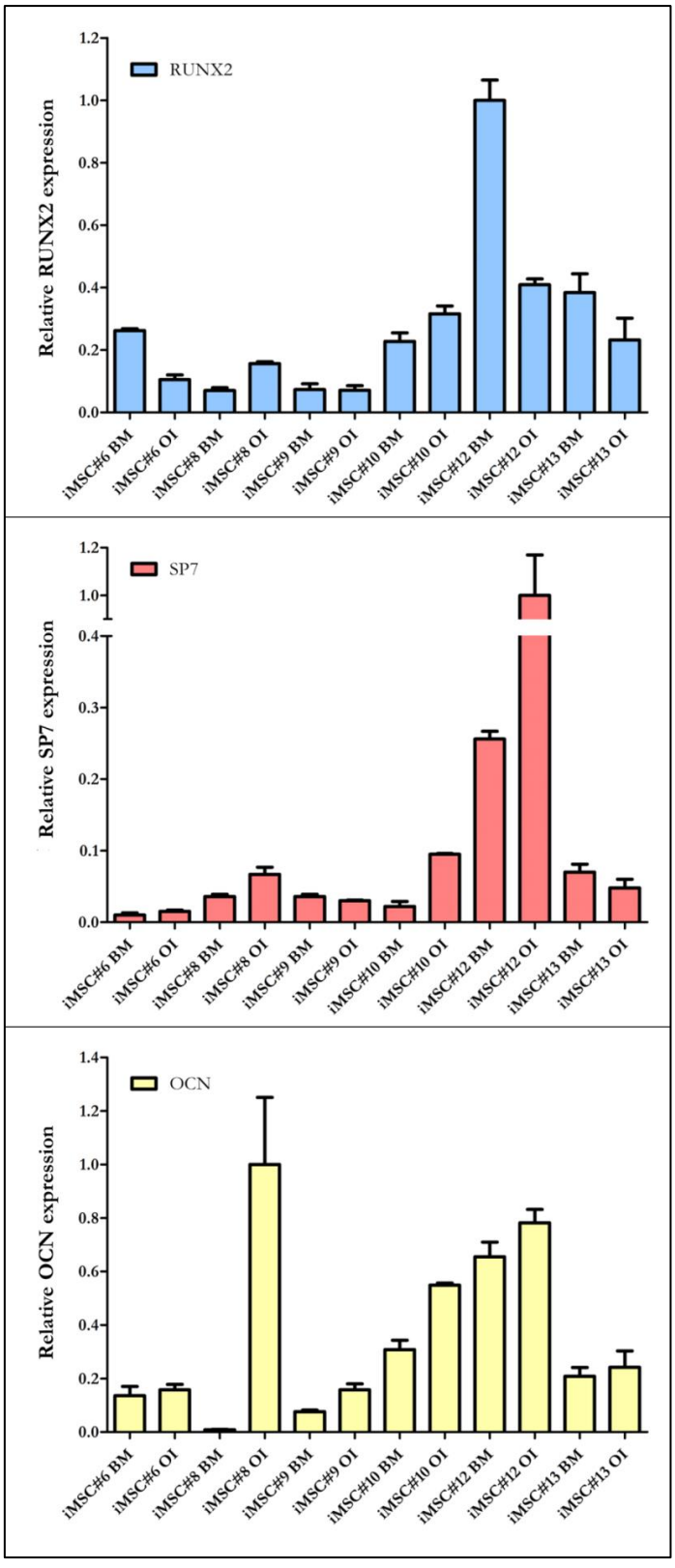

Figure 24. Runx2, Sp7 and OCN RELs in all iMSC lines. Runx2: Runt-related transcription factor 2; Sp7: Sp7 transcription factor (osterix); OCN: bone gamma-carboxyglutamate protein (osteocalcin); iMSC: immortalized mesenchymal stromal cell; BM: basal medium; OI: osteogenic induction.

Three iMSC lines, #6, #9 and #10, were also able to differentiate into the osteogenic lineage after induction in three-dimensional cell culture. iMSC lines #6 and #9 presented a threefold increase in Alizarin Red staining intensity (measured as OD) after differentiation in comparison with the 20%FBS/DMEM control (**Figure 25 a-d**). In contrast, iMSC#10 showed the same intensity after osteogenic induction and after culture in 20%FBS/DMEM because of the high mineralization of the control sample (**Figure 25 e-f**). All iMSC lines presented higher Von Kossa staining intensities after EO than their respective controls (**Figure 25 g-l**). Proteoglycans were not detected in iMSCs aggregates after either osteogenic induction or culture in 20%FBS/DMEM for five weeks (**Figure 25 m-r**). No significant increase or decrease in the amount of collagen fibres was detected after differentiation in comparison with five-week culture in 20%FBS/DMEM (**Figure 25 s-x**), with the exception of iMSC#9.

In addition, three clones (A, B and C) were isolated from iMSC lines #6, #8, #9 and #10, and their osteogenic potential was analysed by osteogenic induction and Alizarin Red staining. All clones were capable of forming a highly mineralized ECM upon osteogenic induction. Some of the clones (#6.C, #8.B, #9.B and #10.A) were capable of spontaneous mineralization to some extent, and one clone (#8.A) spontaneously formed three-dimensional aggregates that stained positive for Alizarin Red (**Figure 26**).

6.3 Adipogenesis

Primary, T-MSC and iMSC adipogenic potentials were compared in cell lines #6 (OA) and #12 (non-OA) by Oil Red O staining, which stains intracellular lipid droplets red. In cell line #6, primary MSC#6 showed the highest potential to differentiate into the adipogenic lineage after 21 days of induction (**Figure 27a**). T-MSC#6 showed a 50% reduction of the stained area in comparison with primary MSC#6, and few pre-adipocytes could be identified (**Figure 27b**). iMSC#6 retained the adipogenic differentiation potential, but the pre-adipocytes formed, although clearly identifiable, were less mature than those formed by primary MSC#6 and contained smaller lipid vacuoles (**Figure 27c**). Consistently, iMSC#6 showed a 70% reduction of the stained area compared with primary MSC#6. MSC#6 cultured in 20%FBS/DMEM were not stained with Oil Red O (**Figure 27d**), but positive staining was observed in controls T-MSC#6 (**Figure 27e**) and iMSC#6 (**Figure 27f**), suggesting some spontaneous adipogenic differentiation.

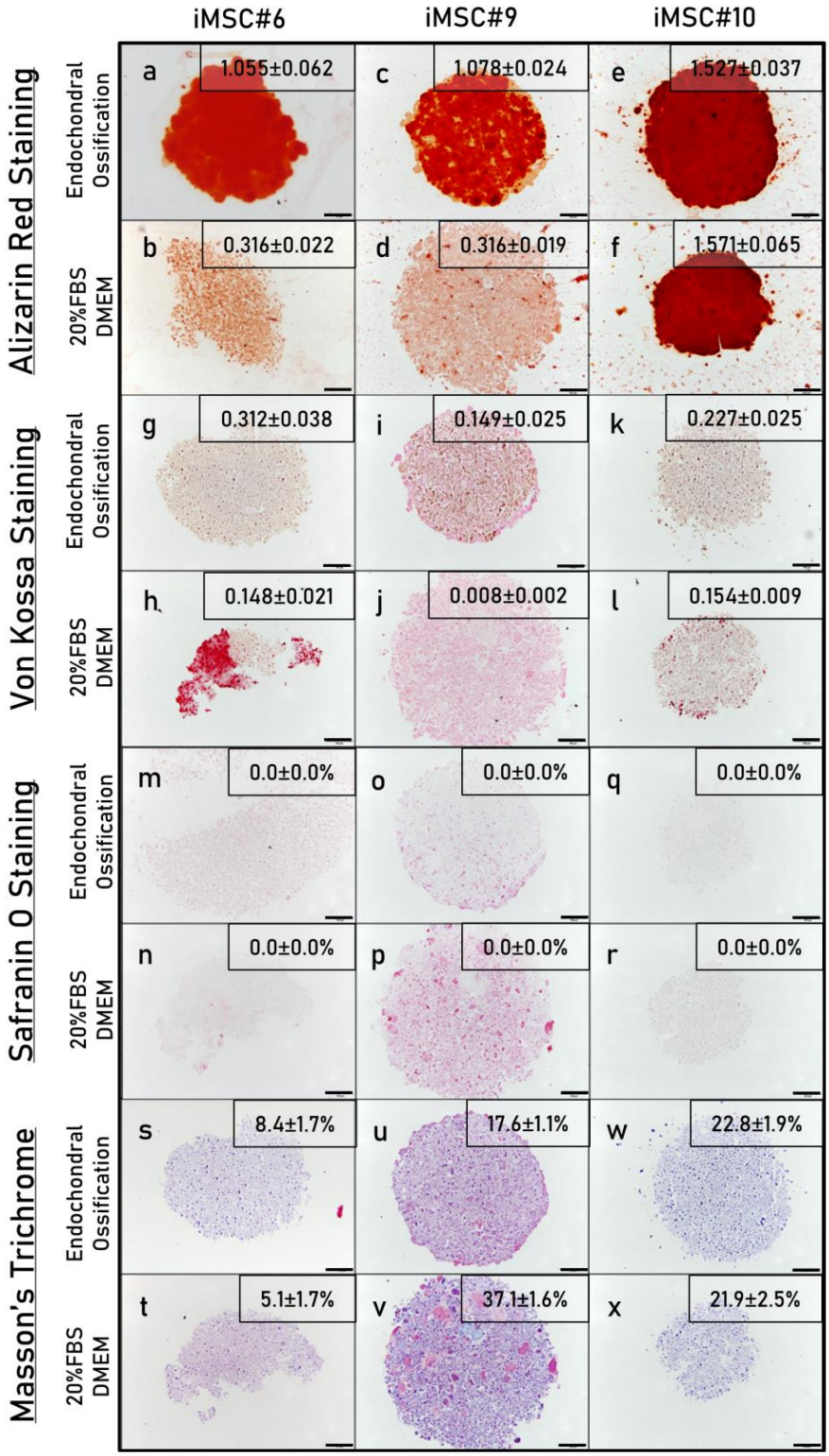

Figure 25. Alizarin Red staining (a-f), Von Kossa staining (g-l), Safranin O staining (m-r) and Masson's Trichrome staining (s-x) of iMSC#6, #9 and #10 after 3D osteogenic induction or five-week culture in 20%FBS/DMEM. Scale bar: 100 μm. Quantification is shown for each sample as percentage of stained area or optical density (OD).

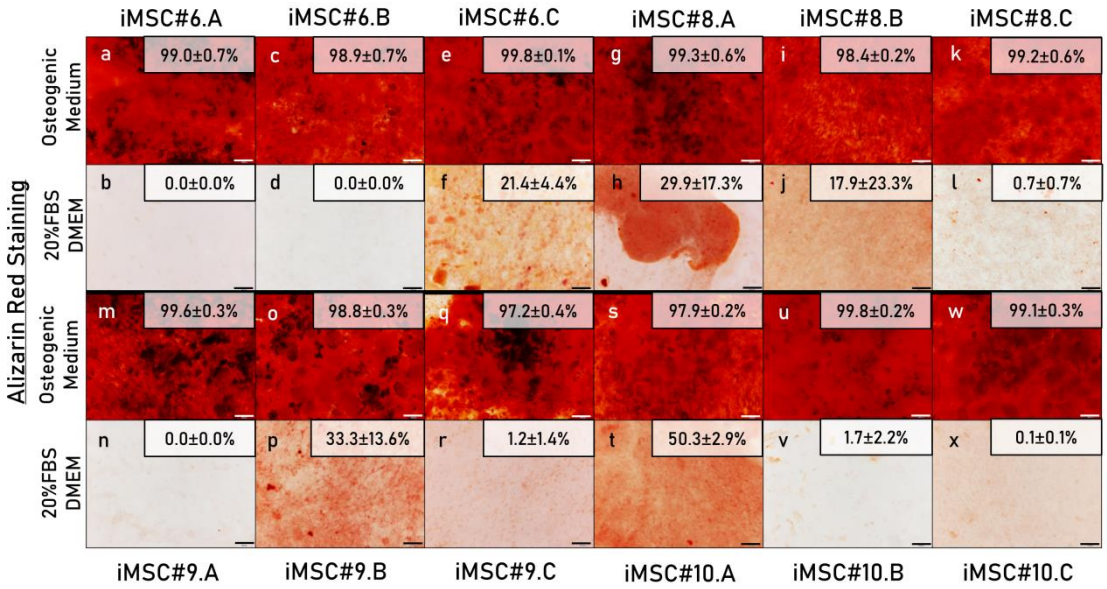

Figure 26. Alizarin Red staining of iMSC-derived clones after 21 days of osteogenic induction. Scale bar: 100 μm.

In cell line #12, primary MSCs (**Figure 28a**) showed a level of Oil Red O staining lower than T-MSCs (**Figure 28b**) and similar to iMSCs (**Figure 28c**), even though adipocytes formed by primary MSCs were more mature in appearance, while those formed by T-MSC#12 and iMSC#12 contained smaller lipid vacuoles (**Figure 28c**). Primary MSC#12, T-MSC#12 and iMSC#12 were barely stained with Oil Red O after culture in 20%FBS/DMEM (**Figure 28 d-f**). Adipogenic-related gene expression was compared in primary, T-MSCs and iMSCs in cell lines #6 (OA) and #12 (non-OA). In cell line #6, the highest RELs of APN and FABP4 were found in primary MSCs, and the lowest levels were found in iMSCs. Conversely, in cell line #12, the highest RELs of both adipogenesis-related genes were found in iMSCs. FABP4 was similarly expressed in MSC#12 and T-MSC#12, while APN was more expressed in primary MSC#12 (**Figure 29**).

The adipogenic potential of all iMSC lines was studied by Oil Red O staining and molecular analysis following culture under adipogenic conditions after reaching more than 100 PDs. All iMSC lines were capable of adipogenic differentiation, but lipid droplets were not formed in all cells, and the adipocytes formed seem immature (**Figure 30**). iMSC lines #8 (**Figure 30b**) and #10 (**Figure 30d**) showed the highest percentages of Oil Red O-stained area, with values similar to those of T-MSCs #6 (**Figure 27b**) and #12 (**Figure 28b**). When comparing the expression of APN and FABP4 among the six iMSC lines, iMSC#10 showed the highest

expression of both adipogenic markers, while iMSC lines #6, #8 and #9 showed very low levels of both genes (**Figure 31**).

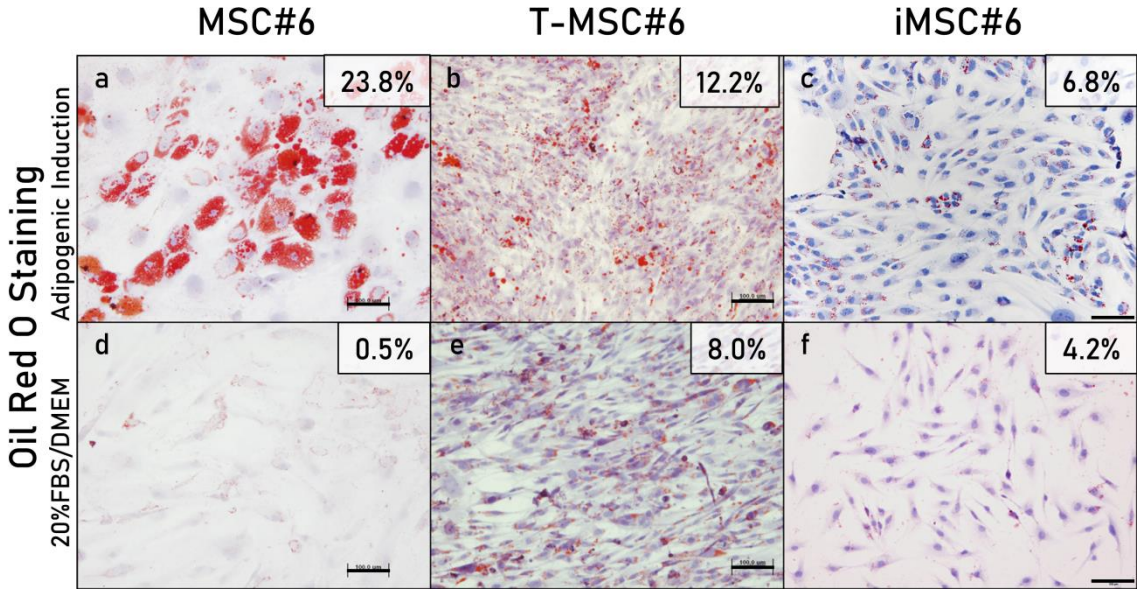

Figure 27. Oil Red O staining of primary MSC#6, T-MSC#6 and iMSC#6 after 21 days of adipogenic induction (a-c) or culture in 20%FBS/DMEM (d-f). Percentage of Oil Red O-stained area for each sample is shown. Scale bar: 50 μm.

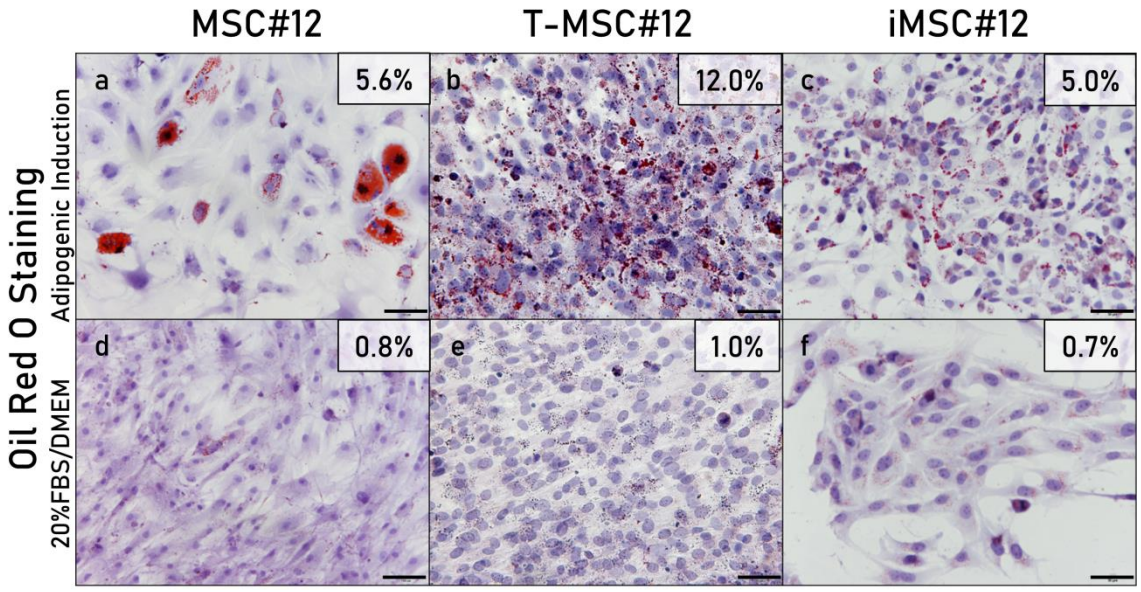

Figure 28. Oil Red O staining of primary MSC#12, T-MSC#12 and iMSC#12 after 21 days of adipogenic induction (a-c) or culture in 20%FBS/DMEM (d-f). Percentage of Oil Red O-stained area for each sample is shown. Scale bar: 50 μm.

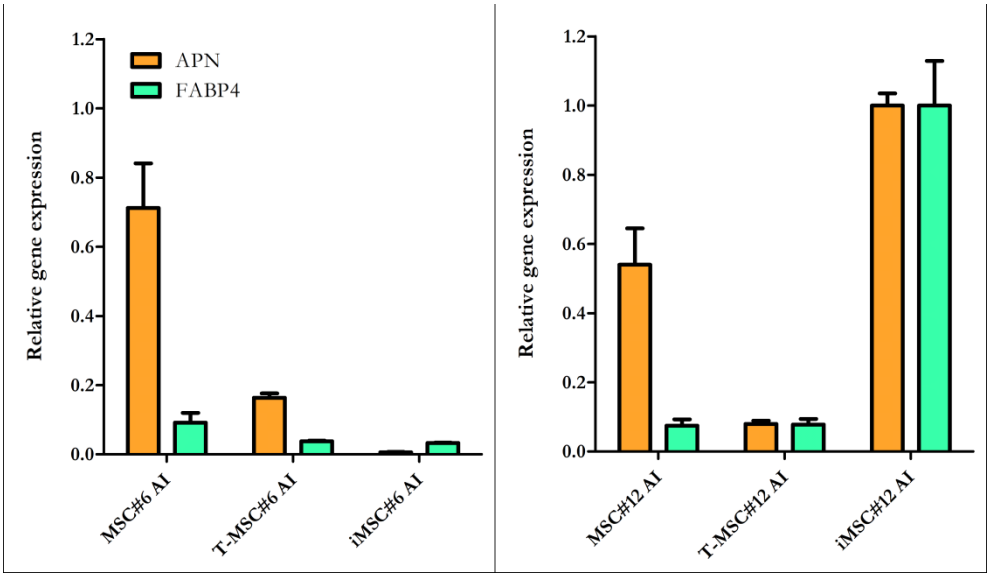

Figure 29. APN and FABP4 RELs in primary MSCs, T-MSCs and iMSCs #6 and #12. APN: adiponectin; FABP4: fatty acid-binding protein 4; AI: adipogenic induction.

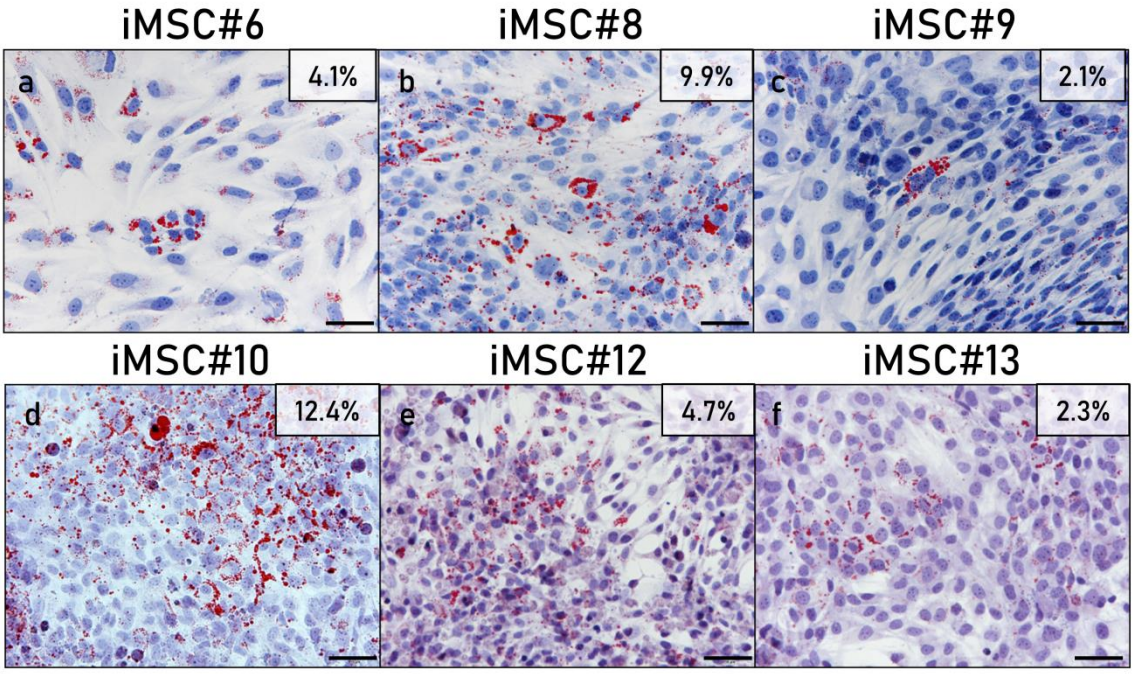

Figure 30. Oil Red O staining of iMSC#6 (a), #8 (b), #9 (c), #10 (d), #12 (e) and #13 (f). Percentage of Oil Red O-stained area for each sample is shown. Scale bar: 50 μm.

6.4 Chondrogenesis

Two iMSC lines, #6 (OA) and #9 (non-OA), as well as T-MSC#6, were cultured under chondrogenic differentiation conditions. Both T-MSC#6 (11th passage) and iMSC#6 (25th passage) were able to differentiate into the chondrogenic lineage after

21 days of induction in three-dimensional cell culture. Histological staining indicated the presence of proteoglycans (stained orange by Safranin O staining; **Figure 32a-b**) and collagen (stained blue by Masson's Trichrome staining; **Figure 32c-d**) in the ECM of the aggregates. Strong aggrecan immunostaining was observed in both T-MSC#6 (**Figure 32e**) and iMSC#6 (**Figure 32f**) aggregates, being almost twice as intense in iMSC#6. Type II collagen immunostaining was intense in T-MSC#6 aggregates (**Figure 32g**) but faint in iMSC#6 (**Figure 32h**). Cell aggregates showed heterogeneous shapes and sizes (**Figure 32**).

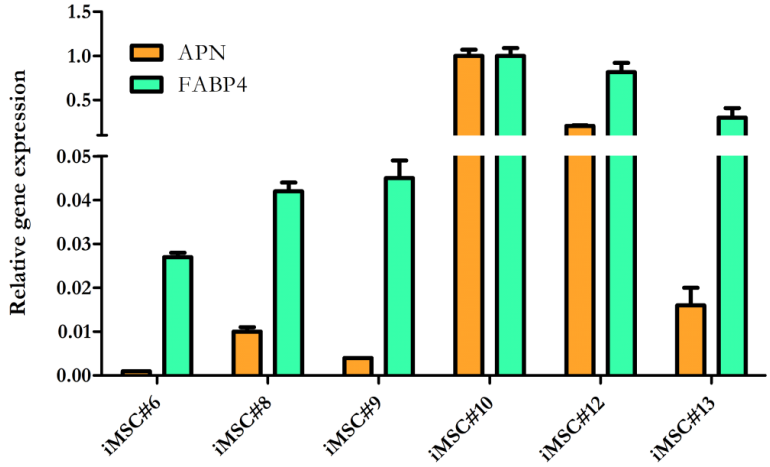

Figure 31. APN and FABP4 RELs in iMSC lines #6, #8, #9, #10, #12 and #13. APN: adiponectin; FABP4: fatty acid-binding protein 4.

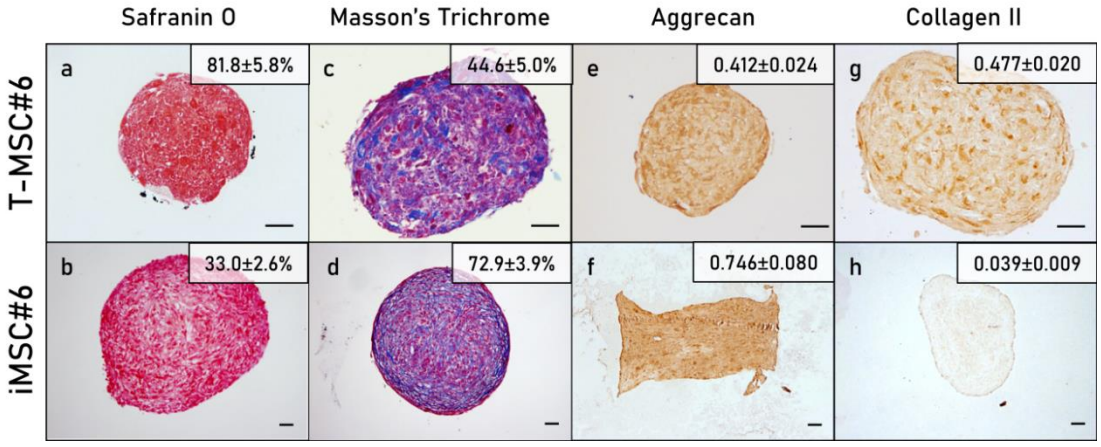

Figure 32. Histochemical and immunohistochemical staining of T-MSC#6 and iMSC#6 aggregates after 21 days of chondrogenic induction: Safranin O staining of T-MSC#6 (a) and iMSC#6 (b); Masson's Thricrome staining of T-MSC#6 (c) and iMSC#6 (d); aggrecan immunostaining of T-MSC#6 (e) and iMSC#6 (f); and type II collagen immunostaining of T-MSC#6 (g) and iMSC#6 (h). Quantification is shown for each sample as the percentage of stained area or optical density (OD). Scale bar: 50 μm.

When compared with their respective controls, both iMSC#6 and iMSC#9 (50th passage) aggregates contained more proteoglycans when chondrogenic differentiation was induced, as shown by orange staining of proteoglycans by Safranin O staining (**Figure 33 a-d**). Greater amounts of collagen were also detected in chondrogenic-induced iMSCs, as shown by the blue staining of collagen fibres by Masson's Trichrome staining (**Figure 33 e-h**). Aggrecan immunostaining was almost four and two times as intense in chondrogenic-induced iMSC#6 and #9, respectively, as in controls (**Figure 33 i-l**). Comparing iMSC#6 and #9, iMSC#6 showed the most intense aggrecan immunostaining after chondrogenic induction, correlating with the highest amount of proteoglycans detected. The amount of total collagen and type II collagen was also higher in iMSC#6. Chondrogenic-induced iMSC#10 and iMSC#13 aggregates were too small to allow for the performance of histological techniques and, therefore, could not be analysed. iMSC#8 and iMSC12 were unable to form aggregates by the hanging drop method employed.

7. Study of the colony-forming ability and oncogenic potential of transduced MSCs

A clonogenic assay was performed to assess the colony formation ability of iMSCs. After one week, all iMSC lines were able to form colonies (**Figure 34**). In addition, a soft agar assay was performed to assess oncogenic potential of iMSCs. After 14 days, two out of six iMSC lines formed colonies in soft agar. Representative micrographs are shown in **Figure 34**. iMSC#6 formed colonies with wide intercellular spaces (**Figure 34a**) and was not able to grow in soft agar (**Figure 34b**). Conversely, iMSC#8 and iMSC#9 formed more compact colonies and were able to grow in soft agar (**Figure 34 c-f**). iMSC#10, #12 and #13 showed a phenotype similar to that of iMSC#6, forming uncompacted colonies and being unable to grow in soft agar (**Figure 34 g-l**).

As for tumour-related gene expression, no significant differences were found in p53 REL between iMSCs and primary MSCs (p-value=0.1727). However, this tumour suppressor was slightly up-regulated in all iMSC lines except for iMSC#8, in comparison with their primary parental cells, and all cell lines showed lower p53 RELs than that of 143B, except for iMSC#12. Following the same trend, tumour suppressor Rb was up-regulated in all iMSC lines, and significant differences were found between iMSCs and their primary parental MSCs (p-value=0.043). Transcription factor E2F, a positive regulator of cell proliferation, was also up-

regulated in all iMSC lines, and significant differences were found between iMSCs and their primary parental MSCs (p-value=0.0022). Both Rb and E2F RELs were higher in iMSCs than in 143B, but no significant differences were found (p-value >0.05). Proto-oncogene RAS was down-regulated in iMSC#8 and up-regulated in iMSC#12, and no significant differences were found between iMSCs and primary MSCs (p-value=0.1320) (**Figure 35**).

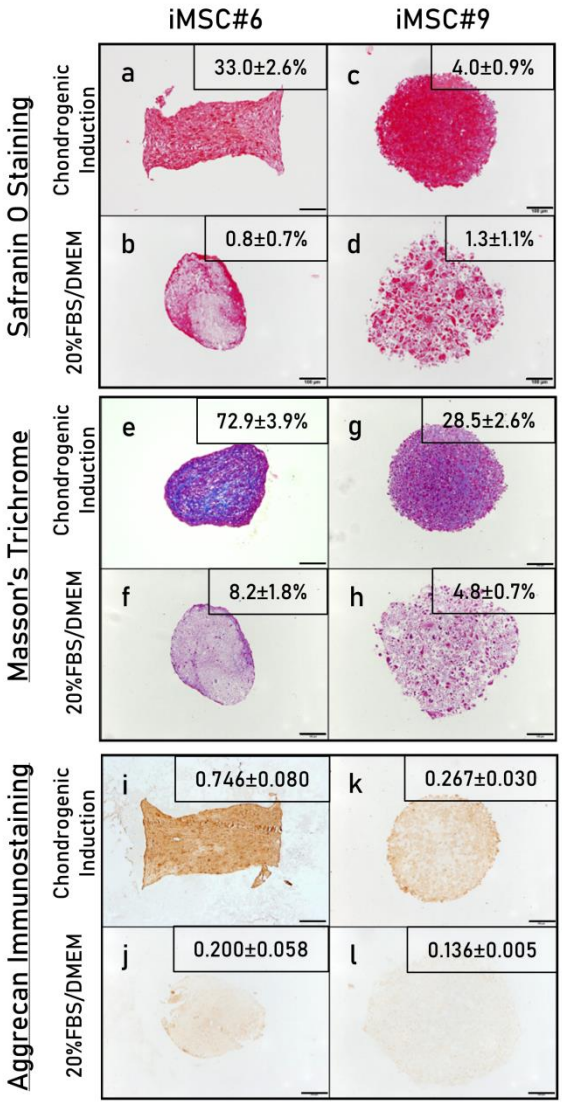

Figure 33. Histochemical and immunohistochemical staining of iMSC#6 and #9 after 21 days of chondrogenic induction or culture in 20%FBS/DMEM: Safranin O staining (a-d), Masson's Trichrome staining (e-h) and aggrecan immunostaining (i-l). Scale bar: 100 μm. Quantification is shown for each sample as percentage of stained area or optical density (OD).

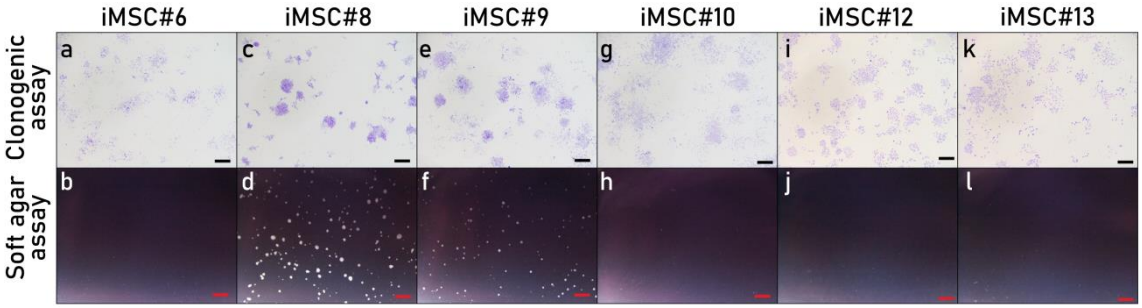

Figure 34. Crystal violet staining to assess the clonogenic potential of iMSC lines (a, c, e, g, i, k) and soft agar assay to assess their oncogenic potential (b, d, f, h, j, l). Scale bar: 1 mm.

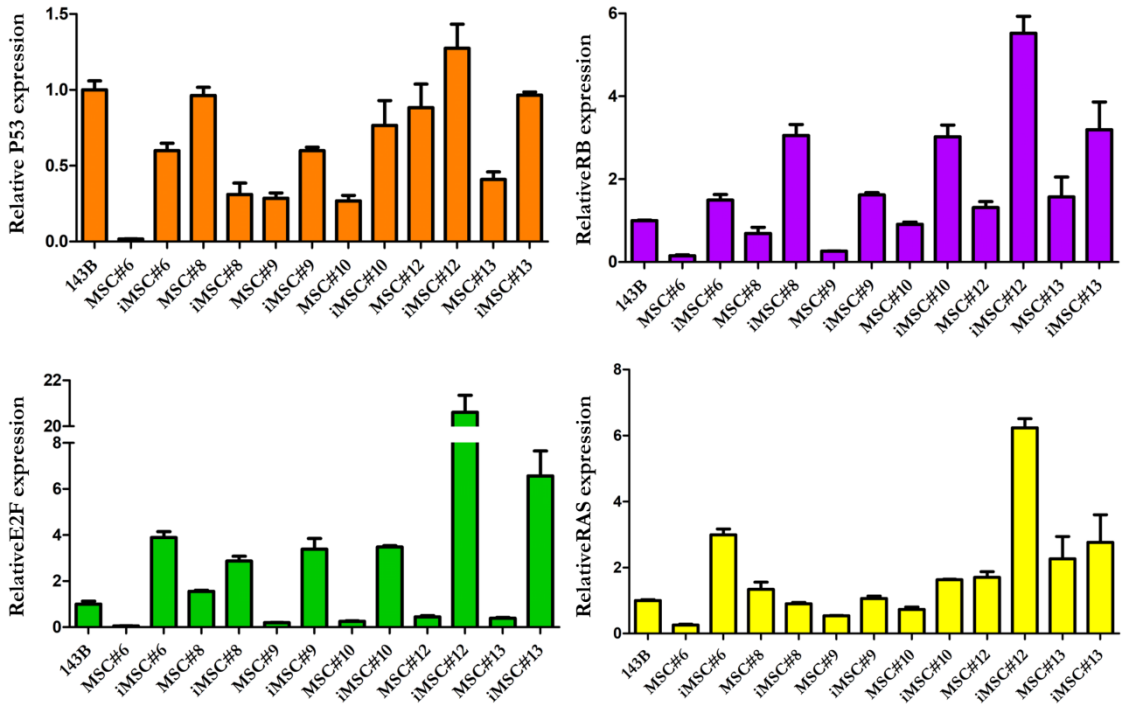

Figure 35. Normalized levels of expression of the tumour-related genes p53, Rb, E2F and RAS in primary MSCs, iMSCs and the osteosarcoma cell line 143B. MSC: mesenchymal stromal cell; iMSC: immortalized MSCs.

8. Analysis of the effect of iron oxide nanoparticles and rotating magnetic field on cell viability and differentiation

ColI scaffolds magnetized with different concentrations of Fe_3O_4@PAA IONs showed a superparamagnetic behaviour at 300 K, whereas a ferromagnetic-like behaviour with a coercive field of 0.03 T was observed at 5K, derived from the existence of a blocked magnetic state at that temperature. As expected, saturation magnetization increased with the magnetic content of the scaffolds: the higher the %Fe_3O_4 used in incubation, the higher the amount of nanoparticles absorbed and

the higher the magnetic signal (**Figure 36**). Saturation magnetization was higher in the magnetization curves at 5K, as expected based on Curie's law, which describes the decrease in magnetization with temperature. In short, the magnetic results confirm that the superparamagnetic behaviour of the IONs at room temperature is preserved after their incorporation into the scaffolds.

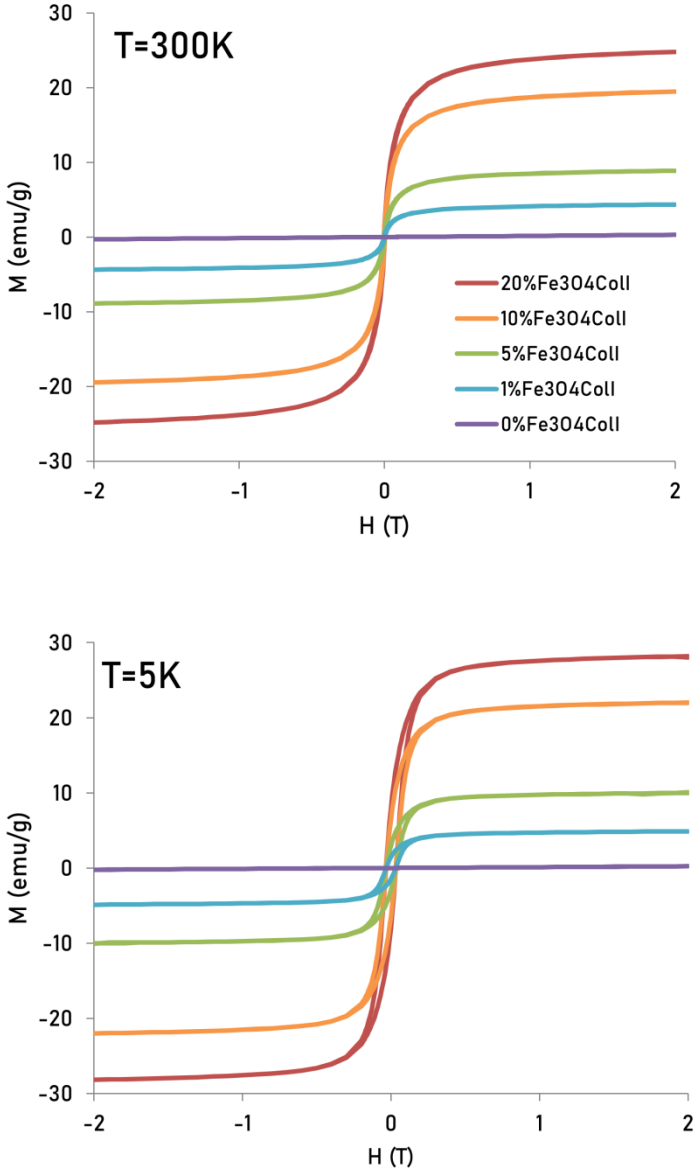

Figure 36. Magnetization curves as a function of the applied magnetic field up to 2 T for CoII scaffolds magnetized with different concentrations of Fe_3O_4@PAA IONs at 300K and 5K under zero-field-cooled conditions.

All concentrations assessed for magnetic labelling of ColI sponges (0, 1, 5, 10 and 20 g/L Fe_3O_4) were found to support iMSC#8.A (a highly osteogenic clone) attachment and growth as in native ColI scaffolds, as shown by cell viability results at 2, 7 and 15 days after seeding (**Figure 37**). Thus, ColI sponges magnetized with the highest Fe_3O_4@PAA concentration (20 g/L Fe_3O_4) were selected for cell differentiation experiments induced by RMF in order to maximize the interaction of the magnetic sponges with the applied magnetic field.

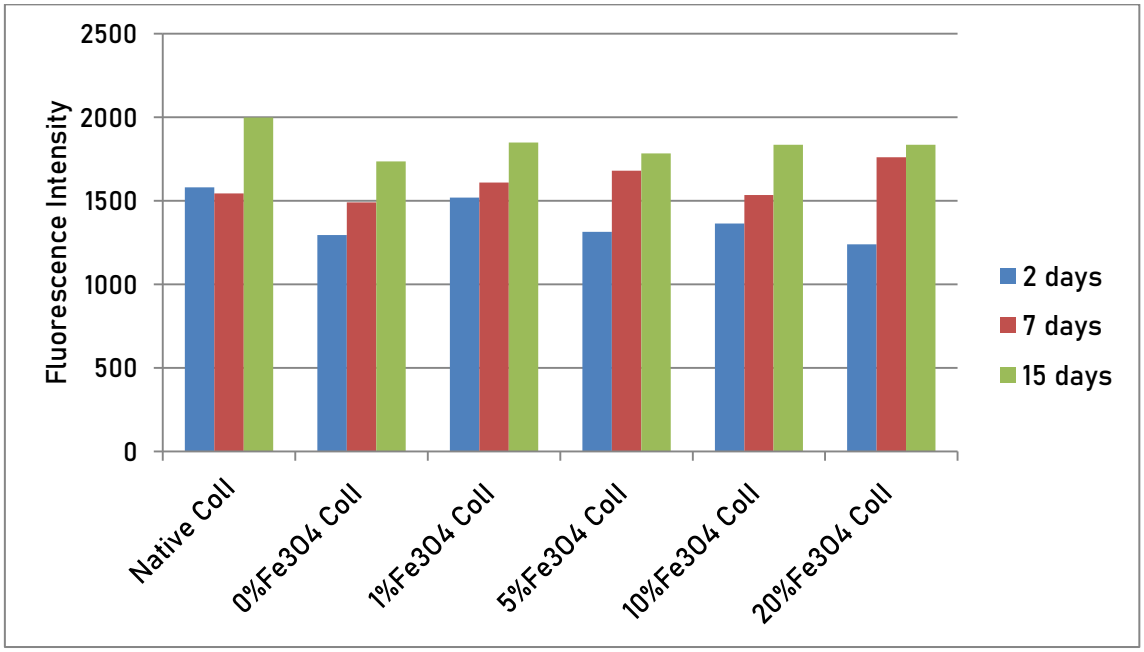

Figure 37. Cell viability measurements carried out 2, 7 and 15 days after seeding for each type of ColI sponges. ColI: type I collagen.

In the same way, none of the concentrations of Fe_3O_4@PAA nanoparticles employed for magnetic labelling of iMSC#8.A (0, 25, 50 and 100 μg/mL Fe) showed a negative effect on cell viability compared with the control. Moreover, iron content of the cells was found to progressively increase with the iron concentration of the ION dispersion used for incubation, as measured by ICP-OES (**Figure 38a**). This confirms that Fe_3O_4@PAA nanoparticles are internalized by iMSC8#A without causing cell toxicity (**Table 8**). This internalization of Fe_3O_4@PAA nanoparticles was also observed by Prussian blue staining (**Figure 38b**), which shows particles located inside the cells, surrounding the nucleus. Once again, the highest Fe_3O_4@PAA nanoparticle concentration (100 μg/mL iron) was chosen for cell differentiation experiments induced by RMF.

Table 8. Iron concentration of the Fe_3O_4@PAA nanoparticle dispersion added to culture medium and amount of iron detected inside the cells after a 24-hour incubation. Millions of viable cells after incubation with Fe_3O_4@PAA are also shown. Results are expressed as mean±standard deviation.

[Fe] (µg/mL)	0	25	50	100
[Fe] (pg/cell)	1.03±0.26	4.43±0.43	7.40±1.04	11.19±0.75
Viable cells (millions)	2.35±0.24	2.75±0.30	1.91±0.23	2.02±0.10

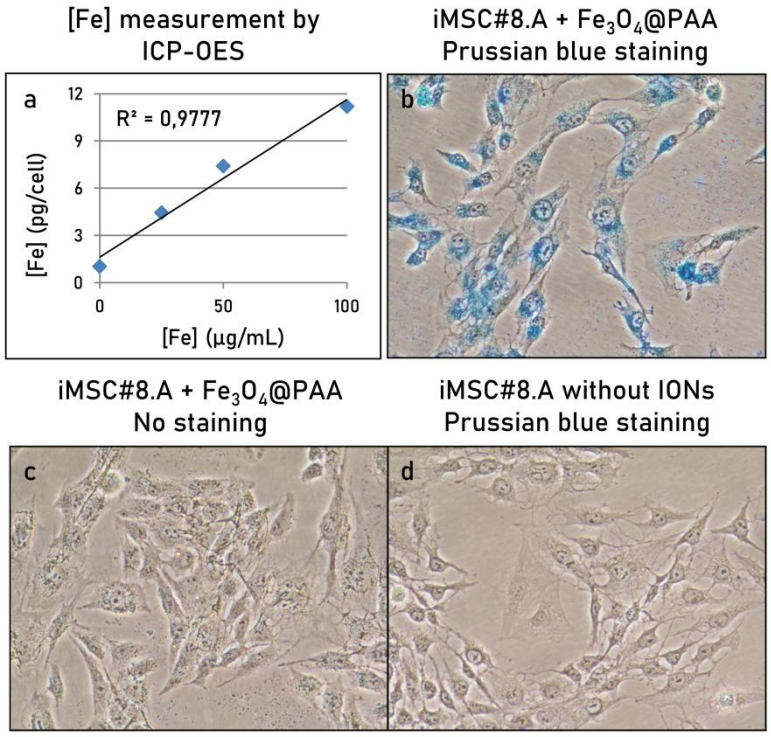

Figure 38. Iron amount inside iMSC#8.A measured by ICP-OES after incubating with Fe_3O_4@PAA nanoparticles (0, 25, 50 and 100 µg/mL Fe) (a) and Prussian blue staining of iMSC#8.A after incubation with the Fe_3O_4@PAA nanoparticle dispersion with the highest iron concentration (b). Both controls without Prussian blue staining (c) or without Fe_3O_4@PAA nanoparticles (d) are shown. IONs are stained blue. Magnification: 10X.

Both types of constructs (magnetically labelled ColI sponges containing iMSC#8.A and ColI sponges containing magnetically labelled iMSC#8.A) were employed for cell differentiation experiments induced by RMF. Three conditions (RMF, rotation only and static culture) and three time points (0, 14 and 21 days) were investigated. Three replicates were included for each condition and time.

After 21 days of culture, iMSC#8.A seeded on magnetically labelled ColI sponges produced little mineralized ECM, and no differences were found among the three

culture conditions tested (**Figure 39**). Magnetically labelled iMSC#8.A seeded on ColI sponges were unable to synthetize ECM under the same conditions, even if the cellularity of the scaffolds was higher (**Figure 40**).

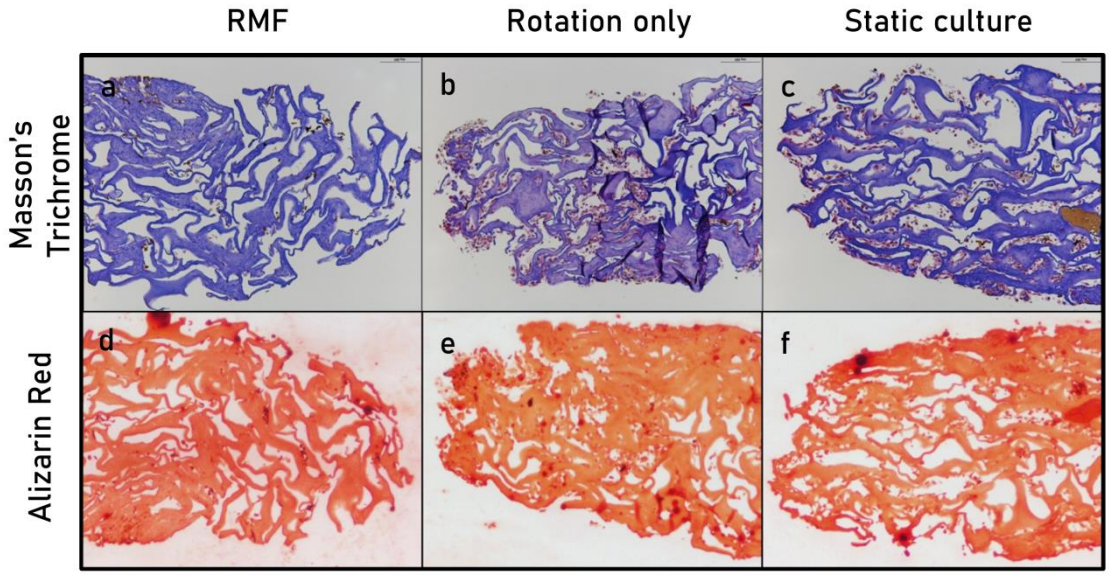

Figure 39. Masson's Trichrome and Safranin O staining of magnetically labelled ColI sponges with iMSC#8.A after 21 days of culture in RMF (a,d), rotation only (b,e) and static culture (c,f). Magnification 10X. RMF: rotating magnetic field.

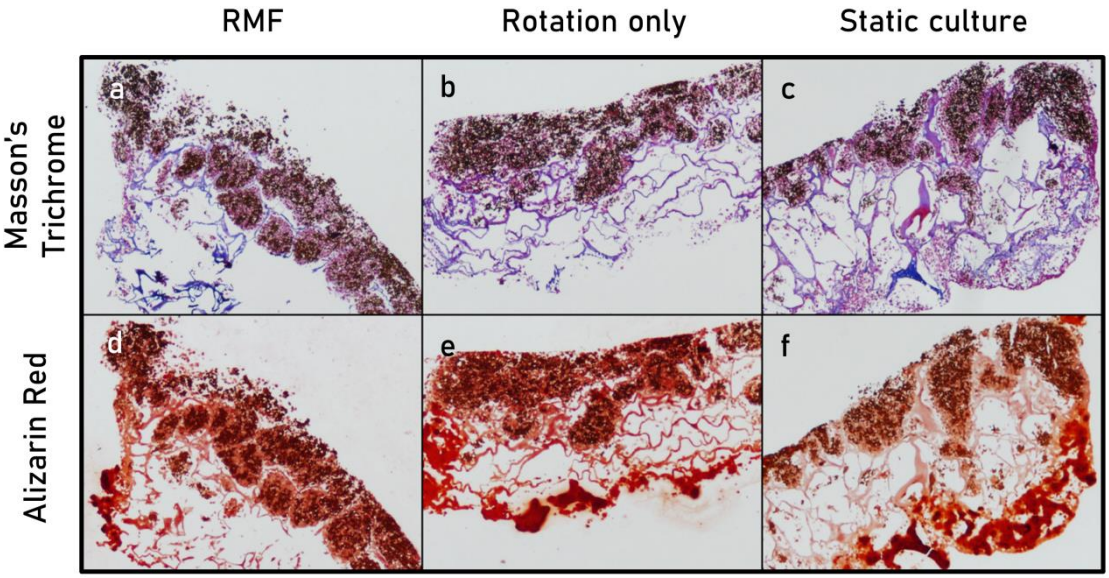

Figure 40. Masson's Trichrome and Safranin O staining of ColI sponges with magnetically labelled iMSC#8.A after 21 days of culture in RMF (a,d), rotation only (b,e) and static culture (c,f). Magnification 10X. RMF: rotating magnetic field.

9. Validation of the immortalization protocol in other cell types present in the synovial joint: chondrocytes and synoviocytes

The established spinoculation parameters were successfully employed for transduction of primary human chondrocytes and synoviocytes. SV40LT-transduced chondrocytes and synoviocytes were selected in puromycin within one week, and selected cells reached the confluence to be trypsinized ten days later. Subsequent hTERT transduction of SV40LT-transduced cells was also achieved. After hygromycin selection, expression of SV40LT and hTERT was detected in the nucleus of transduced cells by immunostaining (**Figure 41**). Unlike iMSCs, hTERT expression in immortalized chondrocytes and synoviocytes showed the same "nucleolar exclusion" pattern as SV40LT.

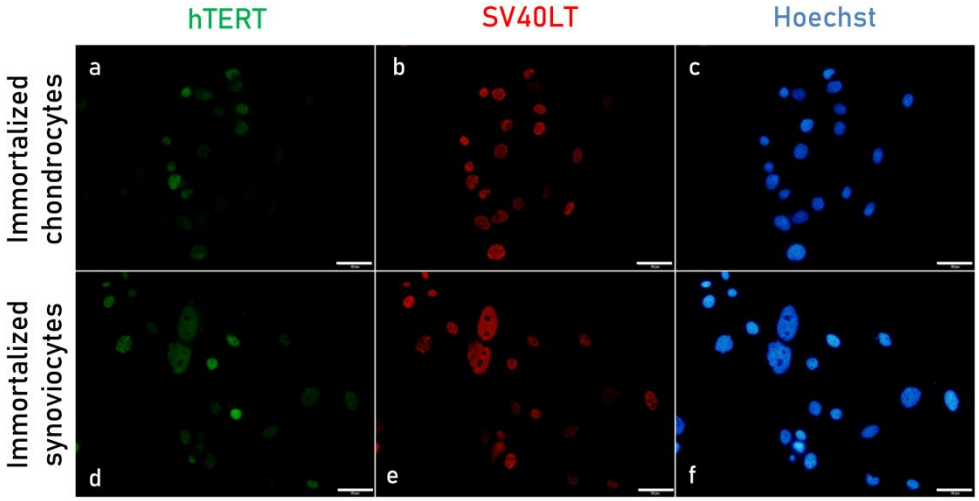

Figure 41. SV40LT and eGFP-hTERT immunostaining and Hoechst staining of immortalized chondrocytes (a, b, c) and synoviocytes (d, e, f). SV40LT is shown in red, eGFP-hTERT is shown in green and Hoechst staining is shown in blue. Scale bar: 50 μm.

Mean generation time of these cell lines was 2.9±0.9 days for immortalized chondrocytes between passages 12 and 28, and 2.1±0.6 days for immortalized synoviocytes between passages 13 and 34. In comparison with iMSCs, the generation time of immortalized chondrocytes was significantly higher (p-value=0.0005). Immortalized chondrocytes were grown over 45 PDs, and immortalized synoviocytes were grown over 60 PDs. Regression analysis showed a constant proliferation rate, with a multiple correlation coefficient R>0.99 (**Figure 42**) for both chondrocytes and synoviocytes and a p-value <0.0001. The percentage of SA-ß-Gal-positive cells was 1.6±0.2% for immortalized chondrocytes (15th-25th

passages) (**Figure 43a**) and 1.8±0.2% for immortalized synoviocytes (20th-30th passages) (**Figure 43b**).

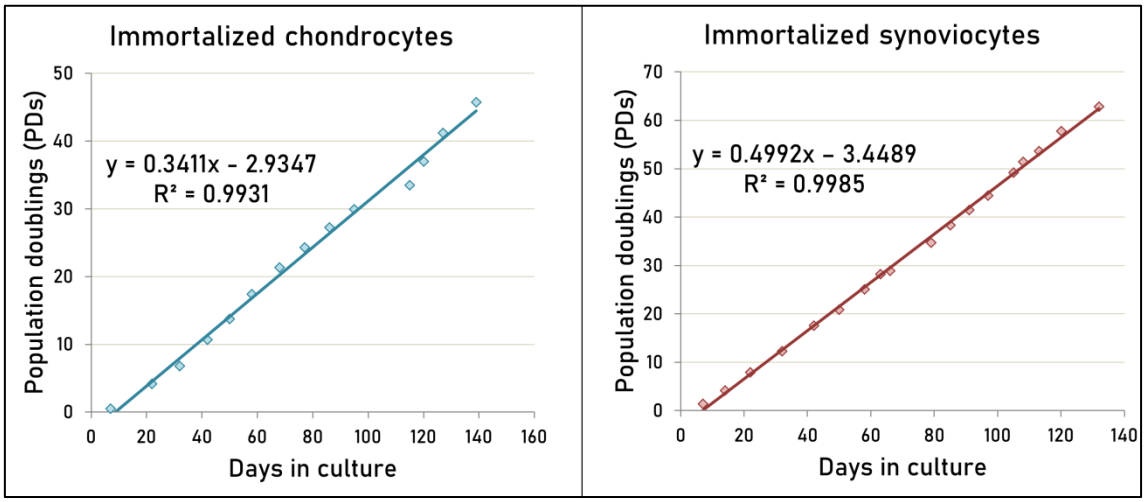

Figure 42. Number of PDs accumulated by immortalized chondrocytes and synoviocytes against days in culture. PDs were calculated as (log *Nf* – log *Ni*)/log 2 (where *Nf* is the final cell population, *Ni* is the number of cells in the inoculum and log is the natural logarithm). PDs: population doublings.

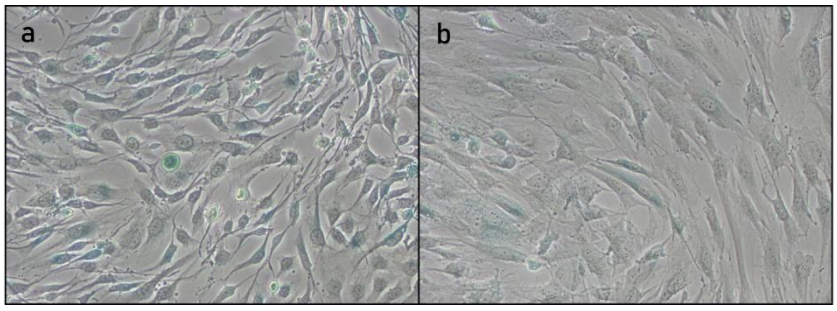

Figure 43. Phase contrast microscopic images of the SA-ß-Gal-stained immortalized chondrocytes (a) and synoviocytes (b). SA-ß-Gal activity is shown in blue. Magnification: 10X. SA-ß-Gal: senescence-associated ß-galactosidase.

Immortalized synoviocytes were 96.5% positive for CD44 and 98.7% positive for CD90. Immortalized chondrocytes presented the ability to form three-dimensional aggregates when subjected to the hanging drop method, and these aggregates presented an ECM containing collagen, as shown by Masson's Tricrome staining (**Figure 44a**), but low amounts of proteoglycans (**Figure 44b**), similarly to primary OA chondrocytes (**Figure 43 c-d**). However, immortalized chondrocytes were unable to form a cartilage-like tissue when seeded on ColI sponges (**Figure 44 e-f**), unlike primary OA chondrocytes (**Figure 44 g-h**).

Analysis of cartilage-related gene expression in cell aggregates of immortalized and primary chondrocytes revealed a loss of the chondrogenic phenotype in immortalized chondrocytes compared with primary chondrocytes, even though Sox9, aggrecan and type II collagen were up-regulated in immortalized chondrocytes after 15 days of three-dimensional culture in chondrogenic medium (**Figure 45**). However, immortalized articular chondrocytes showed more susceptibility to IL-1β than immortalized chondrocyte cell line T/C28a2 (**Figure 46**). Significant differences were found between primary chondrocytes and cell line T/C28a2 (p-value=0.0202), but not between primary and immortalized chondrocytes.

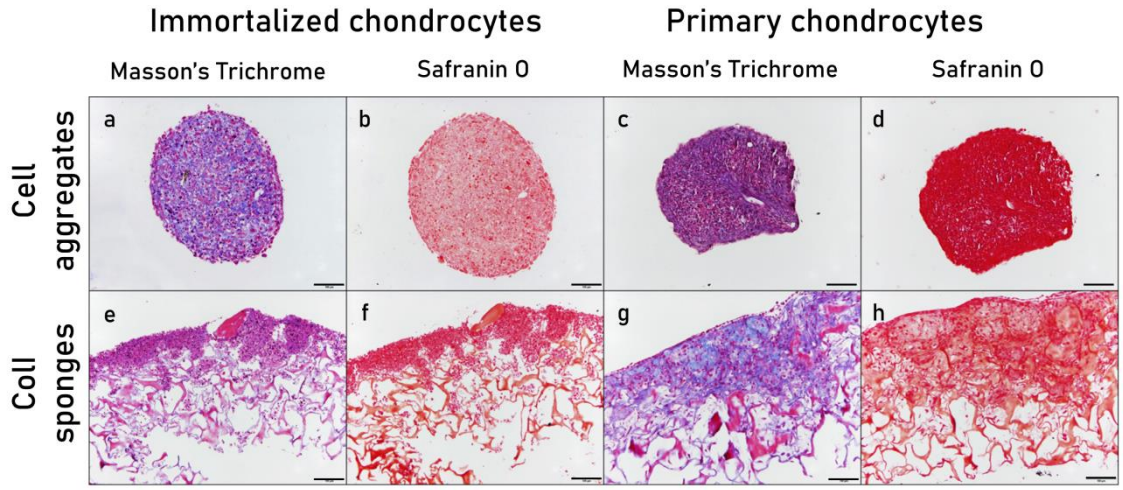

Figure 44. Masson's Trichrome and Safranin O staining of immortalized and primary chondrocytes in the form of cell aggregates (a-d) and seeded on ColI sponges (e-h) after 15 and 30 days of culture in chondrogenic medium, respectively. Scale bar: 100 μm.

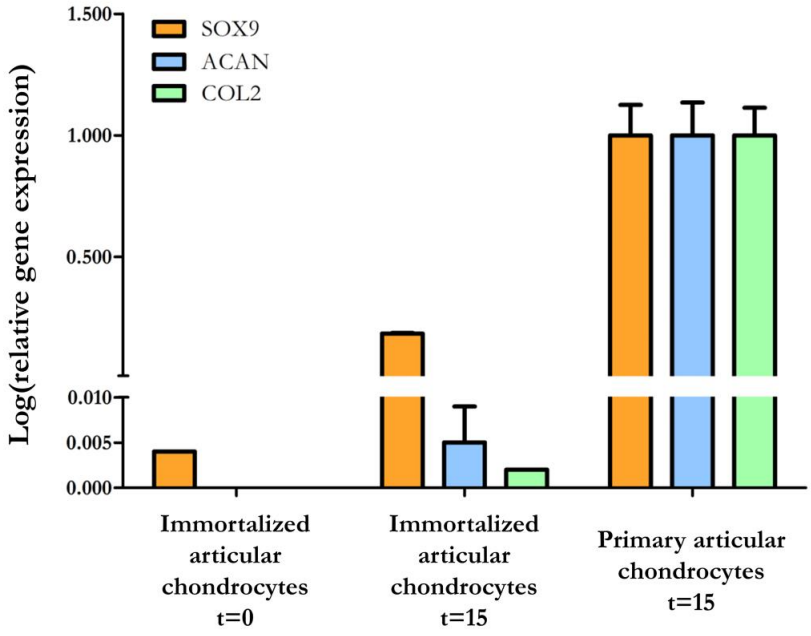

Figure 45. RELs of SOX9, COL2 and ACAN in immortalized and primary chondrocytes at the beginning of the experiment (t=0) and after 15 days of chondrogenic induction (t=15). RELs: relative expression levels; SOX9: SRY-box transcription factor 9; COL2: type II collagen; ACAN: aggrecan.

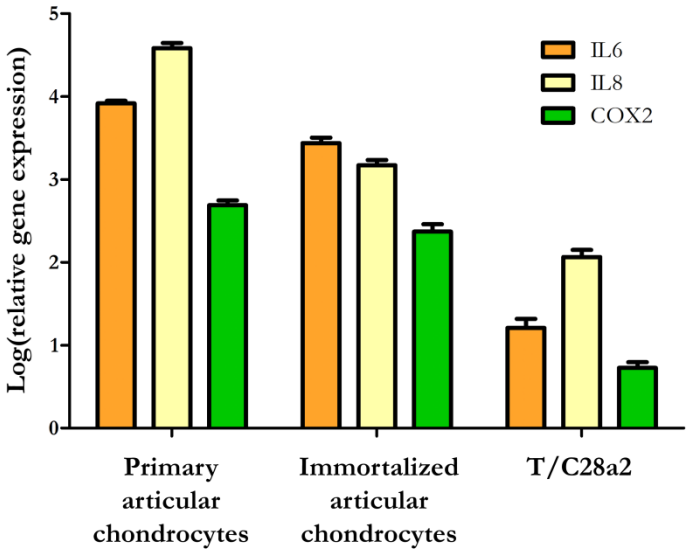

Figure 46. IL6, IL8 and COX2 RELs in primary articular chondrocytes, immortalized articular chondrocytes and T/C28a2 cells after stimulation with IL-1β. IL6: Interleukin 6; IL8: Interleukin 8; COX2: Cyclooxigenase 2; IL-1β: Interleukin 1β.

V. Discussion

Immortalization of mesenchymal stromal cells

MSCs derived from aged donors are prone to senesce during *in vitro* culture, but they could acquire an unlimited proliferation potential if p53 and Rb-mediated pathways and telomere shortening are repressed by transduction of immortalization genes (Koch *et al.*, 2013; Carnero *et al.*, 2015; Szychlinska *et al.*, 2017). A number of immortalized MSC lines have been generated in an attempt to overcome the limitations associated with primary MSCs (Tsai *et al.*, 2010; Bourgine *et al.*, 2014; Skårn *et al.*, 2014; Lee *et al.*, 2015). These cell lines have many *in vitro* applications: testing engineered scaffolds for bone and cartilage repair (Stölzel *et al.*, 2015; Ahlfeld *et al.*, 2017; Akmammedov *et al.*, 2018); generating biotechnological products (Bourgine *et al.*, 2017; Siska *et al.*, 2017); investigating the differentiation process of MSCs at the molecular level (Elsafadi *et al.*, 2017; Aida, Kurihara and Kato, 2018; Wilson *et al.*, 2018) and finding ways to improve the differentiation protocols that are currently in use (Okita *et al.*, 2015). In addition, they can be convenient tools for the development of *in vitro* disease modeling (Ringe and Sittinger, 2009; Moon *et al.*, 2013).

Several approaches have been employed to confer an unlimited proliferation potential to MSCs, mainly involving transduction of viral genes and/or hTERT (Mori *et al.*, 2005; Tsai *et al.*, 2010; Koch *et al.*, 2013; Bourgine *et al.*, 2014; Skårn *et al.*, 2014; Lee *et al.*, 2015). Viral genes such as SV40LT and HPV E6/E7 prevent cell growth arrest by interfering with p53 and Rb-mediated pathways (An, Sáenz Robles and Pipas, 2012; Pal and Kundu, 2020), while hTERT prevents telomere shortening and thus eventual senescence induced by DNA damage (J. Zhang *et al.*, 2016; Heidenreich and Kumar, 2017). It is still unclear which set of genetic alterations are necessary and sufficient for MSC immortalization, but it probably involves abrogation of both stress-induced and replicative senescence. MSCs transduced with only SV40LT (Lee *et al.*, 2015), E6/E7 (Mori *et al.*, 2005) or hTERT (Okamoto *et al.*, 2002; Takeda *et al.*, 2004; Mori *et al.*, 2005; Koch *et al.*, 2013; Dale *et al.*, 2015) finally undergo senescence, while the combination of SV40LT or E6/E7 with hTERT efficiently immortalizes MSCs (Takeda *et al.*, 2004; Mori *et al.*, 2005; Tsai *et al.*, 2010; Koch *et al.*, 2013) and ADSCs (Balducci *et al.*, 2014).

Retroviral transduction of slowly dividing adult human cells is an ineffective process and requires the use of enhancing methods. Spinoculation, employment of chemical adjuvants and addition of transgene expression inductors can improve retroviral

transduction. The enhancement of retroviral infection induced by spinoculation is related to centrifugation speed in a cell type-dependent manner (Introna *et al.*, 1998; Guo *et al.*, 2011; Yan *et al.*, 2015; Simmons and Alberola-Ila, 2016), and thus speed and time of spinoculation should be adapted to each transduction system. In this study, a suitable method for the immortalization of aged MSCs and other types of human adult cells has been developed. For its optimization, several variations were assayed, including SV40LT and hTERT co-transduction and sequential transduction, two incubation times of packaging cells for retrovirus production, two speeds and three time-points of spinoculation, and five different concentrations of VPA, an inductor of transgene expression.

In our system, spinoculation of primary MSCs with hTERT retrovirus triggered general cell death, which may be due to apoptosis induction by hTERT overexpression. It has been described that hTERT transduction can induce apoptosis in primary cells with a short *in vitro* lifespan (Choi and Lee, 2015). Transduction of previously SV40LT-transduced MSCs (T-MSCs) with hTERT did not induce apoptosis, which is consistent with previous reports as well (Choi and Lee, 2015). However, even when employing SV40LT retrovirus, cell survival to spinoculation at 1000 ×*g* was low. This low survival may be attributed to centrifugation-induced stress, as lowering centrifugation speed to 800 ×*g* remarkably improved cell survival. At high speeds, centrifugation-induced stress could cause damage to the cells (Lin *et al.*, 2012). In our study, cell viability measurements showed that the MSC population was reduced after spinoculation in a very variable way. This reduction was attributed to centrifugation rather than infection, since it was also observed in control cells, where no viruses were added. Furthermore, centrifugation-induced stress is known to make cells more susceptible to the toxicity of HDBM (Lin *et al.*, 2012), used in this study as an adjuvant for retroviral infection. Lowering centrifugation time below 45 minutes did not improve cell survival and was unfavourable for infection, consistently with the results obtained by other authors (Ye *et al.*, 2008; Yan *et al.*, 2015).

VPA-induced transgene expression

Because of their polyanionic nature, viral DNA interacts with positively charged histones in the nucleus. In this way, the promoter becomes inaccessible, which results in a loss of gene expression. It has been suggested that this gene silencing could be a defence mechanism against viruses. However, it can be reversed by

histone acetylation through the addition of histone deacetylase inhibitors such as VPA (Joglekar *et al.*, 2014; Zhang, Zhang and Liu, 2019). Our results indicated that VPA does not exert any negative effect on transduced MSC viability, but a negative effect on proliferation while present in the culture medium cannot be discarded.

After puromycin selection of T-MSCs, cell population size decreased for all tested VPA concentrations. However, cells treated with 0.5 mM and 2 mM VPA showed the smallest reduction in cell population. We hypothesize that this can be related to differences in spinoculation efficiency caused by the particular position of each well within the dish when centrifuging and, thus, to the centrifugal force experimented by each well. It should also be noted that, during transduction, transgenes are inserted in different random regions of the genome, with different levels of epigenetic modifications, in each transduced cell. Therefore, each cell may respond differently to the same concentration of VPA (Yang *et al.*, 2014), which probably contributes to the observed variability.

Finally, 2 mM VPA was established as the optimal concentration above 0.5 mM, based on its greater similarity to concentrations established as optimal for other transduction systems (Jäger *et al.*, 2013; Cervera *et al.*, 2015). For instance, Cervera *et al.* (2015) determined that 3.36 mM was the optimal concentration of VPA to increase both gene expression and cell viability in HEK-293 cells, and Fang *et al.* (2017) employed a concentration of 3.5 mM to boost the production of recombinant antibodies with similar results. In addition, Joglekar *et al.* (2014) showed that VPA enhanced gene expression from lentiviral vectors in human HSCs in a concentration-dependent manner, with 1.5 mM being significantly superior to 0.5 mM (Joglekar *et al.*, 2014).

Nevertheless, despite increasing recombinant protein yield, higher concentrations of VPA (3.75-5 mM) have been found to reduce cell viability and cause cell growth arrest in several cell types (Wulhfard *et al.*, 2010; Jäger *et al.*, 2013). Taken together, all these data indicate that VPA concentrations between 1.5 and 3.5 mM may enhance transgene expression more efficiently, but higher concentrations have deleterious effects over cell growth and viability that overcome the beneficial effects over transgene expression.

Transgene expression and proliferation potential of immortalized MSCs

Ten lines of T-MSCs, derived from ten different donors, were generated employing the optimal transduction parameters (48 hour-incubation of ΦNX-A for retrovirus production, spinoculation at 800 ×*g* for 45 minutes and addition of 2 mM VPA after infection). Six of these T-MSC lines were further transduced with hTERT, using the same transduction conditions, to obtain six immortalized MSC (iMSC) lines. Three of these cell lines were derived from OA patients (iMSC#6, iMSC#8 and iMSC#10), while the other three were derived from hip fracture donors without OA (iMSC#9, iMSC#12 and iMSC#13).

In these iMSC lines, SV40LT was located in the nucleoplasm and excluded from the nucleoli, while eGFP-hTERT was preferentially associated with the nucleoli. SV40LT nucleolar exclusion had been previously described in other SV40LT-transduced cell lines (Wong, Kusdra and Collins, 2002). Conversely, intranuclear localization of hTERT changes during the cell cycle: in G1 phase, before DNA replication, hTERT is sequestered in nucleoli; in S/G2 phase, hTERT is released into the nucleoplasm, where it exerts its catalytic activity. Even though SV40LT transduction promotes the release of telomerase from nucleoli to nucleoplasm (Wong, Kusdra and Collins, 2002), association of hTERT with nucleoli suggests that its regulation is not completely lost in iMSCs.

We found that iMSCs retained fibroblast-like morphology after transduction of immortalization genes, as has been previously reported by others (Liu *et al.*, 2013; Skårn *et al.*, 2014; Huang *et al.*, 2015). However, their morphology differed from their primary parental cells: while parental MSCs presented an enlarged cytoplasm after a few passages, characteristic of the senescent phenotype, iMSCs showed less cytoplasm and more prominent nucleoli, characteristics of actively proliferating cells. In addition, iMSCs lacked granular content related to SA-ß-Gal activity (less than 5% of cells were SA-ß-Gal activity-positive), like other immortalized MSC lines (Balducci *et al.*, 2014; Skårn *et al.*, 2014) and unlike late-passage primary MSCs derived from aged donors.

All six iMSC lines showed higher proliferation rates than T-MSCs and MSCs, and T-MSCs proliferated faster than MSCs as well. Accordingly, the expression of PCNA was significantly higher in iMSCs than in their primary parental cells. Faster proliferation has often been observed after SV40LT transduction (Huang *et al.*,

2015) but has not been attributed to hTERT alone (Skårn *et al.*, 2014); however, the combination of SV40LT (or another p53 inhibitor) with hTERT overexpression can exert a synergistic effect in improving MSCs growth rate (Liu *et al.*, 2013; Balducci *et al.*, 2014). From the initial passage to senescence, primary MSCs are not able to carry out more than 30-40 PDs (Bourgine *et al.*, 2014; Skårn *et al.*, 2014; Yang *et al.*, 2018), while immortalized MSCs are able to reach more than 200 PDs (Bourgine *et al.*, 2014; Skårn *et al.*, 2014). All the iMSC lines generated in this study have undergone more than 100 PDs without showing any sign of senescence.

Phenotypical characterization of immortalized MSCs

MSCs are characterized by expressing a set of mesenchymal surface markers, such as CD29, CD44, CD73, CD90 and CD105, while lacking expression of hematopoietic markers CD34 and CD45. Primary MSCs can maintain high levels of mesenchymal surface markers regardless of passage number (Koch *et al.*, 2013; Yang *et al.*, 2018), but some authors have noticed the down-regulation of some of these markers during *in vitro* expansion (Tan, Lui and Rui, 2012; Duan and Chen, 2015) or due to particular culture conditions (Uder *et al.*, 2018).

The expression of these surface markers can be preserved in MSCs after immortalization (Liu *et al.*, 2013; Bourgine *et al.*, 2014; Skårn *et al.*, 2014). In this study, mesenchymal surface markers CD29, CD44 and CD90 were highly expressed in primary MSCs, T-MSCs and iMSCs. CD73 was also highly expressed in primary MSCs and iMSCs, but its expression was lower in T-MSCs. Other authors have described a loss of CD73 after several passages, together with a decrease in the growth rate of MSCs (Harting *et al.*, 2008). Therefore, the lower levels of CD73 expression in T-MSCs could be a sign of aging of these cells, which are not completely immortalized.

CD105 was the most variable of the surface markers studied in this work; its expression was either reduced or increased from primary to immortalized cells, depending on the cell line. Moreover, it was the only mesenchymal surface marker with low expression in immortalized mesenchymal cell line 3a6. The expression of CD105 can be reduced with passaging in primary MSCs (Harting *et al.*, 2008) and immortalized cells (Balducci *et al.*, 2014; Alexander *et al.*, 2015; Takeuchi *et al.*, 2015; Abarrategi *et al.*, 2018). The reason for its variation in iMSCs is difficult to elucidate, as *in vitro* culture-related and immortalization-related effects are undistinguishable.

In this study, four iMSC lines showed relatively high levels of CD105 positivity, while two iMSC lines showed low levels and were less CD105-positive than mesenchymal cell line 3a6. Interestingly, these two cell lines, iMSC#8 and iMSC#9, were the only ones capable of anchorage-independent growth. The exact role of CD105 expression in MSCs is still unclear (Schoonderwoerd, Goumans and Hawinkels, 2020). The two isoforms of CD105, S-endoglin and L-endoglin, which differ only in the length of their cytoplasmic region, are expressed in MSCs (Samoilovich *et al.*, 2018). While L-endoglin expression is related to angiogenesis and tumour development, S-endoglin is anti-angiogenic and its expression supresses tumour invasion (Pérez-Gómez *et al.*, 2005; Henry *et al.*, 2011). S-endoglin expression could be related to MSCs resistance to malignant transformation, and thus the loss of CD105 expression in iMSC#8 and iMSC#9 could be related to the acquisition of oncogenic potential.

It is worth noting that these surface antigens, although traditionally established as a necessary requirement for defining MSCs (Dominici *et al.*, 2006), are also expressed by terminally differentiated MSCs (Ali *et al.*, 2015) and other cell types, such as fibroblasts (Halfon *et al.*, 2011; Samsonraj *et al.*, 2017). In addition, there is no clear relationship between their expression and differentiation potential (Cleary *et al.*, 2016; Uder *et al.*, 2018). Therefore, their usefulness for characterising MSCs is limited.

Differentiation potential of immortalized MSCs

The transduction with immortalization genes alters the expression levels of genes associated with stemness (Qin *et al.*, 2016). One of the genes associated with stemness is OCT4, which has several splice variants; OCT4A is only expressed by pluripotent stem cells, while OCT4B1 is also expressed by human somatic cells and is involved in the regulation and maintenance of an undifferentiated state (Atlasi *et al.*, 2008; Wang and Dai, 2010; Zhou *et al.*, 2019). In primary MSCs, OCT4 expression gradually decreases as the number of passages increases, and higher levels of OCT4 are related to higher viability, proliferation and potency (Han *et al.*, 2014). In this study, OCT4B1 was more expressed in iMSCs than in their primary parental cells, and their up-regulation in iMSCs could indicate a higher level of stemness.

Multi-differentiation potential into osteoblasts, adipocytes and chondroblasts is one of the essential characteristics of MSCs (Dominici *et al.*, 2006; Bianco and Robey, 2015; Uder *et al.*, 2018). The ability of MSCs to differentiate into these three cell lineages may be altered by immortalization. Immortalized MSCs usually have equal or higher osteogenic potential than primary MSCs (Böcker *et al.*, 2008; Lee *et al.*, 2015), while their chondrogenic potential is generally poor (Bourgine *et al.*, 2014; Skårn *et al.*, 2014; Dale *et al.*, 2015; Armbruster *et al.*, 2017), although there are immortalized MSC lines capable of chondrogenesis when cultured in a three-dimensional environment (Stölzel *et al.*, 2015; Prasopthum, Shakesheff and Yang, 2018). In this study, differences were found in the differentiation potential within the cell lines themselves in their different transduction states. In comparison with their primary parental MSCs, iMSCs showed higher osteogenic potential, but also reduced or delayed adipogenesis. Out of all tested iMSC lines, only iMSC#6 showed some degree of chondrogenic potential when cultured in three-dimensional aggregates under chondrogenic stimuli. The multi-differentiation potential of T-MSCs was different from that of primary MSCs and iMSCs as well.

Instead of being a result of either transduction or passaging, the differences found among the multi-differentiation abilities of MSCs, T-MSCs and iMSCs could be derived from the selection of cells during these processes. Not all cells in a MSC population are susceptible to infection and, during spinoculation, only the cells located on those parts of the wells with lower centrifugation-induced stress will survive. Moreover, extensive passaging leads to the selection of the cells with the highest growth rates in polyclonal cultures (Tan, Lui and Rui, 2012). Since MSCs are heterogeneous cell populations, this arbitrary selection of cells will alter their properties, including their multi-differentiation potential.

Variations in the differentiation potential of MSCs exist not only among donors (Baker, Boyette and Tuan, 2015), but also among clones derived from one single donor (Okamoto *et al.*, 2002; James *et al.*, 2015; Stölzel *et al.*, 2015). Characterization and selection of immortalized MSC-derived clones may enable the maintenance of a population of cells with desirable characteristics, such as high osteogenic or chondrogenic capacities (Duan and Chen, 2015; Kouroupis *et al.*, 2018). In the study by Bourgine *et al.* (2014), the clone with the most prominent osteogenic potential was selected, thus obtaining an immortalized MSC line suitable for bone regeneration research. Jayasuriya *et al.* (2018) generated and analysed clonal CPC

lines from knee articular cartilage of OA patients, identifying the existence of two cell populations: one preferentially undergoing chondrogenesis and another one exhibiting higher osteogenic potential. In our study, twelve clones from four iMSC lines were generated for bone tissue engineering studies.

Osteogenesis

Osteogenesis is the default differentiation pathway for MSCs (Bourgine *et al.*, 2014; Somoza *et al.*, 2014; Bianco and Robey, 2015), and immortalized MSCs are able to form bone both *in vitro* (Liu *et al.*, 2015; Harkness *et al.*, 2016; Liang *et al.*, 2016) and *in vivo* (Simonsen *et al.*, 2002; Larsen *et al.*, 2009; Bourgine *et al.*, 2014). All the iMSC lines generated in this study were able to differentiate into the osteogenic lineage. When subjected to osteogenic stimuli, iMSCs deposited a strongly mineralized ECM.

When compared with their primary parental T-MSCs and MSCs, iMSCs showed higher osteogenic potential, as shown by Alizarin Red staining and osteocalcin expression. In the study by Tsai *et al.*, (2010), the hTERT and E6/E7-transduced immortalized MSC line 3a6 was also more osteogenic than their E6/E7 only-transduced counterpart, the KP cells. Conversely, hTERT-transduced but not immortalized MSCs were found to be less osteogenic than their primary parental cells (Dale and Forsyth, 2018). These data suggest that complete immortalization could be beneficial for the bone-forming capacity of MSCs.

ECM mineralization was stronger in T-MSCs than in MSCs in line #6, but similar between T-MSCs and MSCs in line #12. The low level of mineralization detected in osteogenically-induced MSC#6 could be due to differentiation being induced at a late passage, when cells are expected to be aged (Yang *et al.*, 2018). After osteogenic induction, MSCs showed lower levels of osteogenic transcription factors than T-MSCs and iMSCs in cell line #10, while in cell line #12 primary MSCs expressed higher levels of Runx2 than T-MSCs and iMSCs, but iMSCs expressed the higher levels of Sp7. In both lines, iMSCs showed the highest expression of osteocalcin. Commitment of MSCs to OPCs/pre-osteoblasts requires Runx2, and subsequent differentiation into mature osteoblast and osteocalcin production is regulated by a concerted action of Runx2 and Sp7. At the same time, Sp7 is a downstream target of Runx2 (Rashid *et al.*, 2014). High levels of these transcription factors combined with low levels of osteocalcin and mineralization may indicate an immature state of

osteoblasts derived from T-MSCs and MSC#12. Shu *et al.* (2018) proposed that MSCs with higher proliferative activity, such as SV40LT-transduced MSCs, may need a longer time to differentiate.

All iMSC lines produced a mineralized ECM when subjected to osteogenic stimuli. Interestingly, three iMSC lines with higher CD105 expression (iMSC#10, iMSC#12 and iMSC#13) showed weaker mineralization by Alizarin Red staining. Low CD105 positivity has been related to higher osteogenic potential and mineralization efficiency (Leyva-Leyva *et al.*, 2015; Izgi *et al.*, 2017). These three iMSC lines also showed lower expression of CD73, a surface antigen that has been related to increased osteogenic potential (Hau *et al.*, 2017). Furthermore, all iMSC lines up-regulated the expression of osteocalcin after osteogenic induction. Overall, there were small differences between RELs of Runx2 and Sp7 in basal and osteogenic media, which are due to the high expression of these transcription factors in unstimulated MSCs. Runx2 promotes osteoblast differentiation and inhibits adipocyte differentiation of MSCs (Hu *et al.*, 2018). Without any osteogenic stimuli, SV40LT-transduced OPCs show higher levels of Runx2 than primary cells (Alexander *et al.*, 2015). This high expression of bone-related transcription factors, together with reduced adipogenic and chondrogenic potential, could be due to an osteogenic commitment of iMSCs.

In addition, all clones isolated from iMSCs presented a high osteogenic potential, and some of them were also capable of mineralization in the absence of osteogenic stimuli. One of these clones, iMSC#8.A, spontaneously formed mineralized three-dimensional aggregates in the absence of osteogenic stimuli. Strikingly, this clone was derived from iMSC#8, one of the cell lines unable to form three-dimensional aggregates by the hanging drop method.

Adipogenesis

Immortalized MSCs and OPCs have often been reported to be able to differentiate into adipocytes (Wu *et al.*, 2015; Ali *et al.*, 2016; Harkness *et al.*, 2016; Galarza Torre *et al.*, 2018; Fayyad *et al.*, 2019), but their adipogenic potential may be reduced after immortalization (Funes *et al.*, 2007; Dale *et al.*, 2015; James *et al.*, 2015). In this study, all six iMSC lines generated were able to differentiate into the adipogenic lineage to some degree, but they did not give rise to mature adipocytes. As previously mentioned, there is an inverse relationship between osteogenesis and adipogenesis

(Bianco, 2014), and unstimulated iMSCs expressed higher levels of Runx2, which in an inhibitor of adipogenesis (Hu *et al.*, 2018).

The immaturity of the adipocytes generated by iMSCs could indicate that they need more time to reverse their osteogenic commitment and fully differentiate into the adipogenic lineage. Unlike iMSCs and T-MSCs, primary MSCs did form mature adipocytes, as evidenced by Oil Red O staining. Primary MSC#6, which were differentiated at the 6th passage, also showed higher expression levels of adipogenic markers APN and FABP4. MSCs have been described to become more adipogenic during *in vitro* aging (Ok, Song and Hwang, 2018), but the adipogenic potential of iMSCs has been described to be progressively reduced throughout *in vitro* expansions (Koch *et al.*, 2013; James *et al.*, 2015). Similarly to iMSCs, immortalized OCPs and ADSCs, transduced with SV40LT, proliferate faster than their primary parental cells but are less adipogenic (Tátrai *et al.*, 2012; Song *et al.*, 2017).

However, iMSC#12 expressed higher levels of the adipogenic markers APN and FABP4 than their primary parental cells upon adipogenic induction. In addition, this iMSC line expressed the highest levels of these genes among iMSCs. Nevertheless, no differences were found among iMSC lines regarding the level of Oil Red O staining or the maturity of the adipocytes generated. APN and FABP4 are responsible for the formation of mature adipocytes (Moseti, Regassa and Kim, 2016), and their up-regulation upon adipogenic induction demonstrates the potential of iMSCs to differentiate into this cell lineage, but longer exposure to adipogenic stimuli may be needed to overcome their osteogenic commitment and generate mature adipocytes.

Chondrogenesis

Immortalized MSCs are able to up-regulate the expression of Sox9 and type II collagen expression upon chondrogenic stimuli, but show the same predisposition to hypertrophy than primary MSCs (Somoza *et al.*, 2014), with type X collagen expression (Bourgine *et al.*, 2014; Armbruster *et al.*, 2017) and low quality-cartilage production (Nürnberger *et al.*, 2019). In cell line #6, the chondrogenic potential of T-MSCs and iMSCs was evidenced by their ability to produce an extracellular matrix containing collagen and aggrecan. However, notably higher amounts of type II collagen were detected in T-MSC aggregates. Surprisingly, non-OA iMSC line #9

produced cartilage-like tissue of noticeably lower quality than OA iMSC line #6 when cultured in three-dimensional aggregates.

It is still controversial whether the expression of CD105, which is part of the TGF-ß receptor complex, is related to the chondrogenic potential of MSCs (Cleary *et al.*, 2016; Izgi *et al.*, 2017). T-MSC#6 showed higher CD105 positivity than iMSC#6, which, in turn, showed higher CD105 positivity than iMSC#9. The expression of CD73 has also been related to reduced chondrogenic potential (Ode *et al.*, 2013), and both iMSC#6 and iMSC#9 were highly CD73-positive. Unfortunately, the chondrogenic potential of the other iMSC lines generated in this study could not be evaluated due to their inability to form three-dimensional aggregates by the hanging drop method or to the small size of the aggregates after 21 days of chondrogenic induction. Further studies would be needed to confirm whether CD73 and CD105 positivity are related to multi-differentiation potential of iMSCs.

Oncogenic potential of immortalized MSCs

Immortalized MSCs can maintain an unlimited proliferation potential without aberrant growth control (Okamoto *et al.*, 2002; Simonsen *et al.*, 2002; Böcker *et al.*, 2008; Abarrategi *et al.*, 2018). However, oncogenic mutations could arise during passaging (Burns *et al.*, 2017), and immortalized MSCs seeded at low densities during long periods of time could become tumorigenic (Abdallah *et al.*, 2005; Takeuchi *et al.*, 2015). In this study, iMSC lines were evaluated for anchorage-independent growth after reaching more than 100 PDs. Two out of six iMSC lines were able to form colonies in soft agar. Surprisingly, one of these was the only cell line in which expression of the oncogene RAS was down-regulated after immortalization.

The binding of SV40LT to p53 prevents the expression of p53-dependent genes but also stabilizes this protein (An, Sáenz Robles and Pipas, 2012). In addition, since SV40LT inhibition of p53 and Rb occurs at the protein level, mRNAs coding for these proteins may accumulate in SV40LT-transduced cells without effectively triggering senescence. Both p53 and Rb were up-regulated in iMSCs in comparison with their primary parental cells, but these higher levels of p53 and Rb did not correlate with lower levels of E2F, nor did they had any effect on cell proliferation. Other tumour-suppressor genes, such as PTEN, have also been found to be up-regulated after MSC immortalization (Qin *et al.*, 2016).

Importantly, after undergoing oncogenic transformation, immortalized MSCs experience changes in their phenotype and their multi-differentiation potential (Abarrategi *et al.*, 2018). Oncogenic transformation could thus be related to the low chondrogenic potential of iMSC#9 and to the inability of iMSC#8 to form three-dimensional aggregates by the hanging drop method.

Magnetic field-based approaches for tissue engineering

Tissue engineering approaches require three elements: a scaffold to provide structure for tissue growth, cells to produce the desired tissue, and signals able to induce cell proliferation and differentiation (Smith and Grande, 2015). Magnetic field-assisted tissue engineering involves cell or scaffold labelling with magnetic nanoparticles and the application of a magnetic force to induce osteogenic differentiation and mineralisation (Ross *et al.*, 2015; Santos, Reis and Gomes, 2015; Yun *et al.*, 2016; Xia *et al.*, 2018). The preferred cells and scaffolds for bone tissue engineering are bone marrow-derived MSCs (Ng *et al.*, 2017) and type I collagen, which is one of the main components of bone ECM (Nijsure and Kishore, 2018). Both MSCs and scaffolds can be "magnetized" by IONs (Meng *et al.*, 2010; Guldris *et al.*, 2017). Due to their unlimited proliferation potential and osteogenic capacity, immortalized MSCs are suitable tools for screening different regeneration approaches for bone tissue engineering.

In this study, a highly osteogenic iMSC-derived clone, iMSC#8.A, with the ability to spontaneously form mineralized three-dimensional aggregates, was employed to study magnetic field-based approaches for bone tissue engineering. Both iMSCs and ColI scaffolds were efficiently magnetized with IONs, and the addition of IONs neither affects cell viability nor cell proliferation in the scaffolds. However, the application of an RMF was found not to induce osteogenic differentiation of iMSCs in any of the tested conditions. In magnetically labelled ColI scaffolds, the small amount of mineralized ECM produced by iMSC#8.A could be a result of the low cellularity of the scaffolds. The scarcity of cells within the scaffolds could have been caused by the modification of scaffold porosity during the magnetization and drying processes. This would be supported by the higher level of cellularity found in ColI sponges containing magnetically labelled iMSC#8.A, even though these cells were unable to produce a mineralized ECM under the tested conditions. A possible explanation for this null ECM mineralization could lie in the fact that the RMF employed was outside the biological window of iMSCs (Xia *et al.*, 2018).

Immortalization of chondrocytes and synoviocytes

The method developed for the immortalization of aged MSCs was validated in two other cell types from the synovial joint, chondrocytes and synoviocytes, demonstrating its usefulness for the immortalization of other types of human primary cells. In immortalized chondrocytes and synoviocytes, both SV40LT and hTERT were expressed in the nucleoplasm and excluded from the nucleoli. SV40LT transduction has been described to promote the release of telomerase from nucleoli to the nucleoplasm (Wong, Kusdra and Collins, 2002), and this expression pattern suggests that cell cycle-dependent hTERT regulation is lost in immortalized chondrocytes and synoviocytes, unlike in iMSCs.

Human primary synoviocytes tend to senesce in culture after the 9th passage, and their mean generation time is about 7 days (Rosengren, Boyle and Firestein, 2007). Immortalized synoviocytes generated in this study reached a high number of PDs, and their mean generation time was similar to that of iMSCs. As mentioned above, the combination of SV40LT with hTERT can exert a synergistic effect in improving the proliferation rate (Liu *et al.*, 2013; Balducci *et al.*, 2014). Just like iMSCs, a very low percentage of immortalized synoviocytes were SA-ß-Gal activity-positive, which suggest that SV40LT and hTERT transduction is useful to bypass senescence also in synoviocytes. In addition, synoviocytes retained the expression of surface markers CD44 and CD90 despite immortalization. Further studies would be necessary to confirm whether immortalized synoviocytes are phenotypically and functionally equal to primary synoviocytes, for example in terms of the absence of macrophage markers CD14 and CD68 and the production of hyaluronic acid and types I and III collagen (Rosengren, Boyle and Firestein, 2007).

Human articular chondrocytes have limited proliferative capacity and tend to undergo dedifferentiation during *in vitro* expansion. Dedifferentiated chondrocytes acquire fibroblast-like morphology and reduce the expression of articular cartilage markers, such as type II collagen and aggrecan (Duan *et al.*, 2015; Rim, Nam and Ju, 2020). In this study, immortalization allowed OA articular chondrocytes to bypass senescence but did not prevent dedifferentiation, as has been observed by other authors (Grigolo *et al.*, 2002). However, mean generation time of immortalized chondrocytes was higher than that of immortalized MSCs and synoviocytes, suggesting that immortalized chondrocytes retain a higher degree of differentiation.

Immortalized chondrocytes were able to form three-dimensional aggregates similar to those formed by primary OA articular chondrocytes, but, unlike primary OA articular chondrocytes, they were unable to form a cartilage-like tissue when seeded in three-dimensional scaffolds in the tested conditions. Even when cultured in three-dimensional culture, the expression of cartilage ECM-related genes was much lower in immortalized chondrocytes than in primary OA articular chondrocytes. Finger *et al.* (2003) also noted that immortalized chondrocytes showed lower expression of these genes than primary chondrocytes. Even though they did not show the anabolic capacities that are characteristic of primary articular chondrocytes, immortalized chondrocytes generated in this study were able to respond to the inflammatory stimulus of IL-1β similarly to primary articular chondrocytes. IL-1 is the most potent inducer of cartilage degradation (Vincent, 2019). Articular chondrocytes respond to IL-1β by reducing anabolism and increasing catabolism (Jenei-Lanzl, Meurer and Zaucke, 2019), and this cytokine is present at elevated levels in OA cartilage (Mohanraj *et al.*, 2018). IL-1ß-treated articular chondrocytes have been widely used as *in vitro* models to study OA initiation or post-traumatic OA (Lv *et al.*, 2019). Therefore, the ability of immortalized chondrocytes to respond to IL-1β could be an interesting characteristic for the future development of an *in vitro* model of OA for drug screening purposes.

In summary, this study has demonstrated that primary MSCs, articular chondrocytes and fibroblast-like synoviocytes derived from aged and OA donors can be immortalized by sequential spinoculation of SV40LT and hTERT. Immortalized MSCs overcome senescence, acquire an unlimited proliferation potential and maintain most of the characteristics that define MSCs. The high osteogenic potential of these cells and the clones derived from them makes them ideal candidates to form part of *in vitro* tissue engineering models for bone disease and regeneration studies.

VI. Conclusions

The general conclusion of this doctoral thesis is that the immortalization of bone-marrow derived MSCs from OA patients and aged donors allows for the generation of multipotent MSC lines useful for the study of bone repair strategies.

1.1. Retroviral spinoculation with HDBM and induction of transgene expression with VPA is a suitable method for the transduction of senescence-prone, slowly dividing MSCs.

1.2. Immortalized MSC lines can be obtained by sequential transduction of immortalization genes SV40LT and hTERT.

1.3. Transduction of immortalization genes SV40LT and hTERT allows aged and OA MSCs to overcome senescence and acquire an unlimited proliferation potential.

2.1. Immortalized MSCs are phenotypically similar to primary MSCs, but expression of CD73 and especially of CD105 can be altered by immortalization and/or passaging.

2.2. Immortalized MSCs are able to differentiate into the skeletal lineages but are functionally different from primary MSCs, showing enhanced osteogenic potential, lower or delayed adipogenic potential, and poor chondrogenic potential.

2.3. Immortalized MSCs can acquire the ability to grow independently of anchorage and become tumorigenic.

3. Clones can be isolated from immortalized MSCs, and iMSC-derived clones have great mineralization capacity.

4. Fe_3O_4@PAA IONs can be efficiently incorporated in both scaffolds and cells and do not affect cell viability, but RMF did not induce osteogenic differentiation of the selected iMSC clone under the tested conditions.

5. Articular chondrocytes and fibroblast-like synoviocytes can also be immortalized by sequential spinoculation of immortalization genes SV40LT and hTERT.

VII. References

Aasen, T. *et al.* (2008) 'Efficient and rapid generation of induced pluripotent stem cells from human keratinocytes', *Nature Biotechnology*, 26(11), pp. 1276–1284. doi: 10.1038/nbt.1503.

Abarrategi, A. *et al.* (2018) 'c-Fos induces chondrogenic tumor formation in immortalized human mesenchymal progenitor cells', *Scientific Reports*, 8(1), p. 15615. doi: 10.1038/s41598-018-33689-0.

Abdallah, B. M. *et al.* (2005) 'Maintenance of differentiation potential of human bone marrow mesenchymal stem cells immortalized by human telomerase reverse transcriptase gene despite of extensive proliferation', *Biochemical and Biophysical Research Communications*, 326(3), pp. 527–538. doi: 10.1016/j.bbrc.2004.11.059.

Ahlfeld, T. *et al.* (2017) 'Development of a clay based bioink for 3D cell printing for skeletal application', *Biofabrication*, 9(3), p. 034103. doi: 10.1088/1758-5090/aa7e96.

Aida, Y., Kurihara, H. and Kato, K. (2018) 'Wnt3a promotes differentiation of human bone marrow-derived mesenchymal stem cells into cementoblast-like cells', *In Vitro Cellular & Developmental Biology - Animal*, 54(6), pp. 468–476. doi: 10.1007/s11626-018-0265-3.

Akmammedov, R. *et al.* (2018) 'Preparation and characterization of novel chitosan/zeolite scaffolds for bone tissue engineering applications', *International Journal of Polymeric Materials and Polymeric Biomaterials*, 67(2), pp. 110–118. doi: 10.1080/00914037.2017.1309539.

Akter, F. and Ibanez, J. (2016) 'Bone and Cartilage Tissue Engineering', in *Tissue Engineering Made Easy*. Elsevier Inc., pp. 77–97. doi: 10.1016/B978-0-12-805361-4.00008-4.

Alberts, B. *et al.* (2008) *Molecular Biology of the Cell* (5th edn). New York City, NY, USA: Garland Science. ISBN: 978-84-282-1507-7.

Alexander, D. *et al.* (2015) 'Phenotypic Characterization of a Human Immortalized Cranial Periosteal Cell Line', *Cellular Physiology and Biochemistry*, 35(6), pp. 2244–2254. doi: 10.1159/000374029.

Ali, D. *et al.* (2016) 'Epigenetic Library Screen Identifies Abexinostat as Novel Regulator of Adipocytic and Osteoblastic Differentiation of Human Skeletal (Mesenchymal) Stem Cells', *STEM CELLS Translational Medicine*, 5(8), pp. 1036–1047. doi: 10.5966/sctm.2015-0331.

Ali, H. *et al.* (2015) 'Multi-Lineage Differentiation of Human Umbilical Cord Wharton's Jelly Mesenchymal Stromal Cells Mediates Changes in the Expression Profile of Stemness Markers', *PLOS ONE*, 10(4), p. e0122465. doi: 10.1371/journal.pone.0122465.

An, P., Brodsky, J. L. and Pipas, J. M. (2015) 'The conserved core enzymatic activities and the distinct dynamics of polyomavirus large T antigens', *Archives of Biochemistry and Biophysics*, 573, pp. 23–31. doi: 10.1016/j.abb.2015.02.033.

An, P., Sáenz Robles, M. T. and Pipas, J. M. (2012) 'Large T Antigens of Polyomaviruses: Amazing Molecular Machines', *Annual Review of Microbiology*, 66(1), pp. 213–236. doi: 10.1146/annurev-micro-092611-150154.

Anastasov, N. *et al.* (2016) 'Optimized Lentiviral Transduction Protocols by Use of a Poloxamer Enhancer, Spinoculation, and scFv-Antibody Fusions to VSV-G', *Methods in Molecular Biology*, 1448, pp. 49–61. doi: 10.1007/978-1-4939-3753-0_4.

Ansari, S. A. M. K. *et al.* (2019) 'Magnetic iron oxide nanoparticles: Synthesis, characterization and functionalization for biomedical applications in the Central Nervous System', *Materials (Basel)*, 12(3), p. 465. doi: 10.3390/ma12030465.

Arjmand, M. *et al.* (2018) 'Osteogenic differentiation potential of mesenchymal stem cells cultured on nanofibrous scaffold improved in the presence of pulsed electromagnetic field', *Journal of Cellular Physiology*, 233(2), pp. 1061–1070. doi: 10.1002/jcp.25962.

Armbruster, N. *et al.* (2017) 'Rescued Chondrogenesis of Mesenchymal Stem Cells under

Interleukin 1 Challenge by Foamyviral Interleukin 1 Receptor Antagonist Gene Transfer', *Frontiers in Pharmacology*, 8, p. 255. doi: 10.3389/fphar.2017.00255.

Armiento, A. R. *et al.* (2018) 'Biomaterials for articular cartilage tissue engineering: Learning from biology', *Acta Biomaterialia*, 65, pp. 1–20. doi: 10.1016/j.actbio.2017.11.021.

Atlasi, Y. *et al.* (2008) 'OCT4 Spliced Variants Are Differentially Expressed in Human Pluripotent and Nonpluripotent Cells', *STEM CELLS*, 26(12), pp. 3068–3074. doi: 10.1634/stemcells.2008-0530.

Baker, N., Boyette, L. B. and Tuan, R. S. (2015) 'Characterization of bone marrow-derived mesenchymal stem cells in aging', *Bone*, 70, pp. 37–47. doi: 10.1016/j.bone.2014.10.014.

Balducci, L. *et al.* (2014) 'Immortalization of human adipose-derived stromal cells: production of cell lines with high growth rate, mesenchymal marker expression and capability to secrete high levels of angiogenic factors', *Stem Cell Research & Therapy*, 5(3), p. 63. doi: 10.1186/scrt452.

Balducci, L. and Alessandri, G. (2016) 'Isolation, Expansion, and Immortalization of Human Adipose-Derived Mesenchymal Stromal Cells from Biopsies and Liposuction Specimens', *Methods in Molecular Biology*, 1416, pp. 259–274. doi: 10.1007/978-1-4939-3584-0_15.

Baumann, C. A. *et al.* (2019) 'Articular cartilage: Structure and restoration', in *Joint Preservation of the Knee: A Clinical Casebook*. Springer International Publishing, pp. 3–24. doi: 10.1007/978-3-030-01491-9_1.

Bianco, P. (2014) '"Mesenchymal" stem cells', *Annual Review of Cell and Developmental Biology*, 30, pp. 677–704. doi: 10.1146/annurev-cellbio-100913-013132.

Bianco, P. and Robey, P. G. (2015) 'Skeletal stem cells', *Development*, 142(6), pp. 1023–1027. doi: 10.1242/dev.102210.

Blaschke, M. *et al.* (2018) 'Crohn's disease patient serum changes protein expression in a human mesenchymal stem cell model in a linear relationship to patients' disease stage and to bone mineral density', *Journal of Clinical & Translational Endocrinology*, 13, pp. 26–38. doi: 10.1016/j.jcte.2018.06.002.

Böcker, W. *et al.* (2008) 'Introducing a single-cell-derived human mesenchymal stem cell line expressing hTERT after lentiviral gene transfer', *Journal of Cellular and Molecular Medicine*, 12(4), pp. 1347–1359. doi: 10.1111/j.1582-4934.2008.00299.x.

Bomer, N. *et al.* (2015) 'Translating genomics into mechanisms of disease: Osteoarthritis', *Best Practice & Research Clinical Rheumatology*, 29(6), pp. 683–691. doi: 10.1016/j.berh.2016.01.001.

Bourgeois, B. and Madl, T. (2018) 'Regulation of cellular senescence via the FOXO4-p53 axis', *FEBS Letters*, 592(12), pp. 2083–2097. doi: 10.1002/1873-3468.13057.

Bourgine, P. *et al.* (2014) 'Combination of immortalization and inducible death strategies to generate a human mesenchymal stromal cell line with controlled survival', *Stem Cell Research*, 12(2), pp. 584–598. doi: 10.1016/j.scr.2013.12.006.

Bourgine, P. E. *et al.* (2017) 'Engineered Extracellular Matrices as Biomaterials of Tunable Composition and Function', *Advanced Functional Materials*, 27(7), p. 1605486. doi: 10.1002/adfm.201605486.

Burns, J. S. *et al.* (2017) 'Chromosome copy number variation in telomerized human bone marrow stromal cells; insights for monitoring safe *ex-vivo* expansion of adult stem cells', *Stem Cell Research*, 25, pp. 6–17. doi: 10.1016/j.scr.2017.09.006.

Caddeo, S., Boffito, M. and Sartori, S. (2017) 'Tissue engineering approaches in the design of healthy and pathological in vitro tissue models', *Frontiers in Bioengineering and Biotechnology*, 5, p. 40. doi: 10.3389/fbioe.2017.00040.

Caplan, H. *et al.* (2019) 'Mesenchymal Stromal Cell Therapeutic Delivery: Translational Challenges to Clinical Application', *Frontiers in Immunology*, 10, p. 1645. doi: 10.3389/fimmu.2019.01645.

Carnero, A. *et al.* (2015) 'Disruptive chemicals, senescence and immortality', *Carcinogenesis*, 36(Suppl 1), pp. S19–S37. doi: 10.1093/carcin/bgv029.

Cervera, L. *et al.* (2015) 'Selection and optimization of transfection enhancer additives for increased virus-like particle production in HEK293 suspension cell cultures', *Applied Microbiology and Biotechnology*, 99(23), pp. 9935–9949. doi: 10.1007/s00253-015-6842-4.

Chang, B. *et al.* (2018) 'Treatment of osteoporosis, with a focus on 2 monoclonal antibodies', *Medical Science Monitor*, 24, pp. 8758–8766. doi: 10.12659/MSM.912309.

Chen, R. J. *et al.* (2017) 'P53-dependent downregulation of hTERT protein expression and telomerase activity induces senescence in lung cancer cells as a result of pterostilbene treatment', *Cell Death & Disease*, 8(8), p. e2985. doi: 10.1038/cddis.2017.333.

Choi, M. and Lee, C. (2015) 'Immortalization of Primary Keratinocytes and Its Application to Skin Research', *Biomolecules & Therapeutics*, 23(5), pp. 391–399. doi: 10.4062/biomolther.2015.038.

Cleary, M. A. *et al.* (2016) 'Expression of CD105 on expanded mesenchymal stem cells does not predict their chondrogenic potential', *Osteoarthritis and Cartilage*, 24(5), pp. 868–872. doi: 10.1016/j.joca.2015.11.018.

Colnot, C. (2011) 'Cell sources for bone tissue engineering: Insights from basic science', *Tissue Engineering - Part B: Reviews*, 17(6), pp. 449–457. doi: 10.1089/ten.teb.2011.0243.

Dale, T. P. *et al.* (2015) 'Immortalisation with hTERT Impacts on Sulphated Glycosaminoglycan Secretion and Immunophenotype in a Variable and Cell Specific Manner', *PLOS ONE*, 10(7), p. e0133745. doi: 10.1371/journal.pone.0133745.

Dale, T. P. and Forsyth, N. R. (2018) 'Ectopic Telomerase Expression Fails to Maintain Chondrogenic Capacity in Three-Dimensional Cultures of Clinically Relevant Cell Types', *BioResearch Open Access*, 7(1), p. biores.2018.0008. doi: 10.1089/biores.2018.0008.

Dang, P. N. *et al.* (2016) 'Controlled Dual Growth Factor Delivery From Microparticles Incorporated Within Human Bone Marrow-Derived Mesenchymal Stem Cell Aggregates for Enhanced Bone Tissue Engineering via Endochondral Ossification', *STEM CELLS Translational Medicine*, 5(2), pp. 206–217. doi: 10.5966/sctm.2015-0115.

Deng, C. *et al.* (2018) 'Bioactive Scaffolds for Regeneration of Cartilage and Subchondral Bone Interface', *Theranostics*, 8(7), pp. 1940–1955. doi: 10.7150/thno.23674.

Díaz-Prado, S. *et al.* (2012) 'Characterization of microRNA expression profiles in normal and osteoarthritic human chondrocytes', *BMC Musculoskeletal Disorders*, 13(1), p. 144. doi: 10.1186/1471-2474-13-144.

Dominici, M. *et al.* (2006) 'Minimal criteria for defining multipotent mesenchymal stromal cells. The International Society for Cellular Therapy position statement', *Cytotherapy*, 8(4), pp. 315–317. doi: 10.1080/14653240600855905.

Duan, L. *et al.* (2015) 'Cytokine networking of chondrocyte dedifferentiation in vitro and its implications for cell-based cartilage therapy', *American Journal of Translational Research*, 7(2), pp. 194–208.

Duan, P. and Chen, J. (2015) 'Nanomechanical and microstructure analysis of extracellular matrix layer of immortalized cell line Y201 from human mesenchymal stem cells', *Surface and Coatings Technology*, 284, pp. 417–421. doi: 10.1016/j.surfcoat.2015.06.076.

Durgam, S. *et al.* (2016) 'Differential Adhesion Selection for Enrichment of Tendon-Derived Progenitor Cells During In Vitro Culture', *Tissue engineering - Part C: Methods*, 22(8), pp. 801–808. doi:

10.1089/ten.TEC.2016.0152.

Elsafadi, M. *et al.* (2017) 'MicroRNA-4739 regulates osteogenic and adipocytic differentiation of immortalized human bone marrow stromal cells via targeting LRP3', *Stem Cell Research*, 20, pp. 94–104. doi: 10.1016/J.SCR.2017.03.001.

Fang, X. T. *et al.* (2017) 'Efficient and inexpensive transient expression of multispecific multivalent antibodies in Expi293 cells', *Biological Procedures Online*, 19(1), p. 11. doi: 10.1186/s12575-017-0060-7.

Fayyad, A. *et al.* (2019) 'Rosiglitazone Enhances Browning Adipocytes in Association with MAPK and PI3-K Pathways During the Differentiation of Telomerase-Transformed Mesenchymal Stromal Cells into Adipocytes', *International Journal of Molecular Sciences*, 20(7), p. 1618. doi: 10.3390/ijms20071618.

Fellows, C. R. *et al.* (2017) 'Characterisation of a divergent progenitor cell sub-populations in human osteoarthritic cartilage: The role of telomere erosion and replicative senescence', *Scientific Reports*, 7, p. 41421. doi: 10.1038/srep41421.

Finger, F. *et al.* (2003) 'Molecular phenotyping of human chondrocyte cell lines T/C-28a2, T/C-28a4, and C-28/I2', *Arthritis & Rheumatism*, 48(12), pp. 3395–3403. doi: 10.1002/art.11341.

Fox, A. J., Bedi, A. and Rodeo, S. A. (2009) 'The basic science of articular cartilage: Structure, composition, and function', *Sports Health*, 1(6), pp. 461–468. doi: 10.1177/1941738109350438.

Freshney, R. I. (2005) 'Transformation and Immortalization', in *Culture of Animal Cells*. Hoboken, NJ, USA: John Wiley & Sons, Inc. doi: 10.1002/0471747599.cac018.

Funes, J. M. *et al.* (2007) 'Transformation of human mesenchymal stem cells increases their dependency on oxidative phosphorylation for energy production', *Proceedings of the National Academy of Sciences*, 104(15), pp. 6223–8. doi: 10.1073/pnas.0700690104.

Galarza Torre, A. *et al.* (2018) 'An immortalised mesenchymal stem cell line maintains mechano-responsive behaviour and can be used as a reporter of substrate stiffness', *Scientific Reports*, 8(1), p. 8981. doi: 10.1038/s41598-018-27346-9.

Ghassemi, T. *et al.* (2018) 'Current Concepts in Scaffolding for Bone Tissue Engineering', *The archives of bone and joint surgery*, 6(2), pp. 90–99.

Goldring, M. B. *et al.* (1994) 'Interleukin-1β-modulated gene expression in immortalized human chondrocytes', *Journal of Clinical Investigation*, 94(6), pp. 2307–2316. doi: 10.1172/JCI117595.

Goldring, S. R. and Goldring, M. B. (2016) 'Changes in the osteochondral unit during osteoarthritis: Structure, function and cartilage bone crosstalk', *Nature Reviews Rheumatology*, 12(11), pp. 632–644. doi: 10.1038/nrrheum.2016.148.

Goonoo, N. and Bhaw-Luximon, A. (2018) 'Regenerative medicine: Induced pluripotent stem cells and their benefits on accelerated bone tissue reconstruction using scaffolds', *Journal of Materials Research*, 33(11), pp. 1573–1591. doi: 10.1557/jmr.2018.132.

Grayson, W. L. *et al.* (2015) 'Stromal cells and stem cells in clinical bone regeneration', *Nature Reviews Endocrinology*, 11(3), pp. 140–50. doi: 10.1038/nrendo.2014.234.

Grigolo, B. *et al.* (2002) 'Human articular chondrocytes immortalized by HPV-16 E6 and E7 genes: Maintenance of differentiated phenotype under defined culture conditions', *Osteoarthritis and Cartilage*, 10(11), pp. 879–889. doi: 10.1053/joca.2002.0836.

Guldris, N. *et al.* (2017) 'Magnetite Nanoparticles for Stem Cell Labeling with High Efficiency and Long-Term *in Vivo* Tracking', *Bioconjugate Chemistry*, 28(2), pp. 362–370. doi: 10.1021/acs.bioconjchem.6b00522.

Guo, J. *et al.* (2011) 'Spinoculation Triggers Dynamic Actin and Cofilin Activity That Facilitates

HIV-1 Infection of Transformed and Resting CD4 T Cells', *Journal of Virology*, 85(19), pp. 9824–9833. doi: 10.1128/JVI.05170-11.

Halfon, S. *et al.* (2011) 'Markers Distinguishing Mesenchymal Stem Cells from Fibroblasts Are Downregulated with Passaging', *Stem Cells and Development*, 20(1), pp. 53–66. doi: 10.1089/scd.2010.0040.

Han, S. M. *et al.* (2014) 'Enhanced proliferation and differentiation of Oct4- And Sox2-overexpressing human adipose tissue mesenchymal stem cells', *Experimental and Molecular Medicine*, 46(6), p. e101. doi: 10.1038/emm.2014.28.

Harigaya, K. and Handa, H. (1985) 'Generation of functional clonal cell lines from human bone marrow stroma', *Proceedings of the National Academy of Sciences*, 82(10), pp. 3477–3480. doi: 10.1073/pnas.82.10.3477.

Harkness, L. *et al.* (2016) 'CD146/MCAM defines functionality of human bone marrow stromal stem cell populations', *Stem Cell Research & Therapy*, 7(1), p. 4. doi: 10.1186/s13287-015-0266-z.

Hart, N. H. *et al.* (2017) 'Mechanical basis of bone strength: Influence of bone material, bone structure and muscle action', *Journal of Musculoskeletal Neuronal Interactions*, 17(3), pp. 114–139.

Harting, M. T. *et al.* (2008) 'Immunophenotype characterization of rat mesenchymal stromal cells', *Cytotherapy*, 10(3), pp. 243–253. doi: 10.1080/14653240801950000.

Hau, K. L. *et al.* (2017) 'TGFβ-induced osteogenic potential of human amniotic fluid stem cells via CD73-generated adenosine production', *Scientific Reports*, 7(1), p. 6601. doi: 10.1038/s41598-017-06780-1.

Heidenreich, B. and Kumar, R. (2017) 'TERT promoter mutations in telomere biology', *Mutation Research - Reviews in Mutation Research*, 771, pp. 15–31. doi: 10.1016/j.mrrev.2016.11.002.

Henry, L. A. *et al.* (2011) 'Endoglin expression in breast tumor cells suppresses invasion and metastasis and correlates with improved clinical outcome', *Oncogene*, 30(9), pp. 1046–1058. doi: 10.1038/onc.2010.488.

Heras, F. Las and Gahunia, H. K. (2020) 'Growth and development of articular cartilage', in *Articular Cartilage of the Knee: Health, Disease and Therapy*. Springer New York, pp. 71–95. doi: 10.1007/978-1-4939-7587-7_2.

Hildebrandt, C., Büth, H. and Thielecke, H. (2011) 'A scaffold-free in vitro model for osteogenesis of human mesenchymal stem cells', *Tissue and Cell*, 43(2), pp. 91–100. doi: 10.1016/j.tice.2010.12.004.

Hohdatsu, T., Tatekawa, T. and Koyama, H. (1995) 'Enhancement of feline infectious peritonitis virus type I infection in cell cultures using low-speed centrifugation', *Journal of Virological Methods*, 51(2–3), pp. 357–62.

Honoki, K. and Tsujiuchi, T. (2013) 'Senescence bypass in mesenchymal stem cells: A potential pathogenesis and implications of pro-senescence therapy in sarcomas', *Expert Review of Anticancer Therapy*, 13(8), pp. 983–996. doi: 10.1586/14737140.2013.820010.

Hu, L. *et al.* (2018) 'Mesenchymal stem cells: Cell fate decision to osteoblast or adipocyte and application in osteoporosis treatment', *International Journal of Molecular Sciences*, 19(2), p. 306. doi: 10.3390/ijms19020360.

Huang, Y. *et al.* (2015) 'Immortalization and characterization of human dental mesenchymal cells', *Journal of Dentistry*, 43(5), pp. 576–582. doi: 10.1016/j.jdent.2015.02.008.

Hung, S.-C. *et al.* (2004) 'Immortalization without neoplastic transformation of human mesenchymal stem cells by transduction with HPV16E6/E7 genes', *International Journal of Cancer*, 110(3), pp. 313–319. doi: 10.1002/ijc.20126.

Iaquinta, M. R. *et al.* (2019) 'Adult Stem Cells for Bone Regeneration and Repair', *Frontiers in Cell and Developmental Biology*, 7, p. 268. doi: 10.3389/fcell.2019.00268.

Introna, M. *et al.* (1998) 'Rapid retroviral infection of human haemopoietic cells of different lineages: efficient transfer in fresh T cells', *British Journal of Haematology*, 103(2), pp. 449–61.

Izgi, K. *et al.* (2017) 'Long Term Exposure to Myrtucommulone-A Changes CD105 Expression and Differentiation Potential of Mesenchymal Stem Cells', *Tissue Engineering and Regenerative Medicine*, 14(2), pp. 113–121. doi: 10.1007/s13770-016-0020-3.

Jäger, V. *et al.* (2013) 'High level transient production of recombinant antibodies and antibody fusion proteins in HEK293 cells', *BMC Biotechnology*, 13(1), p. 52. doi: 10.1186/1472-6750-13-52.

James, S. *et al.* (2015) 'Multiparameter Analysis of Human Bone Marrow Stromal Cells Identifies Distinct Immunomodulatory and Differentiation-Competent Subtypes', *Stem Cell Reports*, 4(6), pp. 1004–1015. doi: 10.1016/j.stemcr.2015.05.005.

Jayasuriya, C. T. *et al.* (2018) 'Molecular characterization of mesenchymal stem cells in human osteoarthritis cartilage reveals contribution to the OA phenotype', *Scientific Reports*, 8(1), p. 7044. doi: 10.1038/s41598-018-25395-8.

Jenei-Lanzl, Z., Meurer, A. and Zaucke, F. (2019) 'Interleukin-1β signaling in osteoarthritis – chondrocytes in focus', *Cellular Signalling*, 53, pp. 212–223. doi: 10.1016/j.cellsig.2018.10.005.

Jeon, O. H. and Elisseeff, J. (2016) 'Orthopedic tissue regeneration: cells, scaffolds, and small molecules', *Drug Delivery and Translational Research*, 6(2), pp. 105–120. doi: 10.1007/s13346-015-0266-7.

Joglekar, A. V. *et al.* (2014) 'Dissecting the mechanism of histone deacetylase inhibitors to enhance the activity of zinc finger nucleases delivered by integrase-defective lentiviral vectors', *Human Gene Therapy*, 25(7), pp. 599–608. doi: 10.1089/hum.2013.211.

Kim, E. C. *et al.* (2015) 'Effects of moderate intensity static magnetic fields on human bone marrow-derived mesenchymal stem cells', *Bioelectromagnetics*, 36(4), pp. 267–276. doi: 10.1002/bem.21903.

Knuth, C. A. *et al.* (2018) 'Isolating Pediatric Mesenchymal Stem Cells with Enhanced Expansion and Differentiation Capabilities', *Tissue engineering - Part C Methods*, 24(6), pp. 313–321. doi: 10.1089/ten.TEC.2018.0031.

Koch, C. M. *et al.* (2013) 'Pluripotent stem cells escape from senescence-associated DNA methylation changes', *Genome Research*, 23(2), pp. 248–259. doi: 10.1101/gr.141945.112.

Koelling, S. *et al.* (2009) 'Migratory Chondrogenic Progenitor Cells from Repair Tissue during the Later Stages of Human Osteoarthritis', *Cell Stem Cell*, 4(4), pp. 324–335. doi: 10.1016/j.stem.2009.01.015.

Kohler, S. L. *et al.* (2016) 'Germinal Center T Follicular Helper Cells Are Highly Permissive to HIV-1 and Alter Their Phenotype during Virus Replication', *The Journal of Immunology*, 196(6), pp. 2711–2722. doi: 10.4049/jimmunol.1502174.

Kolen'ko, Y. V. *et al.* (2014) 'Large-Scale Synthesis of Colloidal Fe_3O_4 Nanoparticles Exhibiting High Heating Efficiency in Magnetic Hyperthermia', *The Journal of Physical Chemistry C*, 118(16), pp. 8691–8701. doi: 10.1021/jp500816u.

Kotani, H. *et al.* (1994) 'Improved Methods of Retroviral Vector Transduction and Production for Gene Therapy', *Human Gene Therapy*, 5(1), pp. 19–28. doi: 10.1089/hum.1994.5.1-19.

Kouroupis, D. *et al.* (2018) 'MSC functionalization for enhanced therapeutic applications', *Tissue Engineering - Part B: Reviews*, 25(1), pp. 55-77. doi: 10.1089/ten.TEB.2018.0118.

Kraus, V. B. *et al.* (2015) 'Call for standardized definitions of osteoarthritis and risk stratification for clinical trials and clinical use', *Osteoarthritis and Cartilage*, 23(8), pp. 1233–1241. doi: 10.1016/j.joca.2015.03.036.

Kusuyama, J. *et al.* (2018) 'Spleen tyrosine kinase influences the early stages of multilineage differentiation of bone marrow stromal cell lines by regulating phospholipase C gamma activities', *Journal of Cellular Physiology*, 233(3), pp. 2549–2559. doi: 10.1002/jcp.26130.

Larsen, K. H. *et al.* (2009) 'Identifying A Molecular Phenotype for Bone Marrow Stromal Cells With *In Vivo* Bone Forming Capacity', *Journal of Bone and Mineral Research*, 25(4), pp. 796-808. doi: 10.1359/jbmr.091018.

Le, H. *et al.* (2020) 'Mesenchymal stem cells for cartilage regeneration', *Journal of Tissue Engineering*, 11, p. 2041731420943839. doi: 10.1177/2041731420943839.

Leão, R. *et al.* (2018) 'Mechanisms of human telomerase reverse transcriptase (hTERT) regulation: Clinical impacts in cancer', *Journal of Biomedical Science*, 25(1), p. 22. doi: 10.1186/s12929-018-0422-8.

Leber, J. *et al.* (2017) 'Microcarrier choice and bead-to-bead transfer for human mesenchymal stem cells in serum-containing and chemically defined media', *Process Biochemistry*, 59, pp. 255–265. doi: 10.1016/J.PROCBIO.2017.03.017.

Lee, K. S. *et al.* (2015) 'Characterization of a growth-elevated cell line of human bone marrow-derived mesenchymal stem cells by SV40 T-antigen', *Biotechnology and Bioprocess Engineering*, 20(3), pp. 498–505. doi: 10.1007/s12257-014-0730-0.

Leyva-Leyva, M. *et al.* (2015) 'Differential Expression of Adhesion-Related Proteins and MAPK Pathways Lead to Suitable Osteoblast Differentiation of Human Mesenchymal Stem Cells Subpopulations', *Stem Cells and Development*, 24(21), pp. 2577–2590. doi: 10.1089/scd.2015.0070.

Liang, X. *et al.* (2016) 'Dehydroepiandrosterone Stimulation of Osteoblastogenesis in Human MSCs Requires IGF-I Signaling', *Journal of Cellular Biochemistry*, 117(8), pp. 1769–1774. doi: 10.1002/jcb.25475.

Lin, P. *et al.* (2012) 'Efficient Lentiviral Transduction of Human Mesenchymal Stem Cells That Preserves Proliferation and Differentiation Capabilities', *STEM CELLS Translational Medicine*, 1(12), pp. 886–897. doi: 10.5966/sctm.2012-0086.

Liu, B. *et al.* (2015) 'β-catenin signaling induces the osteoblastogenic differentiation of human pre-osteoblastic and bone marrow stromal cells mainly through the upregulation of osterix expression', *International Journal of Molecular Medicine*, 36(6), pp. 1572–1582. doi: 10.3892/ijmm.2015.2382.

Liu, M.-C. *et al.* (2014) 'Establishment of a promising human nucleus pulposus cell line for intervertebral disc tissue engineering', *Tissue engineering - Part C: Methods*, 20(1), pp. 1–10. doi: 10.1089/ten.TEC.2013.0048.

Liu, M. *et al.* (2017) 'Injectable hydrogels for cartilage and bone tissue engineering', *Bone Research*, 5, p. 17014. doi: 10.1038/boneres.2017.14.

Liu, T. M. *et al.* (2013) 'Molecular Basis of Immortalization of Human Mesenchymal Stem Cells by Combination of p53 Knockdown and Human Telomerase Reverse Transcriptase Overexpression', *Stem Cells and Development*, 22(2), pp. 268–278. doi: 10.1089/scd.2012.0222.

Lu, Y. *et al.* (2019) 'Recent advances in cell sheet technology for bone and cartilage regeneration: from preparation to application', *International Journal of Oral Science*, 11(2), p. 17. doi: 10.1038/s41368-019-0050-5.

Lunyak, V. V., Amaro-Ortiz, A. and Gaur, M. (2017) 'Mesenchymal Stem Cells Secretory Responses: Senescence Messaging Secretome and Immunomodulation Perspective', *Frontiers in Genetics*, 8, p. 220. doi: 10.3389/fgene.2017.00220.

Lv, M. *et al.* (2019) 'Identification of Chondrocyte Genes and Signaling Pathways in Response to Acute Joint Inflammation', *Scientific Reports*, 9(1), p. 93. doi: 10.1038/s41598-018-36500-2.

Makris, E. A. *et al.* (2015) 'Repair and tissue engineering techniques for articular cartilage', *Nature Reviews Rheumatology*, 11(1), pp. 21–34. doi: 10.1038/nrrheum.2014.157.

Marolt Presen, D. *et al.* (2019) 'Mesenchymal Stromal Cell-Based Bone Regeneration Therapies: From Cell Transplantation and Tissue Engineering to Therapeutic Secretomes and Extracellular Vesicles', *Frontiers in Bioengineering and Biotechnology*, 7, p. 352. doi: 10.3389/fbioe.2019.00352.

Medeiros Tavares Marques, J. C. *et al.* (2017) 'Identification of new genes associated to senescent and tumorigenic phenotypes in mesenchymal stem cells', *Scientific Reports*, 7(1), p. 17837. doi: 10.1038/s41598-017-16224-5.

Mellor, L. *et al.* (2013) 'Intracellular domain fragment of CD44 alters CD44 function in chondrocytes', *Journal of Biological Chemistry*, 288(36), pp. 25838–25850. doi: 10.1074/jbc.M113.494872.

Meng, J. *et al.* (2010) 'Paramagnetic nanofibrous composite films enhance the osteogenic responses of pre-osteoblast cells', *Nanoscale*, 2(12), pp. 2565–2569. doi: 10.1039/c0nr00178c.

Mohamed-Ahmed, S. *et al.* (2018) 'Adipose-derived and bone marrow mesenchymal stem cells: A donor-matched comparison', *Stem Cell Research and Therapy*, 9(1), p. 168. doi: 10.1186/s13287-018-0914-1.

Mohanraj, B. *et al.* (2018) 'Chondrocyte and mesenchymal stem cell derived engineered cartilage exhibits differential sensitivity to pro-inflammatory cytokines', *Journal of Orthopaedic Research*, 36(11), pp. 2901–2910. doi: 10.1002/jor.24061.

Moiseeva, O. *et al.* (2015) 'Mutant lamin A links prophase to a p53 independent senescence program', *Cell Cycle*, 14(15), pp. 2408–2421. doi: 10.1080/15384101.2015.1053671.

Moll, U. M. and Petrenko, O. (2003) 'The MDM2-p53 Interaction', *Molecular Cancer Research*, 1(14), pp. 1001–1008.

Moon, H. E. *et al.* (2013) 'Mitochondrial Dysfunction of Immortalized Human Adipose Tissue-Derived Mesenchymal Stromal Cells from Patients with Parkinson's Disease', *Experimental Neurobiology*, 22(4), pp. 283–300. doi: 10.5607/en.2013.22.4.283.

Mori, T. *et al.* (2005) 'Combination of hTERT and bmi-1, E6, or E7 Induces Prolongation of the Life Span of Bone Marrow Stromal Cells from an Elderly Donor without Affecting Their Neurogenic Potential', *Molecular and Cellular Biology*, 25(12), pp. 5183–5195. doi: 10.1128/MCB.25.12.5183-5195.2005.

Moseti, D., Regassa, A. and Kim, W. K. (2016) 'Molecular regulation of adipogenesis and potential anti-adipogenic bioactive molecules', *International Journal of Molecular Sciences*, 17(1), p. 124. doi: 10.3390/ijms17010124.

Munisvaradass, R. *et al.* (2017) 'Human CD3+ T-Cells with the Anti-ERBB2 Chimeric Antigen Receptor Exhibit Efficient Targeting and Induce Apoptosis in ERBB2 Overexpressing Breast Cancer Cells', *International Journal of Molecular Sciences*, 18(9), p. 1797. doi: 10.3390/ijms18091797.

Neybecker, P. *et al.* (2020) 'Respective stemness and chondrogenic potential of mesenchymal stem cells isolated from human bone marrow, synovial membrane, and synovial fluid', *Stem Cell Research and Therapy*, 11(1), p. 316. doi: 10.1186/s13287-020-01786-5.

Ng, J. *et al.* (2017) 'Biomimetic Approaches for Bone Tissue Engineering', *Tissue Engineering - Part B: Reviews*, 23(5), pp. 480–493. doi: 10.1089/ten.teb.2016.0289.

Nijsure, M. P. and Kishore, V. (2018) 'Collagen-based scaffolds for bone tissue engineering applications', in *Orthopedic Biomaterials: Advances and Applications*. Springer International Publishing,

pp. 187–224. doi: 10.1007/978-3-319-73664-8_8.

Nürnberger, S. *et al.* (2019) 'Repopulation of an auricular cartilage scaffold, AuriScaff, perforated with an enzyme combination', *Acta Biomaterialia*, 86, pp. 207–222. doi: 10.1016/j.actbio.2018.12.035.

Ode, A. *et al.* (2011) 'CD73 and CD29 concurrently mediate the mechanically induced decrease of migratory capacity of mesenchymal stromal cells', *European Cells and Materials*, 22, pp. 26–42. doi: 10.22203/eCM.v022a03.

Ode, A. *et al.* (2013) 'CD73/5'-ecto-nucleotidase acts as a regulatory factor in osteo-/chondrogenic differentiation of mechanically stimulated mesenchymal stromal cells', *European Cells and Materials*, 25, pp. 37–47. doi: 10.22203/ecm.v025a03.

Ok, J. S., Song, S. B. and Hwang, E. S. (2018) 'Enhancement of replication and differentiation potential of human bone marrow stem cells by nicotinamide treatment', *International Journal of Stem Cells*, 11(1), pp. 13–25. doi: 10.15283/ijsc18033.

Okamoto, T. *et al.* (2002) 'Clonal heterogeneity in differentiation potential of immortalized human mesenchymal stem cells', *Biochemical and Biophysical Research Communications*, 295(2), pp. 354–61. doi: 10.1016/s0006-291x(02)00661-7.

Okita, N. *et al.* (2015) 'Supplementation of strontium to a chondrogenic medium promotes chondrogenic differentiation of human dedifferentiated fat cells', *Tissue Engineering - Part A*, 21(9–10), pp. 1695–704. doi: 10.1089/ten.TEA.2014.0282.

Osterhoff, G. *et al.* (2016) 'Bone mechanical properties and changes with osteoporosis', *Injury*, 47(Suppl 2), pp. S11–S20. doi: 10.1016/S0020-1383(16)47003-8.

Ozono, E., Yamaoka, S. and Ohtani, K. (2013) 'To Grow, Stop or Die? – Novel Tumor-Suppressive Mechanism Regulated by the Transcription Factor E2F', in *Future Aspects of Tumor Suppressor Gene*. InTech. doi: 10.5772/54510.

Pal, A. and Kundu, R. (2020) 'Human Papillomavirus E6 and E7: The Cervical Cancer Hallmarks and Targets for Therapy', *Frontiers in Microbiology*, 10, p. 3116. doi: 10.3389/fmicb.2019.03116.

Paniagua, R. *et al.* (2007) *Citología e histología vegetal y animal* (4th edn). Madrid, Spain: McGraw-Hill - Interamericana de España. ISBN: 978-84-481-5593-3.

Pérez-Gómez, E. *et al.* (2005) 'Characterization of murine S-endoglin isoform and its effects on tumor development', *Oncogene*, 24(27), pp. 4450–4461. doi: 10.1038/sj.onc.1208644.

Petecchia, L. *et al.* (2015) 'Electro-magnetic field promotes osteogenic differentiation of BM-hMSCs through a selective action on Ca^{2+}-related mechanisms', *Scientific Reports*, 5, p. 13856. doi: 10.1038/srep13856.

Phetfong, J. *et al.* (2016) 'Osteoporosis: The current status of mesenchymal stem cell-based therapy', *Cellular and Molecular Biology Letters*, 21, p. 12. doi: 10.1186/s11658-016-0013-1.

Piñeiro-Ramil, M. *et al.* (2018) 'Cell Therapy and Tissue Engineering for Cartilage Repair', in *Cartilage Repair and Regeneration*. InTech. doi: 10.5772/intechopen.70406.

Piñeiro-Ramil, M. *et al.* (2019) 'Usefulness of Mesenchymal Cell Lines for Bone and Cartilage Regeneration Research', *International Journal of Molecular Sciences*, 20(24), p. 6286. doi: 10.3390/ijms20246286.

Piñeiro-Ramil, M. *et al.* (2020) 'Immortalizing Mesenchymal Stromal Cells from Aged Donors while Keeping Their Essential Features', *Stem Cells International*, 2020, p. 5726947. doi: 10.1155/2020/5726947.

Prasopthum, A., Shakesheff, K. M. and Yang, J. (2018) 'Direct three-dimensional printing of polymeric scaffolds with nanofibrous topography', *Biofabrication*, 10(2), p. 025002. doi:

10.1088/1758-5090/aaa15b.

Qin, S. Q. *et al.* (2016) 'Establishment and characterization of fetal and maternal mesenchymal stem/stromal cell lines from the human term placenta', *Placenta*, 39, pp. 134–146. doi: 10.1016/j.placenta.2016.01.018.

Rashid, H. *et al.* (2014) 'Sp7 and Runx2 molecular complex synergistically regulate expression of target genes', *Connective Tissue Research*, 55(Suppl1), pp. 83–87. doi: 10.3109/03008207.2014.923872.

Raya, Á. *et al.* (2010) 'A protocol describing the genetic correction of somatic human cells and subsequent generation of iPS cells', *Nature Protocols*, 5(4), pp. 647–660. doi: 10.1038/nprot.2010.9.

Rim, Y. A., Nam, Y. and Ju, J. H. (2020) 'The role of chondrocyte hypertrophy and senescence in osteoarthritis initiation and progression', *International Journal of Molecular Sciences*, 21(7), p. 2358. doi: 10.3390/ijms21072358.

Ringe, J. and Sittinger, M. (2009) 'Tissue engineering in the rheumatic diseases', *Arthritis Research and Therapy*, 11(1), p. 211. doi: 10.1186/ar2572.

Roca-Lema, D. *et al.* (2019) '*In vitro* anti-proliferative and anti-invasive effect of polysaccharide-rich extracts from trametes versicolor and grifola frondosa in colon cancer cells', *International Journal of Medical Sciences*, 16(2), pp. 231–240. doi: 10.7150/ijms.28811.

Rosengren, S., Boyle, D. L. and Firestein, G. S. (2007) 'Acquisition, culture, and phenotyping of synovial fibroblasts', *Methods in Molecular Medicine*, 135, pp. 365–75.

Roseti, L. *et al.* (2017) 'Scaffolds for Bone Tissue Engineering: State of the art and new perspectives', *Materials Science and Engineering: C*, 78, pp. 1246–1262. doi: 10.1016/j.msec.2017.05.017.

Ross, C. L. *et al.* (2015) 'The effect of low-frequency electromagnetic field on human bone marrow stem/progenitor cell differentiation', *Stem Cell Research*, 15(1), pp. 96–108. doi: 10.1016/j.scr.2015.04.009.

Rotondo, J. C. *et al.* (2019) 'Association Between Simian Virus 40 and Human Tumors', *Frontiers in Oncology*, 9, p. 670. doi: 10.3389/fonc.2019.00670.

Samal, S. K. *et al.* (2015) 'Multilayered Magnetic Gelatin Membrane Scaffolds', *ACS Applied Materials and Interfaces*, 7(41), pp. 23098–23109. doi: 10.1021/acsami.5b06813.

Samoilovich, M. P. *et al.* (2018) 'Endoglin Expression in Non-tumor and Tumor Cells of Different Origin', *Cell and Tissue Biology*, 12(6), pp. 437–447. doi: 10.1134/S1990519X18060111.

Sampah, M. E. S. *et al.* (2015) 'Medroxyprogesterone acetate increases HIV-1 infection of unstimulated peripheral blood mononuclear cells in vitro', *AIDS*, 29(10), pp. 1137–1146. doi: 10.1097/QAD.0000000000000681.

Samsonraj, R. M. *et al.* (2017) 'Concise Review: Multifaceted Characterization of Human Mesenchymal Stem Cells for Use in Regenerative Medicine', *STEM CELLS Translational Medicine*, 6(12), pp. 2173–2185. doi: 10.1002/sctm.17-0129.

Sanjurjo-Rodríguez, C. *et al.* (2014) 'Human Cartilage Tissue Engineering Using Type I Collagen/Heparan Sulfate Scaffolds', *Journal of Regenerative Medicine*, 3(2). doi: 10.4172/2325-9620.1000116.

Santos, L. J., Reis, R. L. and Gomes, M. E. (2015) 'Harnessing magnetic-mechano actuation in regenerative medicine and tissue engineering', *Trends in Biotechnology*, 33(8), pp. 471–479. doi: 10.1016/j.tibtech.2015.06.006.

Scanlan, P. M. *et al.* (2005) 'Spinoculation of heparan sulfate deficient cells enhances HSV-1 entry, but does not abolish the need for essential glycoproteins in viral fusion', *Journal of Virological Methods*,

128(1–2), pp. 104–112. doi: 10.1016/j.jviromet.2005.04.008.

Schmeer, C. *et al.* (2019) 'Dissecting Aging and Senescence-Current Concepts and Open Lessons', *Cells*, 8(11), p. 1446. doi: 10.3390/cells8111446.

Schmidt, J. C. and Cech, T. R. (2015) 'Human telomerase: Biogenesis, trafficking, recruitment, and activation', *Genes and Development*, 29(11), pp. 1095–1105. doi: 10.1101/gad.263863.115.

Schoonderwoerd, M. J. A., Goumans, M. J. T. H. and Hawinkels, L. J. A. C. (2020) 'Endoglin: Beyond the endothelium', *Biomolecules*, 10(2), p. 289. doi: 10.3390/biom10020289.

Shu, Y. *et al.* (2018) 'Reversibly immortalized human umbilical cord-derived mesenchymal stem cells (UC-MSCs) are responsive to BMP9-induced osteogenic and adipogenic differentiation', *Journal of Cellular Biochemistry*, 119(11), pp. 8872–8886. doi: 10.1002/jcb.27140.

Simmons, A. and Alberola-Ila, J. (2016) 'Retroviral Transduction of T Cells and T Cell Precursors', *Methods in Molecular Biology*, 1323, pp. 99–108. doi: 10.1007/978-1-4939-2809-5_8.

Simonsen, J. L. *et al.* (2002) 'Telomerase expression extends the proliferative life-span and maintains the osteogenic potential of human bone marrow stromal cells', *Nature Biotechnology*, 20(6), pp. 592–596. doi: 10.1038/nbt0602-592.

Siska, E. K. *et al.* (2017) 'Generation of an immortalized mesenchymal stem cell line producing a secreted biosensor protein for glucose monitoring', *PLOS ONE*, 12(9), p. e0185498. doi: 10.1371/journal.pone.0185498.

Skårn, M. *et al.* (2014) 'Generation and Characterization of an Immortalized Human Mesenchymal Stromal Cell Line', *Stem Cells and Development*, 23(19), pp. 2377–2389. doi: 10.1089/scd.2013.0599.

Smith, B. D. and Grande, D. A. (2015) 'The current state of scaffolds for musculoskeletal regenerative applications', *Nature Reviews Rheumatology*, 11(4), pp. 213–222. doi: 10.1038/nrrheum.2015.27.

Somoza, R. A. *et al.* (2014) 'Chondrogenic differentiation of mesenchymal stem cells: challenges and unfulfilled expectations', *Tissue engineering - Part B: Reviews*, 20(6), pp. 596–608. doi: 10.1089/ten.TEB.2013.0771.

Song, D. *et al.* (2017) 'BMP9 induces osteogenesis and adipogenesis in the immortalized human cranial suture progenitors from the patent sutures of craniosynostosis patients', *Journal of Cellular and Molecular Medicine*, 21(11), pp. 2782–2795. doi: 10.1111/jcmm.13193.

Sreekumar, V. *et al.* (2018) 'Resveratrol protects primary cilia integrity of human mesenchymal stem cells from cigarette smoke to improve osteogenic differentiation in vitro', *Archives of Toxicology*, 92(4), pp. 1525–1538. doi: 10.1007/s00204-017-2149-9.

Steele, A. K. *et al.* (2014) 'Microbial exposure alters HIV-1-induced mucosal CD4+ T cell death pathways *ex vivo*', *Retrovirology*, 11(1), p. 14. doi: 10.1186/1742-4690-11-14.

Stewart, S. *et al.* (2015) 'Bone Regeneration', in *Translational Regenerative Medicine*. Elsevier Inc., pp. 313–333. doi: 10.1016/B978-0-12-410396-2.00024-4.

Stölzel, K. *et al.* (2015) 'Immortalised human mesenchymal stem cells undergo chondrogenic differentiation in alginate and PGA/PLLA scaffolds', *Cell and Tissue Banking*, 16(1), pp. 159–170. doi: 10.1007/s10561-014-9457-6.

Stranford, D. M. *et al.* (2017) 'A Systematic Evaluation of Factors Affecting Extracellular Vesicle Uptake by Breast Cancer Cells', *Tissue engineering - Part A*, 23(21–22), pp. 1274–1282. doi: 10.1089/ten.TEA.2017.0158.

Su, N. *et al.* (2019) 'Bone function, dysfunction and its role in diseases including critical illness', *International Journal of Biological Sciences*, 15(4), pp. 776–787. doi: 10.7150/ijbs.27063.

Su, P. *et al.* (2018) 'Mesenchymal stem cell migration during bone formation and bone diseases therapy', *International Journal of Molecular Sciences*, 19(8), p. 2343. doi: 10.3390/ijms19082343.

Sugimoto, A. *et al.* (2017) 'Piezo type mechanosensitive ion channel component 1 functions as a regulator of the cell fate determination of mesenchymal stem cells', *Scientific Reports*, 7(1), p. 17696. doi: 10.1038/s41598-017-18089-0.

Sultana, Z. *et al.* (2018) 'Is there a role for placental senescence in the genesis of obstetric complications and fetal growth restriction?', *American Journal of Obstetrics and Gynecology*, 218(Suppl2) pp. S762–S773. doi: 10.1016/j.ajog.2017.11.567.

Swift, S. *et al.* (2001) 'Rapid Production of Retroviruses for Efficient Gene Delivery to Mammalian Cells Using 293T Cell-Based Systems', in *Current Protocols in Immunology*. Hoboken, NJ, USA: John Wiley & Sons, Inc., p. Unit 10.17C. doi: 10.1002/0471142735.im1017cs31.

Szychlinska, M. A. *et al.* (2017) 'Mesenchymal Stem Cell-Based Cartilage Regeneration Approach and Cell Senescence: Can We Manipulate Cell Aging and Function?', *Tissue engineering - Part B: Reviews*, 23(6), pp. 529–539. doi: 10.1089/ten.TEB.2017.0083.

Takeda, Y. *et al.* (2004) 'Can the life span of human marrow stromal cells be prolonged by bmi-1, E6, E7, and/or telomerase without affecting cardiomyogenic differentiation?', *The Journal of Gene Medicine*, 6(8), pp. 833–845. doi: 10.1002/jgm.583.

Takeuchi, M. *et al.* (2015) 'Transcriptional Dynamics of Immortalized Human Mesenchymal Stem Cells during Transformation', *PLOS ONE*, 10(5), p. e0126562. doi: 10.1371/journal.pone.0126562.

Tamaddon, M. *et al.* (2018) 'Osteochondral tissue repair in osteoarthritic joints: clinical challenges and opportunities in tissue engineering', *Bio-Design and Manufacturing*, 1(2), pp. 101–114. doi: 10.1007/s42242-018-0015-0.

Tan, Q., Lui, P. P. Y. and Rui, Y. F. (2012) 'Effect of In Vitro Passaging on the Stem Cell-Related Properties of Tendon-Derived Stem Cells—Implications in Tissue Engineering', *Stem Cells and Development*, 21(5), pp. 790–800. doi: 10.1089/scd.2011.0160.

Tátrai, P. *et al.* (2012) 'Combined introduction of Bmi-1 and hTERT immortalizes human adipose tissue-derived stromal cells with low risk of transformation', *Biochemical and Biophysical Research Communications*, 422(1), pp. 28–35. doi: 10.1016/j.bbrc.2012.04.088.

Thalmeier, K. *et al.* (1994) 'Establishment of two permanent human bone marrow stromal cell lines with long-term post irradiation feeder capacity', *Blood*, 83(7), pp. 1799–1807.

Tsai, C.-C. *et al.* (2010) 'Overexpression of hTERT increases stem-like properties and decreases spontaneous differentiation in human mesenchymal stem cell lines', *Journal of Biomedical Science*, 17(1), p. 64. doi: 10.1186/1423-0127-17-64.

Uder, C. *et al.* (2018) 'Mammalian MSC from selected species: Features and applications', *Cytometry Part A*, 93(1), pp. 32–49. doi: 10.1002/cyto.a.23239.

Vaamonde-García, C. *et al.* (2012) 'Mitochondrial dysfunction increases inflammatory responsiveness to cytokines in normal human chondrocytes', *Arthritis & Rheumatism*, 64(9), pp. 2927–2936. doi: 10.1002/art.34508.

Vandesompele, J. *et al.* (2002) 'Accurate normalization of real-time quantitative RT-PCR data by geometric averaging of multiple internal control genes', *Genome biology*, 3(7). doi: 10.1186/gb-2002-3-7-research0034.

Vas, W. J. *et al.* (2017) 'Biomimetic strategies for fracture repair: Engineering the cell microenvironment for directed tissue formation', *Journal of Tissue Engineering*, 8, p. 2041731417704791. doi: 10.1177/2041731417704791.

Vinatier, C. and Guicheux, J. (2016) 'Cartilage tissue engineering: From biomaterials and stem cells

to osteoarthritis treatments', *Annals of Physical and Rehabilitation Medicine*, 59(3), pp. 139–144. doi: 10.1016/j.rehab.2016.03.002.

Vincent, T. L. (2019) 'Il-1 in osteoarthritis: Time for a critical review of the literature', *F1000Research*, 8, p. 934. doi: 10.12688/f1000research.18831.1.

Wagner, W. *et al.* (2009) 'Aging and replicative senescence have related effects on human stem and progenitor cells', *PLoS ONE*, 4(6), p. e5846. doi: 10.1371/journal.pone.0005846.

Wang, Q. *et al.* (2016) 'Response of MAPK pathway to iron oxide nanoparticles in vitro treatment promotes osteogenic differentiation of hBMSCs', *Biomaterials*, 86, pp. 11–20. doi: 10.1016/j.biomaterials.2016.02.004.

Wang, X. and Dai, J. (2010) 'Concise review: Isoforms of OCT4 contribute to the confusing diversity in stem cell biology', *Stem Cells*, 28(5), pp. 885–893. doi: 10.1002/stem.419.

Wellinger, R. J. (2014) 'In the end, what's the problem?', *Molecular Cell*, 53(6), pp. 855–856. doi: 10.1016/j.molcel.2014.03.008.

Williams, R. *et al.* (2010) 'Identification and clonal characterisation of a progenitor cell sub-population in normal human articular cartilage', *PLoS ONE*, 5(10), p. e13246. doi: 10.1371/journal.pone.0013246.

Wilson, K. M. *et al.* (2018) 'Glycans modify mesenchymal stem cell differentiation to impact on the function of resulting osteoblasts', *Journal of Cell Science*, 131(4), p. jcs209452. doi: 10.1242/jcs.209452.

de Windt, T. S. *et al.* (2014) 'Concise Review: Unraveling Stem Cell Cocultures in Regenerative Medicine: Which Cell Interactions Steer Cartilage Regeneration and How?', *STEM CELLS Translational Medicine*, 3(6), pp. 723–733. doi: 10.5966/sctm.2013-0207.

Wolbank, S. *et al.* (2009) '*Telomerase* Immortalized Human Amnion- and Adipose-Derived Mesenchymal Stem Cells: Maintenance of Differentiation and Immunomodulatory Characteristics', *Tissue Engineering - Part A*, 15(7), pp. 1843–1854. doi: 10.1089/ten.tea.2008.0205.

Wong, J. M. Y., Kusdra, L. and Collins, K. (2002) 'Subnuclear shuttling of human telomerase induced by transformation and DNA damage', *Nature Cell Biology*, 4(9), pp. 731–736. doi: 10.1038/ncb846.

Wu, Y. *et al.* (2015) 'TrAmplification of Human Dental Follicle Cells by piggyBac Transposon - Mediated Reversible Immortalization System', *PLOS ONE*, 10(7), p. e0130937. doi: 10.1371/journal.pone.0130937.

Wulhfard, S. *et al.* (2010) 'Valproic acid enhances recombinant mRNA and protein levels in transiently transfected Chinese hamster ovary cells', *Journal of Biotechnology*, 148(2–3), pp. 128–132. doi: 10.1016/j.jbiotec.2010.05.003.

Xia, Y. *et al.* (2018) 'Magnetic field and nano-scaffolds with stem cells to enhance bone regeneration', *Biomaterials*, 183, pp. 151–170. doi: 10.1016/j.biomaterials.2018.08.040.

Yan, R. *et al.* (2015) 'Spinoculation Enhances HBV Infection in NTCP-Reconstituted Hepatocytes', *PLOS ONE*, 10(6), p. e0129889. doi: 10.1371/journal.pone.0129889.

Yang, W. C. *et al.* (2014) 'Addition of valproic acid to CHO cell fed-batch cultures improves monoclonal antibody titers', *Molecular Biotechnology*, 56(5), pp. 421–428. doi: 10.1007/s12033-013-9725-x.

Yang, Y.-H. K. *et al.* (2018) 'Changes in phenotype and differentiation potential of human mesenchymal stem cells aging *in vitro*', *Stem Cell Research & Therapy*, 9(1), p. 131. doi: 10.1186/s13287-018-0876-3.

Ye, L. *et al.* (2008) 'Centrifugal enhancement of hepatitis C virus infection of human hepatocytes', *Journal of Virological Methods*, 148(1–2), pp. 161–165. doi: 10.1016/j.jviromet.2007.11.002.

Yun, H. M. *et al.* (2016) 'Magnetic nanocomposite scaffolds combined with static magnetic field in the stimulation of osteoblastic differentiation and bone formation', *Biomaterials*, 85, pp. 88–98. doi: 10.1016/j.biomaterials.2016.01.035.

Zhang, C., Zhang, G. and Liu, D. (2019) 'Histone deacetylase inhibitors reactivate silenced transgene *in vivo*', *Gene Therapy*, 26(3–4), pp. 75–85. doi: 10.1038/s41434-018-0053-4.

Zhang, J. *et al.* (2016) 'Ageing and the telomere connection: An intimate relationship with inflammation', *Ageing Research Reviews*, 25, pp. 55–69. doi: 10.1016/j.arr.2015.11.006.

Zhang, W. *et al.* (2016) 'Current research on pharmacologic and regenerative therapies for osteoarthritis', *Bone Research*, 4, p. 15040. doi: 10.1038/boneres.2015.40.

Zhao, J. J. *et al.* (2003) 'Human mammary epithelial cell transformation through the activation of phosphatidylinositol 3-kinase', *Cancer Cell*, 3(5), pp. 483–495.

Zhou, B. O. *et al.* (2014) 'Leptin-receptor-expressing mesenchymal stromal cells represent the main source of bone formed by adult bone marrow', *Cell Stem Cell*, 15(2), pp. 154–168. doi: 10.1016/j.stem.2014.06.008.

Zhou, J. min *et al.* (2019) 'OCT4B1 Promoted EMT and Regulated the Self-Renewal of CSCs in CRC: Effects Associated with the Balance of miR-8064/PLK1', *Molecular Therapy - Oncolytics*, 15, pp. 7–20. doi: 10.1016/j.omto.2019.08.004.

Zhou, Y., Tsai, T.-L. and Li, W.-J. (2017) 'Strategies to retain properties of bone marrow-derived mesenchymal stem cells *ex vivo*', *Annals of the New York Academy of Sciences*, 1409(1), pp. 3–17. doi: 10.1111/nyas.13451.

VIII. Annexes

Annex I – Ethics committee approval

XUNTA DE GALICIA
CONSELLERÍA DE SANIDADE
Secretaría Xeral Técnica

Secretaria Técnica
Comité Autonómico de Ética da Investigación de Galicia
Secretaria Xeral. Consellería de Sanidade
Edificio Administrativo San Lázaro
15703 SANTIAGO DE COMPOSTELA
Tel: 881 546425; ceic@sergas.es

galicia

DICTAMEN DEL COMITÉ DE ÉTICA DE LA INVESTIGACIÓN DE A CORUÑA-FERROL

Carlos Rodríguez Moreno, Secretario del Comité de Ética de la Investigación de A Coruña-Ferrol

CERTIFICA:

Que este Comité evaluó en su reunión del día 2016/588 el estudio:

Título: Generación y caracterización de líneas celulares mesenquimales para la investigación en enfermedades reumáticas
Promotor: Silvia María Díaz Prado, Isaac Manuel Fuentes Boquete
Tipo de estudio: Outros
Version:
Código del Promotor:
Código de Registro: 2016/588

Y, tomando en consideración las siguientes cuestiones:

- La pertinencia del estudio, teniendo en cuenta el conocimiento disponible, así como los requisitos legales aplicables, y en particular la Ley 14/2007, de investigación biomédica, el Real Decreto 1716/2011, de 18 de noviembre, por el que se establecen los requisitos básicos de autorización y funcionamiento de los biobancos con fines de investigación biomédica y del tratamiento de las muestras biológicas de origen humano, y se regula el funcionamiento y organización del Registro Nacional de Biobancos para investigación biomédica, la ORDEN SAS/3470/2009, de 16 de diciembre, por la que se publican las Directrices sobre estudios Posautorización de Tipo Observacional para medicamentos de uso humano, y el la Circular nº 07 / 2004, investigaciones clínicas con productos sanitarios.
- La idoneidad del protocolo en relación con los objetivos del estudio, justificación de los riesgos y molestias previsibles para el sujeto, así como los beneficios esperados.
- Los principios éticos de la Declaración de Helsinki vigente.
- Los Procedimientos Normalizados de Trabajo del Comité.

Emite un **INFORME FAVORABLE** para la realización del estudio **por el/la investigador/a del centro**:

Centros	Investigadores Principales
INIBIC-C.H. Universitario de A Coruña	Silvia María Díaz Prado, Isaac Manuel Fuentes Boquete

Firmado digitalmente por: RODRIGUEZ MORENO CARLOS - 05614327G
ND: CN = RODRIGUEZ MORENO CARLOS - 05614327G C = ES
Fecha: 2016.12.22 12:29:58 +02'00'

XUNTA DE GALICIA
CONSELLERÍA DE SANIDADE
Secretaría Xeral Técnica

Secretaria Técnica
Comité Autonómico de Ética da Investigación de Galicia
Secretaria Xeral. Consellería de Sanidade
Edificio Administrativo San Lázaro
15703 SANTIAGO DE COMPOSTELA
Tel: 881 546425; ceic@sergas.es

galicia

Y hace constar que:

1. El Comité Territorial de Ética de la Investigación de A Coruña-Ferrol cumple los requisitos legales vigentes (R.D 223/2004 de ensayos clínicos, y la Ley 14/2007 de Investigación Biomédica).
2. El Comité Territorial de Ética de la Investigación de A Coruña-Ferrol tanto en su composición como en sus PNTs cumple las Normas de Buena Práctica Clínica (CPMP/ICH/135/95).
3. La composición actual del Comité Territorial de Ética de la Investigación de A Coruña-Ferrol es:

Salvador Pita Fernández (Presidente). Médico especialista en Medicina Familiar y Comunitaria. Área de Gestión Integrada A Coruña.
Lucía Fuster Sanjurjo (Vicepresidenta). Farmacéutica. Especialista en Farmacia Hospitalaria. Área de Gestión Integrada Ferrol
Carlos Rodríguez Moreno (Secretario). Médico especialista en Farmacología Clínica. Área de Gestión Integrada Santiago
Natalia Cal Purriños (Vicesecretaria). Licenciada en derecho. Fundación "Profesor Nóvoa Santos". A Coruña
Juana Mª Cruz del Rio. Trabajadora social. Consellería de Sanidad
Begoña Graña Suárez. Médica especialista en Oncología Médica. Área de Gestión Integrada A Coruña
Angel Lopez-Silvarrey Varela. Médico especialista en Pediatría. Área de Gestión Integrada A Coruña
Alejandro Pazos Sierra. Médico. Universidad de A Coruña
Gonzalo Peña Pérez. Médico especialista en Cardiología. Hospital de San Rafael. A Coruña
José Mª Rumbo Prieto. Diplomado en enfermería. Área de Gestión Integrada Ferrol
María Isabel Sastre Gervás. Farmacéutica Atención Primaria. Área de Gestión Integrada A Coruña

Para que conste donde proceda, y a petición del promotor / investigador, en Santiago de Compostela,

El secretario

Firmado digitalmente por: RODRIGUEZ MORENO CARLOS - 05614327G
ND: CN = RODRIGUEZ MORENO CARLOS - 05614327G C = ES
Fecha: 2016.12.22 12:30:08 +02'00'

Annex II – Patient informed consent

INFORMACIÓN PARA EL PACIENTE Y CONSENTIMIENTO INFORMADO

D. / Dña.:

INTRODUCCIÓN.-

Se le propone participar en un proyecto de investigación sobre enfermedades del aparato locomotor que será realizado por el Servicio de Reumatología del Complejo Hospitalario Universitario A Coruña, bajo la dirección del **Dr. Blanco.**

Este proyecto será realizado en la Unidad de Investigación del C.H.U. A Coruña.

OBJETIVO DEL PROYECTO.-

El objetivo de este estudio se centra en estudiar los mecanismos que participan en la patogénesis de las enfermedades del aparato locomotor.

DESCRIPCIÓN DEL PROYECTO.-

Usted ha sido sometido a una intervención quirúrgica en la que se le han extraído tejidos articulares los cuales, siguiendo la normativa de eliminación de residuos biológicos, serán incinerados. Si usted decide participar en este estudio, sus tejidos, en lugar de ser eliminados, serán enviados a la Unidad de Investigación del C.H.U. A Coruña para que se almacenen en el Banco de Muestras de dicho Hospital para, posteriormente, realizar los estudios de investigación encaminados a conocer mejor por qué se producen algunas enfermedades del aparato locomotor.

Así mismo se le solicita autorización para la extracción de saliva o 10ml de sangre, siendo extraída esta última siguiendo el procedimiento rutinario para efectuar análisis estándar de sangre.

RIESGOS.-

Usted no va a sufrir ningún tipo de inconveniente o riesgo físico adicional al de la propia intervención quirúrgica a la que se le ha sometido, por consentir la utilización de las muestras que se le han extraído durante la misma.

COMPENSACIÓN.-

Usted no recibirá ningún tipo de compensación económica o de cualquier otro tipo por su participación, independientemente de que los resultados de los estudios que se van a realizar puedan dar lugar a patentes con fines médicos.

CONFIDENCIALIDAD.-

Toda la información que se obtenga de analizar su muestra, así como toda la información clínica referente a usted utilizada en las investigaciones futuras, será considerada confidencial y tratada en consecuencia, de acuerdo con lo establecido en la Ley Orgánica 15/1999, de 13 de Diciembre, de Protección de Datos de Carácter Personal y la Ley 14/2007, de 3 de Julio de Investigación Biomédica.

Para garantizar la confidencialidad de su identidad (asegurar que la información de su muestra de sangre no se relaciona con su identidad), su muestra sólo irá identificada desde el mismo momento de la extracción con un código. Sólo este código, y nunca su identidad aparecerá en las bases de datos donde figure la información clínica o genética referida a usted. La relación entre su código y su identidad quedará custodiada por el personal autorizado del equipo investigador, adoptándose las medidas necesarias para que tal información no esté disponible salvo para el personal autorizado, el cual tiene el deber legal de guardar secreto. De esta manera podemos asegurar que cualquier información que se obtenga a partir de su muestra de sangre permanezca confidencial.

Es importante que entienda que existe la posibilidad de que sus datos y parte de su muestra sean transferidos a otros equipos de investigación que trabajen en el mismo campo. En tal caso, se asegurará que estos datos sean tratados con la misma confidencialidad descrita anteriormente.

Por otro lado, es posible que los resultados de las investigaciones sean publicados en la literatura científica, pero entendiendo estos resultados como los obtenidos de la totalidad de las muestras, no los resultados individuales. Si este fuera el caso, su identidad permanecerá completamente confidencial y nunca formará parte de ninguna publicación.

Con su aceptación a participar en el proyecto, usted accede a que esta información pueda ser transferida en las mencionadas condiciones.

NUEVOS HALLAZGOS Y RESULTADOS.-

Como ya se ha descrito, se adoptarán estrictas medidas de seguridad para garantizar la confidencialidad de los resultados de los estudios realizados.

La evaluación de los resultados se hará sólo por grupos (por ejemplo, hombres / mujeres, grupos de edad, etc.) y no de forma individual. Debe comprender que los resultados de valor que se pudieran obtener provendrían del estudio de múltiples muestras, y en ningún caso de la suya exclusivamente.

Las implicaciones médicas de los resultados de las distintas pruebas, si es que los hay, sólo serán conocidas cuando se hayan completado los proyectos de investigación.

Usted debe saber que, en cumplimiento de la Ley 14/2007, de 3 de Julio, de Investigación Biomédica, tiene derecho a conocer o no, la información obtenida con el análisis de sus muestras.

En el caso de que usted decida no ser informado, la ley establece que cuando la información obtenida sea necesaria para evitar un grave perjuicio para la salud de sus familiares biológicos, se podrá informar a los afectados o a sus representantes legales.

PARTICIPACIÓN VOLUNTARIA.-

Su participación en el proyecto de investigación es totalmente voluntaria.

Si firma el consentimiento informado, confirmará que desea participar.

Puede negarse a participar o retirar su consentimiento en cualquier momento posterior a la firma sin tener que explicar los motivos.

Si decide retirar su consentimiento, su muestra será destruida y sólo se guardará la información obtenida hasta ese momento.

Su no-participación o retirada posterior del consentimiento no afectará en modo alguno a su asistencia médica presente o futura.

OBTENCIÓN DE INFORMACIÓN ADICIONAL.-

Usted puede contactar con cualquier miembro del Servicio de Reumatología del C.H.U. A Coruña si le surge cualquier duda sobre su participación en este proyecto o sobre sus derechos como paciente, en el teléfono 981176399.

En todo momento se pondrán los medios necesarios para facilitarle la información más adecuada.

SERVIZO GALEGO de SAÚDE | Complexo Hospitalario Universitario A Coruña A Coruña

CONSENTIMIENTO INFORMADO DEL PACIENTE

Yo, _____(nombre del paciente),

He leído la información que se me ha entregado.

He podido hacer preguntas sobre el proyecto.

He recibido suficiente información sobre el mismo.

He hablado de ello con_____

Comprendo que mi participación es voluntaria.

Comprendo que puedo retirar mi consentimiento:

1º. Cuando quiera.

2º. Sin tener que dar explicaciones.

3º. Sin que esto repercuta en mis cuidados médicos.

Presto libremente mi conformidad para participar en el proyecto.

FIRMA DEL PACIENTE	**Nombre**	**Fecha**

He explicado por completo los detalles relevantes de este proyecto al donante y/o la persona autorizada a dar el consentimiento en su nombre.

FIRMA	**Nombre**	**Fecha**

SERVIZO GALEGO de SAÚDE | Complexo Hospitalario Universitario A Coruña A Coruña

CONSENTIMIENTO INFORMADO DEL ACOMPAÑANTE

Yo, _____(nombre del acompañante del paciente), con DNI:_____ y en calidad de _____(parentesco con el donante) certifico que a _____(nombre del paciente),

Se le ha leído la información establecida en este escrito.

Se le ha entregado copia de esta información.

Ha podido hacer preguntas sobre el proyecto.

Ha recibido suficiente información sobre el mismo.

Hemos hablado de ello con_____

Comprende que su participación es voluntaria.

Comprende que puede retirar su consentimiento:

1º. Cuando quiera.

2º. Sin tener que dar explicaciones.

3º. Sin que esto repercuta en sus cuidados médicos.

Presta libremente su conformidad para participar en el proyecto.

Me autoriza a firmar en su nombre.

FIRMA DEL ACOMPAÑANTE DEL PACIENTE **Nombre** **Fecha**

He explicado por completo los detalles relevantes de este proyecto al donante y/o la persona autorizada a dar el consentimiento en su nombre.

FIRMA **Nombre** **Fecha**

Annex III – Plasmid sequencing results

Sequence 1. Alignment of the sequence obtained from the plasmid pBABE-puro-SV40LT employing the plasmid pBABE_F1 with the sequence provided by *Addgene*.

```
pBABE-puro-SV40LT_seq          CAGAGAGGAATCTTTGCAGCTAATGGACCTTCTAGGTCTTGAAAGGAGTGCCTGGGGGAA
pBABE-puro-SV40LT_addgene      CAGAGAGGAATCTTTGCAGCTAATGGACCTTCTAGGTCTTGAAAGGAGTGCCTGGGGGAA
                               ************************************************************

pBABE-puro-SV40LT_seq          TATTCCTCTGATGAGAAAGGCATATTTAAAAAAATGCAAGGAGTTTCATCCTGATAAAGG
pBABE-puro-SV40LT_addgene      TATTCCTCTGATGAGAAAGGCATATTTAAAAAAATGCAAGGAGTTTCATCCTGATAAAGG
                               ************************************************************

pBABE-puro-SV40LT_seq          AGGAGATGAAGAAAAAATGAAGAAAATGAATACTCTGTACAAGAAAATGGAAGATGGAGT
pBABE-puro-SV40LT_addgene      AGGAGATGAAGAAAAAATGAAGAAAATGAATACTCTGTACAAGAAAATGGAAGATGGAGT
                               ************************************************************

pBABE-puro-SV40LT_seq          AAAATATGCTCATCAACCTGACTTTGGAGGCTTCTGGGATGCAACTGAGATTCCAACCTA
pBABE-puro-SV40LT_addgene      AAAATATGCTCATCAACCTGACTTTGGAGGCTTCTGGGATGCAACTGAGATTCCAACCTA
                               ************************************************************

pBABE-puro-SV40LT_seq          TGGAACTGATGAATGGGAGCAGTGGTGGAATGCCTTTAATGAGGAAAACCTGTTTTGCTC
pBABE-puro-SV40LT_addgene      TGGAACTGATGAATGGGAGCAGTGGTGGAATGCCTTTAATGAGGAAAACCTGTTTTGCTC
                               ************************************************************

pBABE-puro-SV40LT_seq          AGAAGAAATGCCATCTAGTGATGATGAGGCTACTGCTGACTCTCAACATTCTACTCCTCC
pBABE-puro-SV40LT_addgene      AGAAGAAATGCCATCTAGTGATGATGAGGCTACTGCTGACTCTCAACATTCTACTCCTCC
                               ************************************************************

pBABE-puro-SV40LT_seq          -AAAAAGAAGAGAAAGGTAGAAGACCCCAAGGACTTTCCTTCAGAATTGCTAAGTTTTTT
pBABE-puro-SV40LT_addgene      AAAAAAGAAGAGAAAGGTAGAAGACCCCAAGGACTTTCCTTCAGAATTGCTAAGTTTTTT
                                ************************************************************

pBABE-puro-SV40LT_seq          GAGTCATGCTGTGTTTAGTAATAGAACTCTTGCTTGCTTTGCTATTTACACCACAA--GG
pBABE-puro-SV40LT_addgene      GAGTCATGCTGTGTTTAGTAATAGAACTCTTGCTTGCTTTGCTATTTACACCACAAAGGA
                               ********************************************************  *

pBABE-puro-SV40LT_seq          AAAAGCTGCACTGCTATACA--AAAATTATGG-AAAATATTCTGTAACCTTTATAAGTAG
pBABE-puro-SV40LT_addgene      AAAAGCTGCACTGCTATACAAGAAAATTATGGAAAAATATTCTGTAACCTTTATAAGTAG
                               ********************  ********** **************************

pBABE-puro-SV40LT_seq          GCATAACAGTTATAATCATAACATACTGTTTTTTCTTACTCCACACAGGCATAGAGTGTC
pBABE-puro-SV40LT_addgene      GCATAACAGTTATAATCATAACATACTGTTTTTTCTTACTCCACACAGGCATAGAGTGTC
                               ************************************************************

pBABE-puro-SV40LT_seq          TGCTATTAATAACTATGCTC-AAAATTGTGTACCTTTAGCTTTT--ATTTGTAA
pBABE-puro-SV40LT_addgene      TGCTATTAATAACTATGCTCAAAAATTGTGTACCTTTAGCTTTTTAATTTGTAA
                               ******************* **********************  ********
```

Sequence 2. Alignment of the sequence obtained from the plasmid pBABE-hygro-hTERT employing the plasmid hTERT_R with hTERT transcript variant X1.

```
Seq_pBABE-hTERT             TGCA-GAGACCAGCC--GTGAGGGATGCCGTCGTCATCGAGCAGAGCTC--TCCTGAATG
hTERT_variant_X1            TGCAGGAGACCAGCCCGCTGAGGGATGCCGTCGTCATCGAGCAGAGCTCCTCCCTGAATG
                            **** **********   ******************************   ********

Seq_pBABE-hTERT             A-GCCAGCA--GGCCT-TTCGACGTCTT-CTACGCTTCATGTGCCAACACGCCGTGC-CA
hTERT_variant_X1            AGGCCAGCAGTGGCCTCTTCGACGTCTTCCTACGCTTCATGTGCCACCACGCCGTGCGCA
                            * *******  ***** ********** ********** ********** ** **

Seq_pBABE-hTERT             TCA-GGGCAAGTCCTACGTCCAGTGCCAGGGGATCCCGCA-GGCTCCATCCTCT-CACG-
hTERT_variant_X1            TCAGGGGCAAGTCCTACGTCCAGTGCCAGGGGATCCCGCAGGGCTCCATCCTCTCCACGC
                            *** ********************************** ************* ****

Seq_pBABE-hTERT             TGCTCTGCAGCGTG-GCTACGGCGACATGGAGAACAAGCTGTTTGC-GGGATTCGGCGGG
hTERT_variant_X1            TGCTCTGCAGCCTGTGCTACGGCGACATGGAGAACAAGCTGTTTGCGGGGATTCGGCGGG
                            ********** ** ****************************** *************

Seq_pBABE-hTERT             AC-GGCTGCT-CTGCGTTTG--GGATGATTTCTTGTTGGTGACACCTCACCTCACCCACG
hTERT_variant_X1            ACGGGCTGCTCCTGCGTTTGGTGGATGATTTCTTGTTGGTGACACCTCACCTCACCCACG
                            ** ******* *********  ************************************

Seq_pBABE-hTERT             CGAGAACCTTCCTCAGGA-CCTGGTCCGAGGTGTCCCTGAGTATGG-TGCGTGGTGAACT
hTERT_variant_X1            CGAAAACCTTCCTCAGGACCCTGGTCCGAGGTGTCCCTGAGTATGGCTGCGTGGTGAACT
                            *** ************** ************************** *************

Seq_pBABE-hTERT             TG-GGAAGACAGTGGTGAACTTCCCTGTAGAAGACGAGGCCCTGGGTGGCACGGCTTTTG
hTERT_variant_X1            TGCGGAAGACAGTGGTGAACTTCCCTGTAGAAGACGAGGCCCTGGGTGGCACGGCTTTTG
                            ** ************************************************************

Seq_pBABE-hTERT             TTCAGATGCCGGCCCACGGCCTATT-CCCTGGTGCGGCCTGCTGCTGGATACCCGGACCC
hTERT_variant_X1            TTCAGATGCCGGCCCACGGCCTATTCCCCTGGTGCGGCCTGCTGCTGGATACCCGGACCC
                            ************************ **********************************

Seq_pBABE-hTERT             TGGAGGTGCAGAGCGACTACTCCAGCTATGCCCGGA-CTCCATCAGAGCCAGTCTCACCT
hTERT_variant_X1            TGGAGGTGCAGAGCGACTACTCCAGCTATGCCCGGACCTCCATCAGAGCCAGTCTCACCT
                            ********************************** ***********************

Seq_pBABE-hTERT             TCAACCGCGGCTTCAAGGCTGGGAGGAACATGCGTCGCAAACT-TTTGGGGTCTTGCGGC
hTERT_variant_X1            TCAACCGCGGCTTCAAGGCTGGGAGGAACATGCGTCGCAAACTCTTTGGGGTCTTGCGGC
                            ***************************************** ****************

Seq_pBABE-hTERT             TGAAGTGTCACAGCCTGTTTCTGGATTTGCAGGTGAACAGCCTCCAGACGGTGTGCACCA
hTERT_variant_X1            TGAAGTGTCACAGCCTGTTTCTGGATTTGCAGGTGAACAGCCTCCAGACGGTGTGCACCA
                            ************************************************************

Seq_pBABE-hTERT             ACATCTACAAGATCCTCCTGCTGCAGGCGTACAGG-CCCACGCATGTGTGCAACAGCTCC
hTERT_variant_X1            ACATCTACAAGATCCTCCTGCTGCAGGCGTACAGGTTTCACGCATGTGTGCTGCAGCTCC
                            ********************************   *************  *******

Seq_pBABE-hTERT             CATTTCATCAGCAAG-TTGGAAGAACCCCACATTCCTGCGCTG
hTERT_variant_X1            CATTTCATCAGCAAGTTTGGAAGAACCCCACATT---------
                            *************** ******************
```

Annex IV – geNorm analysis of candidate reference genes

GAPDH					
	RPLP	TBP	β-ACTINA	RNA 18S	YWHAZ
iMSC#6 BM	0.780	-0.695	-1.115	0.760	-0.165
iMSC#6 OI	-1.220	-1.045	-1.240	2.070	-0.800
iMSC#6 AI	0.285	-0.390	-1.675	0.220	-0.220
iMSC#6 CI	-0.625	-0.825	-1.525	0.055	-1.065
MSC#6 BM	-0.570	-0.235	-0.650	0.335	0.050
MSC#6 AI	-0.030	0.155	-1.815	0.810	0.170
iMSC#9 BM	-0.335	-0.345	0.000	-0.005	-0.005
iMSC#9 OI	-2.210	-1.435	-1.275	2.615	-0.520
iMSC#9 AI	-0.600	-0.890	-0.460	-0.590	-0.165
MSC#9 BM	-1.060	0.570	-1.305	-0.770	0.055
MSC#9 OI	-2.895	-0.235	-2.205	1.245	-0.830
MSC#9 AI	-2.095	-1.780	-1.460	2.660	-0.675
RPLP					
	GAPDH	TBP	β-ACTINA	RNA 18S	YWHAZ
iMSC#6 BM	-0.780	-1.475	-1.895	-0.020	-0.945
iMSC#6 OI	1.220	0.175	-0.020	3.290	0.420
iMSC#6 AI	-0.285	-0.675	-1.960	-0.065	-0.505
iMSC#6 CI	0.625	-0.200	-0.900	0.680	-0.440
MSC#6 BM	0.570	0.335	-0.080	0.905	0.620
MSC#6 AI	0.030	0.185	-1.785	0.840	0.200
iMSC#9 BM	0.335	-0.010	0.335	0.330	0.330
iMSC#9 OI	2.210	0.775	0.935	4.825	1.690
iMSC#9 AI	0.600	-0.290	0.140	0.010	0.435
MSC#9 BM	1.060	1.630	-0.245	0.290	1.115
MSC#9 OI	2.895	2.660	0.690	4.140	2.065
MSC#9 AI	2.095	0.315	0.635	4.755	1.420

TBP					
	GAPDH	RPLP	β-ACTINA	RNA 18S	YWHAZ
iMSC#6 BM	0.695	1.475	-0.420	1.455	0.530
iMSC#6 OI	1.045	-0.175	-0.195	3.115	0.245
iMSC#6 AI	0.390	0.675	-1.285	0.610	0.170
iMSC#6 CI	0.825	0.200	-0.700	0.880	-0.240
MSC#6 BM	0.235	-0.335	-0.415	0.570	0.285
MSC#6 AI	-0.155	-0.185	-1.970	0.655	0.015
iMSC#9 BM	0.345	0.010	0.345	0.340	0.340
iMSC#9 OI	1.435	-0.775	0.160	4.050	0.915
iMSC#9 AI	0.890	0.290	0.430	0.300	0.725
MSC#9 BM	-0.570	-1.630	-1.875	-1.340	-0.515
MSC#9 OI	0.235	-2.660	-1.970	1.480	-0.595
MSC#9 AI	1.780	-0.315	0.320	4.440	1.105
ACTB					
	GAPDH	RPLP	TBP	RNA 18S	YWHAZ
iMSC#6 BM	1.115	1.895	0.420	1.875	0.950
iMSC#6 OI	1.240	0.020	0.195	3.310	0.440
iMSC#6 AI	1.675	1.960	1.285	1.895	1.455
iMSC#6 CI	1.525	0.900	0.700	1.580	0.460
MSC#6 BM	0.650	0.080	0.415	0.985	0.700
MSC#6 AI	1.815	1.785	1.970	2.625	1.985
iMSC#9 BM	0.000	-0.335	-0.345	-0.005	-0.005
iMSC#9 OI	1.275	-0.935	-0.160	3.890	0.755
iMSC#9 AI	0.460	-0.140	-0.430	-0.130	0.295
MSC#9 BM	1.305	0.245	1.875	0.535	1.360
MSC#9 OI	2.205	-0.690	1.970	3.450	1.375
MSC#9 AI	1.460	-0.635	-0.320	4.120	0.785

RNA18S					
	GAPDH	RPLP	TBP	β-ACTINA	YWHAZ
iMSC#6 BM	-0.760	0.020	-1.455	-1.875	-0.925
iMSC#6 OI	-2.070	-3.290	-3.115	-3.310	-2.870
iMSC#6 AI	-0.220	0.065	-0.610	-1.895	-0.440
iMSC#6 CI	-0.055	-0.680	-0.880	-1.580	-1.120
MSC#6 BM	-0.335	-0.905	-0.570	-0.985	-0.285
MSC#6 AI	-0.810	-0.840	-0.655	-2.625	-0.640
iMSC#9 BM	0.005	-0.330	-0.340	0.005	0.000
iMSC#9 OI	-2.615	-4.825	-4.050	-3.890	-3.135
iMSC#9 AI	0.590	-0.010	-0.300	0.130	0.425
MSC#9 BM	0.770	-0.290	1.340	-0.535	0.825
MSC#9 OI	-1.245	-4.140	-1.480	-3.450	-2.075
MSC#9 AI	-2.660	-4.755	-4.440	-4.120	-3.335
YWHAZ					
	GAPDH	RPLP	TBP	β-ACTINA	RNA 18S
iMSC#6 BM	0.165	0.945	-0.530	-0.950	0.925
iMSC#6 OI	0.800	-0.420	-0.245	-0.440	2.870
iMSC#6 AI	0.220	0.505	-0.170	-1.455	0.440
iMSC#6 CI	1.065	0.440	0.240	-0.460	1.120
MSC#6 BM	-0.050	-0.620	-0.285	-0.700	0.285
MSC#6 AI	-0.170	-0.200	-0.015	-1.985	0.640
iMSC#9 BM	0.005	-0.330	-0.340	0.005	0.000
iMSC#9 OI	0.520	-1.690	-0.915	-0.755	3.135
iMSC#9 AI	0.165	-0.435	-0.725	-0.295	-0.425
MSC#9 BM	-0.055	-1.115	0.515	-1.360	-0.825
MSC#9 OI	0.830	-2.065	0.595	-1.375	2.075
MSC#9 AI	0.675	-1.420	-1.105	-0.785	3.335

M VALUES				
	M1	M2	M3	M4
YWHAZ	0.767	0.607	0.505	0.492
GAPDH	0.783	0.690	0.560	0.512
β-ACTINA	0.927	0.788	0.703	0.590
TBP	0.971	0.794	0.705	
RPLP	1.214	1.024		
RNA 18S	1.541			

Annex V – Pre-doctoral scientific production

Scientific papers

Piñeiro-Ramil M, Castro-Viñuelas R, Sanjurjo-Rodríguez C, Rodríguez-Fernández S, Hermida-Gómez T, Blanco-García FJ, Fuentes-Boquete IM, Díaz-Prado SM. Immortalizing Mesenchymal Stromal Cells from Aged Donors While Keeping Their Essential Features. *Stem Cells Int.* 2020;2020:5726947. doi: 0.1155/2020/5726947.

Castro-Viñuelas R, Sanjurjo-Rodríguez C, **Piñeiro-Ramil M**, Hermida-Gómez T, Rodríguez-Fernández S, Oreiro-Villar N, de Toro-Santos FJ, Fuentes-Boquete IM, Blanco-García FJ, Díaz-Prado SM. Generation and characterization of human induced pluripotent stem cells (iPSCs) from hand osteoarthritis patient-derived fibroblasts. *Sci Rep.* 2020;10(1):4272. doi: 10.1038/s41598-020-61071-6.

Sanjurjo-Rodríguez C, Castro-Viñuelas R, **Piñeiro-Ramil M**, Rodríguez-Fernández S, Fuentes-Boquete IM, Blanco-García FJ, Díaz-Prado SM. Versatility of Induced Pluripotent Stem Cells (iPSCs) for Improving the Knowledge on Musculoskeletal Diseases. *Int. J. Mol. Sci.* 2020;21(17), 6124. doi: 10.3390/ijms21176124

Castro-Viñuelas R, Sanjurjo-Rodríguez C, **Piñeiro-Ramil M**, Rodríguez-Fernández S, Fuentes-Boquete IM, Blanco-García FJ, Díaz-Prado SM. Generation of a human control iPS cell line (ESi080-A) from a donor with no rheumatic diseases. *Stem Cell Res.* 2020;43:101683. doi: 10.1016/j.scr.2019.101683.

Piñeiro-Ramil M, Sanjurjo-Rodríguez C, Castro-Viñuelas R, Rodríguez-Fernández S, Fuentes-Boquete IM, Blanco-García FJ, Díaz-Prado SM. Usefulness of Mesenchymal Cell Lines for Bone and Cartilage Regeneration Research. *Int J Mol Sci.* 2019;20(24). pii: E6286. doi: 10.3390/ijms20246286.

Castro-Viñuelas R, Sanjurjo-Rodríguez C, **Piñeiro-Ramil M**, Hermida-Gómez T, Fuentes-Boquete IM, de Toro-Santos FJ, Blanco-García FJ, Díaz-Prado SM. Induced Pluripotent Stem Cells for Cartilage Repair: Current Status and Future Perspectives. *Eur Cell Mater.* 2018;36:96-109. doi: 10.22203/eCM.v036a08.

Piñeiro-Ramil M, Castro-Viñuelas R, Sanjurjo-Rodríguez C, Hermida-Gómez T, Gómez, Fuentes-Boquete I, de Toro-Santos FJ, Blanco-García FJ, Díaz-Prado SD (2018). Cell Therapy and Tissue Engineering for Cartilage Repair. Cartilage Repair and Regeneration (Ed. Alessandro Zorzi). Intech. ISBN: 978-953-51-3789-4.

Book chapters

Piñeiro-Ramil M, Castro-Viñuelas R, Sanjurjo-Rodríguez C, Hermida-Gómez T, Gómez, Fuentes-Boquete I, de Toro-Santos FJ, Blanco-García FJ, Díaz-Prado SD (2018). Cell Therapy and Tissue Engineering for Cartilage Repair. Cartilage Repair and Regeneration (Ed. Alessandro Zorzi). Intech. ISBN: 978-953-51-3789-4.

Oral communications at congresses

Generation of mesenchymal stromal cell lines from osteoarthritic patients. M. Pineiro-Ramil, R. Castro-Vinuelas, C. Sanjurjo-Rodriguez, S. Rodriguez-Fernandez, T. Hermida-Gomez, J. De Toro Santos, F. Blanco-Garcia, I. Fuentes-Boquete, S. Diaz-Prado. 5th European Society of Tissue Regeneration in Orthopaedics and Traumatology (E.S.T.R.O.T.) Congress, 7th May 2019, Málaga (Spain).

Generación y caracterización de línes celulares mesenquimales "artrósicas" y "sanas". M. Piñeiro-Ramil, R. Castro-Viñuelas, C. Sanjurjo-Rodríguez, S. Rodríguez-Fernández, T. Hermida-Gómez, F. Blanco-García, I. Fuentes-Boquete1 y S. Díaz-Prado. XLV Congreso Nacional de la Sociedad Española de Reumatología, 24 de mayo de 2019, Valencia (Spain). Reumatología Cínica Vol. 15, Especial Congreso. ISSN:1699-258X.

Generación de líneas celulares mesenquimales de pacientes con artrosis y donantes sanos. M. Piñeiro-Ramil, R. Castro-Viñuelas, C. Sanjurjo-Rodríguez, S. Rodríguez-Fernández, T. Hermida-Gómez, F. Blanco-García, I. Fuentes-Boquete1 y S. Díaz-Prado. X Xornada de Investigación en Terapia Celular e Medicina Rexenerativa da Rede de Investigación en Células Nai e Terapia Celular (REDICENT), 9 de novembro de 2017, Centro de Investigacións Científicas Avanzadas (CICA), Universidade da Coruña (UDC), A Coruña (Spain).

Posters at congresses

M. Piñeiro-Ramil, R. Castro-Viñuelas, C. Sanjurjo-Rodríguez, T. Hermida-Gómez, F. Blanco-García, I. Fuentes-Boquete, S. Díaz-Prado. Immortalization of "osteoarthritis" and "healthy" mesenchymal stromal cells without loss of mesenchymal features. 2019 OARSI World Congress on Osteoarthritis, June 2019, Toronto, Canada. *Osteoarthritis and Cartilage*, Vol. 27, Number 6, S424-425. ISSN: 1063-4584.

R. Castro-Viñuelas, C. Sanjurjo-Rodríguez, **M. Piñeiro-Ramil**, T. Hermida-Gómez, J. de Toro-Santos, F. Blanco-García, I. Fuentes-Boquete, S. Díaz-Prado. Generation of human induced pluripotent stem cells (iPSC) from hand osteoarthritis patient-derived fibroblasts. *Osteoarthritis and Cartilage*, Vol. 27, Number 6, S428-429 (Abstracts from the 2019 OARSI World Congress on Osteoarthritis, June 2019, Toronto, Canada). ISSN: 1063-4584.

R. Castro-Viñuelas, C. Sanjurjo-Rodríguez, **M. Piñeiro-Ramil**, T. Hermida-Gómez, J. de Toro-Santos, F. Blanco-García, I. Fuentes-Boquete, S. Díaz-Prado. Generation of Human Induced Pluripotent Stem Cell Lines from Patients with Hand Osteoarthritis. *Arthritis & Rheumatology*, Vol. 70, Supplement 9. ACR Annual Meeting, October 19-24 2018, Chicago, USA. ISSN: 2326-5191.

M. Piñeiro-Ramil, R. Castro-Viñuelas, C. Sanjurjo-Rodríguez, T. Hermida-Gómez, F. Blanco-García, F.J. de-Toro-Santos, I. Fuentes-Boquete, S. Díaz-Prado. Generation and characterization of human bone marrow-mesenchymal stromal cell lines. II CINBIO Annual Meeting. University of Vigo, June 2018.

Rodríguez-Fernández S, Álvarez-Portela M, Rendal-Vázquez ME, Montero-Salinas A, **Piñeiro-Ramil M**, Castro-Viñuelas R, de Rojas VA, Sánchez-Ibáñez J, Fuentes-Boquete IM, Díaz Prado S. Cell viability assay in corneal endothelium. II Annual Meeting CINBIO. Biology Faculty, University of Vigo, 25 June 2018.

M. Piñeiro Ramil, R. Castro-Viñuelas, C. Sanjurjo-Rodríguez, T. Hermida Gómez, I. Fuentes Boquete, F.J. de Toro Santos, F.J. Blanco García y S. Díaz Prado. Generación de una línea celular mesenquimal artrósica para investigación en Medicina Regenerativa. XLIV Congreso Nacional de la Sociedad Española de Reumatología, A Coruña, 22-25 de mayo de 2018. Reumatología Clínica Vol. 14 (Especial Congreso), Mayo 2018. ISSN: 1699-258X.

R. Castro-Viñuelas, C. Sanjurjo-Rodríguez, **M. Piñeiro Ramil**, T. Hermida Gómez, I.M. Fuentes Boquete, F.J. de Toro Santos, F.J. Blanco García y S.M. Díaz Prado. Generación de una línea de células madre pluripotentes inducidas a partir de pacientes con artrosis de manos. XLIV Congreso Nacional de la Sociedad Española de Reumatología, A Coruña, 22-25 de mayo de 2018. Reumatología Clínica Vol. 14 (Especial Congreso), Mayo 2018. ISSN: 1699-258X.

M. Piñeiro-Ramil, R. Castro-Viñuelas, C. Sanjurjo-Rodríguez, T. Hermida-Gómez, I. Fuentes-Boquete, J. de Toro-Santos, F. Blanco-García, S. Díaz-Prado. Generation of osteoarthitis and healthy mesenchymal cell lines for research on regenerative medicine for osteoarthritis. OARSI World Congress on Osteoarthritis, April 2018, Liverpool, UK. *Osteoarthritis and Cartilage*, Vol. 26 Supplement 1, S150.

R. Castro-Viñuelas, C. Sanjurjo-Rodríguez, **M. Piñeiro-Ramil**, T. Hermida-Gómez, I. Fuentes-Boquete, J. de Toro-Santos, F. Blanco-García, S. Díaz-Prado. Establishment of an induced pluripotent stem cell line from hand osteoarthritic patients. *Osteoarthritis and Cartilage*, Vol. 26 Supplement 1, S297-8 (Abstracts from the 2018 OARSI World Congress on Osteoarthritis, April 26-29 2018, Liverpool, UK).

Abstracts accepted for publication

Castro-Viñuelas R, Sanjurjo-Rodríguez C, **Piñeiro-Ramil M**, Rodríguez-Fernández S, Fuentes-Boquete IM, Blanco-García FJ, Díaz-Prado SM. Comparison of three different chondrogenic differentiation protocols to obtain chondrocyte-like cells from induced pluripotent stem cells. *Osteoarthritis and Cartilage* 2020;28(S34). doi: 10.1016/j.joca.2020.02.056.

Piñeiro-Ramil M, Castro-Viñuelas R, Sanjurjo-Rodríguez C, Rodríguez-Fernández S, Hermida-Gómez T, de-Toro-Santos FJ, Blanco-García FJ, Fuentes-Boquete IM, Díaz-Prado SM. AB0102 Generation of osteoarthritic mesenchymal stromal cell lines. *Annals of the Rheumatic Diseases* 2019;78:1512-1513. doi: 10.1136/annrheumdis-2019-eular.6717.

Annex VI – Certificate of research stay at INL

INTERNATIONAL IBERIAN NANOTECHNOLOGY LABORATORY

Braga, 11th of December 2019

DECLARATION

The International Iberian Nanotechnology Laboratory (hereinafter INL) is the first International Organisation worldwide in the field of nanoscience and nanotechnology, providing a basis for scientific and technological cooperation by carrying out both fundamental and applied research, as well as research essentially related thereto.

The INL hereby declares that Ms. Maria Piñeiro Ramil, born on 25th of January 1993, citizen of the Kingdom of Spain, with DNI Card number 54125629M, has conducted a research stay at INL concerning a study "Magnetic-based approaches for bone tissue engineering with mesenchymal stromal cell lines", under the supervision of Dr. Manuel Bañobre, who is Leader of the Nanomedicine Research Group in the Life Sciences Department at INL, from 16th of September 2019 to 20th of December 2019.

INTERNATIONAL IBERIAN NANOTECHNOLOGY LABORATORY

Fernando Torres
Chief Administration Officer
International Iberian Nanotechnology Laboratory- INL

TE/HR/039/0.0

Annex VII – Extended abstract in Galician

Xeración e caracterización de liñas celulares mesenquimais para investigación en rexeneración osteocondral

As patoloxías do óso e da cartilaxe son enfermidades moi comúns e que afectan á calidade de vida dos doentes de forma significativa. Debido ao aumento da esperanza de vida da poboación, a incidencia destas doenzas, como a osteoporose e as enfermidades reumáticas, incluída a artrose, tamén está aumentando. Entre estas patoloxías, a artrose é a enfermidade das articulacións máis común nas persoas de idade avanzada. Esta enfermidade está caracterizada pola degradación da matriz extracelular da cartilaxe, causada polo desequilibro entre o anabolismo e o catabolismo dos condrocitos, e polo ambiente micro-inflamatorio. Hoxe en día, non existe ningún tratamento capaz de restaurar as propiedades fisiolóxicas dos tecidos óseo e cartilaxinoso.

As células mesenquimais estromais *(MSC)* son células proxenitoras das liñaxes esqueléticas que se caracterizan pola súas capacidades de auto-renovación e multi-diferenciación. Estas células localízanse na medula ósea e son capaces de dar lugar a distintos tipos celulares (osteoblastos, condrocitos e adipocitos) tanto *in vivo* como *in vitro*. Debido ás súas características, as células *MSC* constitúen unha fonte celular prometedora para a rexeneración do óso e da cartilaxe. Así a todo, estas células perden as súas capacidades de proliferación e diferenciación coa expansión en cultivo celular e coa idade do doante, polo que a investigación con *MSC* procedentes de persoas con enfermidades dexenerativas do óso e da cartilaxe para a rexeneración destes tecidos está moi limitada.

O proceso polo cal as *MSC* perden o seu potencial de proliferación en cultivo coñécese como senescencia. A senescencia celular é causada polo encurtamento dos telómeros ou por outros tipos de estrés celular. Crese que o arresto do crecemento *in vitro* das *MSC* se produce, nun primeiro momento, debido á senescencia inducida por estrés, que está regulada polas rutas das proteínas *p53* e *Rb*. En calquera caso, se as células conseguen evitar a senescencia inducida por estrés, acabarán acadando a senescencia replicativa, que se produce nas células somáticas como consecuencia do encurtamento dos telómeros en cada división celular, por mor da ausencia de telomerase. As *MSC* senescentes perden a súa capacidade de formación de colonias

e sofren cambios no seu potencial de diferenciación ata se converter en células máis adipoxénicas e menos osteoxénicas.

Esta tendencia das *MSC* á senescencia en cultivo pódese evitar mediante a súa inmortalización, coa que as células adquiren unha capacidade de proliferación ilimitada. Para conseguir a inmortalización das *MSC* é necesario interromper as rutas das proteínas *p53* e *Rb*, ademais de introducir un mecanismo que permita a replicación dos telómeros. Diversos xenes virais, como o antíxeno T grande do virus de simio 40 *(SV40LT)*, son capaces de unirse ás proteínas *p53* e *Rb* e inhibir a súa acción. Este xene, o *SV40LT*, foi amplamente utilizado para a inmortalización de diversos tipos celulares, como as *MSC* da medula ósea e as células osteoproxenitoras e condroproxenitoras presentes noutros tecidos. A expresión do *SV40LT* incrementa a esperanza de vida e a velocidade de proliferación das *MSC*, pero non permite a replicación dos telómeros e, polo tanto, non evita a senescencia replicativa.

O mecanismo máis habitual para permitir a replicación dos telómeros en células somáticas en cultivo é á súa transdución coa transcriptase reversa da telomerase humana *(hTERT)*. Ao igual que ocorre coa transdución do *SV40LT*, a transdución da *hTERT* pode non ser suficiente para á inmortalización das *MSC* e doutras células proxenitoras humanas, xa que non permite a inhibición das rutas que conducen á senescencia inducida por estrés. Pola contra, a combinación dos xenes *SV40LT* e *hTERT* si permite a completa inmortalización das *MSC*, e está asociada a unha maior velocidade de proliferación das células transducidas.

A inmortalización de células somáticas humanas adoita levarse a cabo mediante transdución con vectores retrovirais ou lentivirais. A principal limitación dos vectores retrovirais é que só son capaces de infectar células en división activa, polo que son moi ineficientes á hora de infectar células que proliferan lentamente, como son as MSC de doantes de idade avanzada. Para transducir estas células é necesario empregar estratexias que aumenten a eficiencia da infección retroviral. Unha das estratexias máis empregadas para incrementar a eficiencia da retrotransdución é a inoculación centrífuga. O aumento da eficiencia da infección mediante inoculación centrífuga depende do tipo celular e está relacionado coa velocidade de centrifugación, polo que os parámetros de velocidade e o tempo de centrifugación deben ser optimizados para cada sistema de transdución (constituído polas células que se van transducir e o virus empregado). Para un maior incremento da eficiencia

da transdución, pódense empregar adxuvantes químicos e inhibidores das histona deacetilases, que impiden o silenciamento dos transxenes.

Despois da inmortalización das células é necesario caracterizar as liñas celulares xeradas e comprobar que a transdución dos xenes de inmortalización permite a estas células inmortalizadas evitaren a senescencia, adquirindo un potencial de proliferación ilimitado. Tamén é necesario comprobar que as células inmortalizadas manteñen as características das células primarias; en caso das *MSC*, o potencial de diferenciación cara a osteoblastos, condrocitos e adipocitos e a expresión dos marcadores de superficie mesenquimais. Por último, é importante investigar se a inmortalización causou a adquisición dun fenotipo oncoxénico.

Tendo en conta todo isto, establecéronse os obxectivos deste traballo de investigación, que foron: (1) xerar liñas celulares mesenquimais derivadas das *MSC* de pacientes con artrose e doantes sen artrose; (2): analizar fenotípica e funcionalmente as liñas celulares xeradas; (3) illar clons das liñas celulares mesenquimais xeradas e analizar o seu potencial de diferenciación osteoxénica; (4) testar estratexias baseadas no magnetismo para a enxeñaría tisular do óso, empregando as liñas celulares xeradas; e (5) validar o método de inmortalización noutros tipos celulares presentes na articulación sinovial: condrocitos e sinoviocitos.

Para levar a cabo o primeiro obxectivo foi necesario establecer un protocolo de inmortalización axeitado para células de crecemento lento e con tendencia á senescencia en cultivo, como son as *MSC* derivadas de doantes de idade avanzada. Para a transdución das *MSC*, empregáronse vectores retrovirais producidos por células empaquetadoras *Phoenix*. Á súa vez, para a transfección das células *Phoenix*, empregáronse dous plásmidos: un coa secuencia do *SV40LT* e un xene de resistencia a puromicina *(pBABE-SV40LT-puro)* e outro coa secuencia da *hTERT* fusionada á proteína fluorescente verde *(GFP)* e un xene de resistencia a higromicina *(pBABE-eGFP-hTERT-hygro)*. Probáronse dous tempos de incubación das células Phoenix para a produción de retrovirus (24 e 48 horas), dúas velocidades (800 ×*g* e 1000 ×*g*) e tres tempos (60, 45 e 60 minutos) de inoculación centrífuga e distintas concentracións de ácido valproico (0, 0,5, 1, 2, 3 e 5 mM) para á indución da expresión transxénica. Tamén se probaron diferentes estratexias de transdución, incluídas a co-infección e a infección secuencial de ambos os transxenes.

Debido a que a transdución con *hTERT* non permitía a supervivencia das *MSC*, como xa se tiña observado noutros tipos celulares cunha curta esperanza de vida *in vitro*, optouse por transducir secuencialmente as *MSC* primeiro có *SV40LT* e despois coa *hTERT*. A supervivencia das *MSC* ao proceso de inoculación centrífuga foi máis alta a 800 ×*g* que a 1000 ×*g*, o que probablemente se deba ao estrés celular inducido pola centrifugación. A redución do tempo de centrifugación de 60 a 45 minutos mellorou a supervivencia celular, mentres que unha redución adicional a 30 minutos non mellorou a supervivencia e resultou prexudicial para a eficiencia da transdución. A eficiencia da transdución viuse incrementada pola adición de ácido valproico. Para determinar a concentración óptima deste inhibidor de histona deacetilases, realizáronse medidas de viabilidade celular (1) antes da inoculación centrífuga, (2) despois da inoculación centrífuga, (3) despois de tres días de incubación con ácido valproico e (4) despois de realizar a selección das células transducidas en puromicina, en tres experimentos de transdución independentes con virus portadores da secuencia do *SV40LT*. Estas medidas de viabilidade celular confirmaron que o ácido valproico incrementaba a eficiencia da transdución, pero tamén indicaron que concentracións elevadas desta substancia (3-5 mM) resultaban prexudiciais para o crecemento e viabilidade celular, polo que se estableceu a concentración óptima en 2 mM.

Empregando este método de inmortalización (transdución secuencial de hTERT e SV40LT mediante inoculación centrífuga a 800 ×*g* durante 45 minutos e incubación con ácido valproico 2mM), fomos capaces de xerar seis liñas de células mesenquimais, derivadas das *MSC* obtidas de tres pacientes con artrose e tres doantes sen artrose. Este método tamén permitiu a inmortalización de condrocitos derivados da cartilaxe do xeonllo dun paciente con artrose e de sinoviocitos derivados da membrana sinovial do xeonllo dun doante de idade avanzada. Tras a inmortalización, comprobouse mediante inmunofluorescencia que os transxenes *SV40LT* e *hTERT* se expresaban no núcleo das células inmortalizadas. O *SV40LT* presentou un padrón de expresión de "exclusión nucleolar", mentres que a *hTERT* presentou unha expresión máis variable, localizándose tanto nos nucléolos como no nucleoplasma. Non obstante, observouse que esta proteína se atopaba asociada cos nucléolos nas *MSC* inmortalizadas *(iMSC)* e, pola contra, estaba excluída deles nos condrocitos e sinoviocitos inmortalizados. A localización nucleolar da *hTERT* está regulada polo ciclo celular, pero a transdución co *SV40LT* é suficiente para promover a súa liberación dos nucléolos ao nucleoplasma. Polo tanto, a asociación

da *hTERT* cos nucléolos nas *iMSC* podería indicar que a regulación desta proteína co ciclo celular se conserva nestas células a pesar da inmortalización.

A transdución con estes xenes de inmortalización permitiu ás *MSC*, aos condrocitos e aos sinoviocitos adquiriren un potencial de proliferación ilimitado. Todas as liñas celulares xeradas presentaron menos dun 5% de células positivas para actividade β-galactosidase asociada á senescencia, o que indica que a transdución destes xenes permite a evasión da senescencia e é suficiente para a inmortalización destes tipos celulares, aínda que as células sexan procedentes de donantes de idade avanzada ou de pacientes con patoloxías que afectan aos tecidos da articulación da que se obteñen as células. Con respecto á actividade β-galactosidase asociada á senescencia, atopáronse diferenzas significativas entre as *iMSC* e as *MSC* primarias. A transducións cos xenes de inmortalización tamén aumentou a velocidade de proliferación das *MSC*. O tempo de duplicación foi de 1,9±0,8 días para as *iMSC* derivadas de pacientes con artrose e de 2,0±0,7 días para as *iMSC* derivadas de doantes sen artrose. O tempo de duplicación dos sinoviocitos inmortalizados resultou similar ao das *iMSC* (2,1±0,6 días), pero o dos condrocitos inmortalizados foi más longo (2,9±0,9 días), se cadra indicando un estado máis diferenciado dos condrocitos inmortalizados. En concordancia con este incremento na capacidade de proliferación das *iMSC*, a expresión do antíxeno nuclear de proliferación celular *(PCNA)* tamén resultou máis alta nas *iMSC* que nas *MSC* primarias. Non se atoparon diferenzas significativas entre *iMSC* derivadas de pacientes con artrose e as *iMSC* derivadas de doantes sen artrose en canto á velocidade de proliferación, a actividade β-galactosidase asociada á senescencia nin a expresión de *PCNA*.

Tamén se estudou a expresión de sete marcadores de superficie, cinco de células mesenquimais (CD29, CD44, CD73, CD90 e CD105) e dous de células hematopoiéticas (CD34 e CD45) nas *MSC* primarias, transducidas co *SV40LT* e inmortalizadas, así como na liña celular mesenquimal 3a6. En todos os casos, máis dun 90% das células foron positivas para CD29, CD44 e CD90. A expresión de CD73 foi alta nas *MSC* primarias e inmortalizadas, pero máis baixa nas células transducidas co *SV40LT*, o que podería ser un signo do envellecemento destas células, que non están completamente inmortalizadas. A expresión de CD105 foi a máis variable; atopouse tanto reducida como aumentada a través dos diferentes estados de transdución dende as *MSC* primarias ata as *iMSC*, dependendo da liña celular. CD105 tamén foi o único marcador cunha baixa expresión na liña celular

3a6. Outros autores tamén teñen atopado variacións na expresións de CD105 nas *MSC* ao longo de sucesivos subcultivos ou coa inmortalización. Todas as células foron negativas para os marcadores de células hematopoiéticas CD34 e CD45.

A expresión da isoforma *OCT4B1* do factor de transcrición *OCT4*, relacionada coa multipotencia das células somáticas, tamén se analizou nas *MSC* primarias e inmortalizadas e resultou máis alta nas *iMSC* que nas *MSC* primarias. Nas células primarias, a expresión de *OCT4* redúcese co número de subcultivos e asóciase á alta viabilidade, proliferación e multipotencia. A alta expresión de *OCT4B1* nas *iMSC* pode indicar un alto nivel de multipotencia. Outros autores tamén describiron como a inmortalización das *MSC* altera o nivel de expresión dos xenes relacionados coa multipotencia.

O potencial de diferenciación das *iMSC* xeradas, así como das células transducidas só co *SV40LT* e das células primarias, tamén foi analizado. Fixéronse experimentos de diferenciación celular cara a osteoblastos, condrocitos e adipocitos e analizáronse mediante tinturas histolóxicas (Vermello Alizarina, *Oil Red O*, Safranina O e Tricrómico de Masson) e análise da expresión de xenes relacionados coa osteoxénese (Runx2, Sp7 e osteocalcina) e a adipoxénese (*FABP4* e adiponectina). Todas as liñas mesenquimais xeradas, así como os clons derivados delas, presentaron unha alta capacidade de diferenciación osteoxénica. Ao seren sometidas a estímulos osteoxénicos, as *iMSC* formaron unha matriz máis intensamente mineralizada e expresaron maiores niveis de osteocalcina que as súas *MSC* primarias parentais. A osteoxénese é a ruta de diferenciación predeterminada das *MSC*, polo que as *MSC* inmortalizadas adoitan conservar a habilidade de formar óso tanto *in vitro* como *in vivo*. Pola contra, ao seren sometidas a estímulos adipoxénicos, as *iMSC* deron lugar a adipocitos máis inmaturos que as súas *MSC* primarias parentais. Esta inmadurez dos adipocitos xerados polas *iMSC* pode suxerir que estas células precisan de máis tempo para reverter á súa tendencia cara á diferenciación osteoxénica.

Só dúas das liñas celulares xeradas, unha derivada dun paciente con artrose e outra derivada dun doante sen artrose, foron analizadas tras seren sometidas a estímulos condroxénicos. As outras liñas xeradas non puideron ser analizadas debido á súa incapacidade para formar agregados tridimensionais polo método empregado, ou debido ao pequeno tamaño dos agregados despois do período de diferenciación condroxénica. Tras o período de diferenciación condroxénica, as *MSC* derivadas do

paciente con artrose presentaron unha maior capacidade para formar unha matriz extracelular con coláxeno e proteoglicanos que as *iMSC* derivadas do doante sen artrose. Non obstante, o potencial de diferenciación condroxénico de ambas as liñas celulares foi limitado. As *MSC* inmortalizadas mostran a mesma tendencia á hipertrofia que as *MSC* primarias cando son sometidas a estímulos condroxénicos, con presenza de coláxeno tipo X e a produción dun tecido cartilaxinoso non hialino. As capacidades anabólicas dos condrocitos para dar lugar á esta matriz extracelular tamén se viron reducidas nos condrocitos inmortalizados con respecto aos condrocitos primarios. Non obstante, os condrocitos inmortalizados si conservaron a capacidade para responder ao estímulo inflamatorio da IL-1β de xeito similar aos condrocitos primarios.

Outros autores tamén teñen descrito que a capacidade das *MSC* para diferenciarse cara ás tres liñaxes esqueléticas pode variar co número de subcultivos e coa inmortalización. As *MSC* inmortalizadas adoitan ter un potencial de diferenciación osteoxénica igual o maior que o das súas células parentais primarias, mentres que o seu potencial de diferenciación condroxénica é habitualmente limitado. Tamén é posible que as diferenzas atopadas no potencial de diferenciación entre os diferentes estados de transdución dunha mesma liña celular sexan debido á selección arbitraria de células durante a inoculación centrífuga. Neste proceso, as únicas células infectadas serán aquelas que sexan susceptibles á infección e que estean localizadas naquelas partes da placa onde o estrés inducido pola centrifugación é menor. Xa que as *MSC* existen como poboacións heteroxéneas, esta selección arbitraria alterará as súas propiedades, incluído o seu potencial de multi-diferenciación.

As *MSC* inmortalizadas poden adquirir un potencial de diferenciación ilimitado sen un control aberrante do crecemento. Non obstante, poden aparecer mutacións oncoxénicas durante o seu cultivo *in vitro*, e as *MSC* inmortalizadas cultivadas a baixas densidades durante longos períodos de tempo poden acabar converténdose en células tumorais. Neste estudo, dúas das seis liñas celulares mesenquimais xeradas tiveron capacidade de crecemento independente de ancoraxe, o que indica a súa transformación tumoral. Sorprendentemente, unha destas liñas celulares foi a única na que a expresión do oncoxene Ras se reduciu en comparación coas súas células parentais primarias.

Como parte deste estudo, illáronse tres clons a partir de cada unha das catro primeiras liñas celulares mesenquimais xeradas. Todos estes clons presentaron unha

alta capacidade osteoxénica e algúns deles tamén presentaron unha tendencia espontánea cara a esta ruta de diferenciación. Un destes clons, *iMSC#8.A*, presentou a habilidade de formar agregados tridimensionais mineralizados en ausencia de estímulos osteoxénicos. Sorprendentemente, este clon foi derivado dunha das liñas celulares incapaces de formar agregados tridimensionais polo método empregado para a súa diferenciación condroxénica. Polas súas características, este clon foi seleccionado para testar estratexias baseadas no magnetismo para a enxeñaría tisular do óso.

A enxeñaría tisular require tres elementos: un material que permita o crecemento das células, células que produzan o tecido desexado e sinais capaces de induciren a proliferación e a diferenciación das células. As estratexias baseadas no magnetismo implican a magnetización dos materiais ou das células e a aplicación dun campo magnético para inducir a diferenciación osteoxénica. Neste estudo magnetizáronse materiais de coláxeno I e o clon *iMSC#8.A* para investigar o efecto do campo magnético rotatorio sobre a diferenciación osteoxénica destas células. Tanto as células como os materiais de coláxeno foron magnetizados de forma eficiente polas nanopartículas de ferro empregadas, como comprobamos mediante *SQUID*, *ICP* e tintura Azul de Prusia, e a incorporación das nanopartículas de ferro nos materiais e nas células non produciu toxicidade celular. Así a todo, o campo magnético rotatorio non induciu a diferenciación osteoxénica das *iMSC#8.A* nas condicións testadas. É posible que o campo magnético empregado non tivese a intensidade adecuada para a estimulación das *MSC*.

En resumo, este estudo demostra que as *MSC* primarias, os condrocitos articulares e os sinoviocitos derivados de pacientes con artrose e doantes de idade avanzada poden ser inmortalizados por transdución secuencial dos xenes *SV40LT* e *hTERT*, mediante inoculación centrífuga e coa adición de ácido valproico. As células inmortalizadas evitan a senescencia celular, obteñen un potencial de proliferación ilimitado e, no caso das *iMSC*, manteñen as características definitorias das *MSC*. O elevado potencial osteoxénico destas células e dos clons derivados delas convérteas en boas candidatas para formaren parte de modelos *in vitro* de enxeñaría tisular co fin de estudar as enfermidades do óso e investigar a rexeneración deste tecido.